1977

Upper Photospheric Temperature Models Of K Giants With Emphasis On A Comparison Of The Smr(+ Super-metal Rich) K Giants With Normal K Giants

Krishna Desikachary

NOTICE

The quality of this microfiche is heavily dependent upon the quality of the original thesis submitted for microfilming. Every effort has been made to ensure the highest quality of reproduction possible.

If pages are missing, contact the university which granted the degree.

Some pages may have indistinct print especially if the original pages were typed with a poor typewriter ribbon or if the university sent us a poor photocopy.

Previously copyrighted materials (journal articles, published tests, etc.) are not filmed.

Reproduction in full or in part of this film is governed by the Canadian Copyright Act, R.S.C. 1970, c. C-30. Please read the authorization forms which accompany this thesis.

THIS DISSERTATION HAS BEEN MICROFILMED EXACTLY AS RECEIVED

AVIS

La qualité de cette microfiche dépend grandement de la qualité de la thèse soumise au microfilmage. Nous avons tout fait pour assurer une qualité supérieure de reproduction.

S'il manque des pages, veuillez communiquer avec l'université qui a conféré le grade.

La qualité d'impression de certaines pages peut laisser à désirer, surtout si les pages originales ont été dactylographiées à l'aide d'un ruban usé ou si l'université nous a fait parvenir une photocopie de mauvaise qualité.

Les documents qui font déjà l'objet d'un droit d'auteur (articles de revue, examens publiés, etc.) ne sont pas microfilmés.

La reproduction, même partielle, de ce microfilm est soumise à la Loi canadienne sur le droit d'auteur, SRC 1970, c. C-30. Veuillez prendre connaissance des formules d'autorisation qui accompagnent cette thèse.

LA THÈSE A ÉTÉ MICROFILMÉE TELLE QUE NOUS L'AVONS REÇUE

The University of Western Ontario

Faculty of Graduate Studies
Stevenson-Lawson Building
London, Canada N6A 5B8

In the interests of facilitating research by others at this institution and elsewhere, I hereby grant a licence to:

THE UNIVERSITY OF WESTERN ONTARIO

to make copies of my thesis

UPPER PHOTOSPHERIC TEMPERATURE MODELS OF K GIANTS WITH EMPHASIS ON A COMPARISON OF THE SMR K GIANTS WITH NORMAL K GIANTS

or substantial parts thereof, the copyright which is invested in me, provided that the licence is subject to the following conditions:

1. Only single copies shall be made or authorized to be made at any one time, and only in response to a written request from the library of any University or similar institution on its own behalf or on behalf of one of its users.

2. This licence shall continue for the full term of the copyright, or for so long as may be legally permitted.

3. The Universal Copyright Notice shall appear on the title page of all copies of my thesis made under the authority of this licence.

4. This licence does not permit the sale of authorized copies at a profit, but does permit the collection by the institution or institutions concerned of charges covering actual costs.

5. All copies made under the authority of this licence shall bear a statement to the effect that the copy in question "is being made available in this form by the authority of the copyright owner solely for the purpose of private study and research and may not be copied or reproduced except as permitted by the copyright laws without written authority from the copyright owner."

6. The foregoing shall in no way preclude my granting to the National Library of Canada a licence to reproduce my thesis and to lend or sell copies of the same. For this purpose it shall also be permissible for the University of Western Ontario to submit my thesis to the National Library of Canada.

B Gordon
(signature of witness)

K Desikachary
(signature of student)

SEPTEMBER 15, 1977
(date)

Ph.D.
(degree)

ASTRONOMY
(department of student)

UPPER PHOTOSPHERIC TEMPERATURE MODELS OF K GIANTS

WITH EMPHASIS ON

A COMPARISON OF THE SMR K GIANTS WITH NORMAL K GIANTS

by

Krishna Desikachary

Department of Astronomy

Submitted in partial fulfillment of the requirements

for the degree of Doctor of Philosophy

Faculty of Graduate Studies

The University of Western Ontario

London, Ontario

July, 1977

ABSTRACT

In this thesis the upper photospheric $T(\bar{\tau})$ distributions of six K giant stars have been derived using the Ca II K wing profiles. The stars included in this study are the normal K giants β Gem, ε Cyg, α Ari and κ Oph, and the SMR (Super Metal Rich) K giants α Ser and β Oph.

Observations of the K line were obtained photoelectrically at the Coude focus of the 48 inch telescope of the University of Western Ontario Observatory. A resolution of 0.5Å was used to measure the K wing ($\Delta\lambda < 7$Å), while a value of 0.2Å was used to measure the window at $\lambda 3950.8$Å, with respect to which the K wing was normalized.

The normalized profiles were interpreted to yield upper photospheric $T(\bar{\tau})$ models, using the LTE-PCS formulation of Ayres (1975) for the K wing formation. The abundance of Ca used in line synthesis was selfconsistently derived by synthesizing the far wing profile of the Ca II λ8498 line.

A comparison of the upper photospheric $T(\bar{\tau})$ models of the normal stars with those obtained for the SMR stars has revealed that the latter stars are cooler by about 180K. The extent of this differential (SMR-Normal) cooling is in accordance with a similar result obtained by Peterson (1976) in a comparison of the SMR prototype μ Leo with the normal K giants κ Oph and ι Dra. Despite this agreement in a differential sense, in an absolute sense our K line upper photospheric models are considerably (up to 300K) hotter than the empirical $T(\bar{\tau})$ models derived by Peterson.

LIST OF FIGURES

ACKNOWLEDGEMENTS

Several people have contributed to the completion of this thesis project. The foremost among them is my thesis supervisor, Dr.D.F.Gray, whose constant interest, guidance and encouragement were of great value. He was always willing to discuss my problems. More specifically, I must record my indebtedness to him for helping me with observations and for letting me use his computer programs. Drs. J.M.Marlborough and W.H.Wehlau, the other members of my thesis committee, have greatly contributed to the quality of presentation through their constructive criticism. Talking my problems (both scientific and personal) with Dr. J.D.Landstreet has been a great source of inspiration.

My colleaques, the fellow graduate students, provided moral support. Mrs. Rasche drew substantial portion of the diagrams included in this thesis. To these people I am highly indebted. The International Astronomical Union facilitated my journey from India to Canada by providing a travel grant. The Government of Ontario partly supported my stay here by awarding a graduate scholarship. I am thankful to the generosity of these organisations.

Finally, Miss Alice Croft provided cheerful inspiration during the tiring period of thesis writing. It is hard to find adequate words to express my gratitude to her.

TABLE OF CONTENTS

LIST OF TABLES

LIST OF FIGURES

NOTATION

In order to aid the readability of this thesis, we summarise the most often encountered symbols and abbreviations below.

BTM	Basic temperature model
E_c	Continuous opacity enhancement factor
E_6	Van der Waals enhancement factor
HSRA	Harvard-Smithsonian Reference Atmospheric model for the Sun (Gingerich et al.,1971)
KREe	Radiative equilibrium model of the solar atmosphere computed by Kurucz (1974)
LTE	Local thermodynamic equilibrium
NLTE	Non-local thermodynamic equilibrium (Kinetic equilibrium)
NCS	Noncoherent scattering (Complete redistribution)
PCS	Partial coherent scattering (Partial redistribution)
ST	Spinrad & Taylor (1969)
SMR	Super Metal Rich
TEM	Temperature enhancement model
T_{min}	Temperature minimum
VP	Van Paradijs (1976)
Γ_R	Radiation damping width
Γ_4	Stark broadening width
Γ_6	Van der Waals broadening width
$\bar{\tau}$	Continuum optical depth at the standard wavelength, $\lambda = 5000\text{Å}$
τ_c	Continuum optical depth at any other wavelength

CHAPTER I

INTRODUCTION

The Ca II H & K lines have recently been exploited to derive the temperature structure and other physical properties of the upper photosphere and lower chromosphere regions in late type stars. The K line wings are especially suited to derive the upper photospheric temperature structure because the frequency dependence of the opacity is strongly dependent upon the assumed temperature structure. Ideally, within a small frequency band the K line contains the same amount of information as the whole range of continuum flux measurements, and is simpler to observe than the continuum flux. Furthermore, LTE seems to be a good approximation for the formation of the K wings, which makes the numerical approach simpler. Not surprisingly therefore, the analysis of the K line has gained considerable interest in recent times. However, recent work by Milkey and his associates (Milkey, Ayres & Shine, 1975; Shine, Milkey & Mihalas, 1975) has shown that partial coherency effects in the transfer equation become important and should be properly taken into account. Ayres (1975) and Ayres & Linsky (1976) have respectively formulated the LTE and non-LTE versions of the K line synthesis taking partial coherency effects into account. These formulations, abbreviated respectively by LTE-PCS and NLTE-PCS, are more complicated than the simple LTE approach but are still tractable. Ayres and coworkers have applied

these techniques to interpret the K line profiles of the Sun (Ayres & Linsky, 1976), Procyon (Ayres & Linsky, 1974), Arcturus (Ayres & Linsky, 1975), and α Cen A,B (Ayres et. al., 1976).

1.1. THIS INVESTIGATION

Encouraged by the success of the above analyses, here we apply the LTE-PCS formulation of Ayres (1975) to the interpretation of the K wings in some K giant stars to derive upper photospheric temperature models. The stars included in this program are β Gem (K0 III), ε Cyg (K0 III), α Ser (K2 III), β Oph (K2 III), κ Oph (K2 III) and α Ari (K2 III). In addition, Arcturus (K2IIIp) and the Sun (G2 V) are also included to provide a comparison between this work and that of Ayres and his associates. β Gem, ε Cyg, κ Oph and α Ari are the normal composition K giants which bracket the Te, log g values of the highly blanketed stars α Ser and β Oph (cf. Fig.1.1). α Ser and β Oph are also classified as the SMR (Super Metal Rich) stars according to Spinrad & Taylor's (1969) narrow band photometry. In this investigation we compare the upper photospheric temperature structures of these highly blanketed and SMR stars with the normal K giants.

1.2. THE SMR PHENOMENON AND THE CONTEXT OF THIS INVESTIGATION

In order to place this investigation in proper context, it is necessary to give a brief account of the "SMR Phenomenon", and also the effect of line blanketing on the

temperature structure of the photosphere. The so called SMR stars were discovered by Spinrad & Taylor (1969) in their extensive photometric survey of K type stars as having metal abundances in excess of the Hyades stars. Their technique consisted of isolating and measuring certain linefree (continuum) points and also some of the strong atomic and molecular spectral features through photoelectric narrow band photometry and relating these measurements to abundances by a simple theory. In this way they found many SMR stars in the general galactic field as well as in the old galactic clusters M67 and NGC188. They also argued that such spacial distribution of the SMR stars is indicative of a primordial enrichment of the galactic disk rather than the generally accepted view of a gradual enrichment. This controversy focussed the attention of many investigators on these stars, and they became the subject of many high dispersion abundance analyses (Strom, Strom & Carbon, 1971; Blanc Vaziaga, Cayrel & Cayrel, 1973; Oinas, 1974; Peterson, 1976). However, apart from one or two elements, these studies failed to confirm the existence of the expected overall metal enhancement. Of these studies, those by Strom et al. and Peterson are extremely interesting insofar as they propose a decrease in the boundary temperature as the cause of the selective enhancement of the strong line features of the Spinrad & Taylor's narrow band photometry, hence that of the SMR phenomenon. Peterson, in her extensive and careful comparison of the normal K giant stars κ Oph and ι Dra with the prototype SMR K giant μ Leo, has provided compelling

evidence that the SMR phenomenon is caused by a temperature drop of about 180K in the upper photosphere of μ Leo compared to κ Oph. This temperature drop affects the ionization equilibrium of the elements with low ionization potentials and results in selective enhancement of the strong line features that form the basis for SMR classification. She has also shown that the weak line strengths are about the same in all the three stars, thus disproving any selective enhancement in the overall metal content. However, she has found that CN lines are 50% stronger in μ Leo than in κ Oph, as a result of a 200% enhancement of Nitrogen in the former star. The CN molecule has many absorption lines in the near infrared where the most of the K giant flux is emitted. These lines then cause backwarming of the deeper photospheric layers while cooling the shallower layers through their blocking action on the outward flow of radiation in the star. Thus, according to Peterson, the SMR phenomenon is caused by an increase in the Nitrogen abundance, which strengthens the CN molecular features, which in turn cool the upper photosphere while heating the deeper layers. However, the data used by Peterson are not particularly suited to derive the upper photospheric temperature structure. So, it will be very interesting to use a very strong absorption feature like the K line, which is a better diagnostic for the upper photospheric temperature structure, and quantitatively compare the SMR and normal K giant stars. With this goal in mind, we have set out to compare the SMR stars α Ser and

β Oph with several normal K giant stars. It would have been preferable to include the SMR prototype μ Leo in this investigation, but it is too faint. α Ser is SMR insofar as it exhibits strong Na I D and CN features (Spinrad & Taylor, 1969); according to Greene (1969) it also has a higher C/O ratio and higher Nitrogen abundance than the Sun, which explains the enhanced CN strength. Through a curve of growth analysis, Griffin (1969) has shown that α Ser has ≃ 1.5 times higher metal abundance than the Sun. All these facts point towards a lower boundary temperature for this star. This expectation is further strengthened by Fig.1.1, taken from van Paradijs (1976), where the line blocking coefficients of five K2 III stars, including α Ser, β Oph and μ Leo are plotted. These three stars have much larger blocking fractions than the normal K2 giants α Ari and ε Sco. What is more interesting is that both α Ser and β Oph have comparable blocking fractions to μ Leo. This fact leads to the conclusion that even though α Ser and β Oph are not the prototypes of the group, they are still strong members of the group, hence their analysis can be expected to shed some light on the SMR group of stars as a whole.

We should qualify the above statements by mentioning that β Oph was not explicitly classified as SMR by Spinrad and Taylor. Nonetheless, in many physical aspects this star appears to be almost identical to α Ser. For example, both stars have very similar Spinrad & Taylor's T_1 CN indices; as shown in Fig.1.1 they also have very similar line

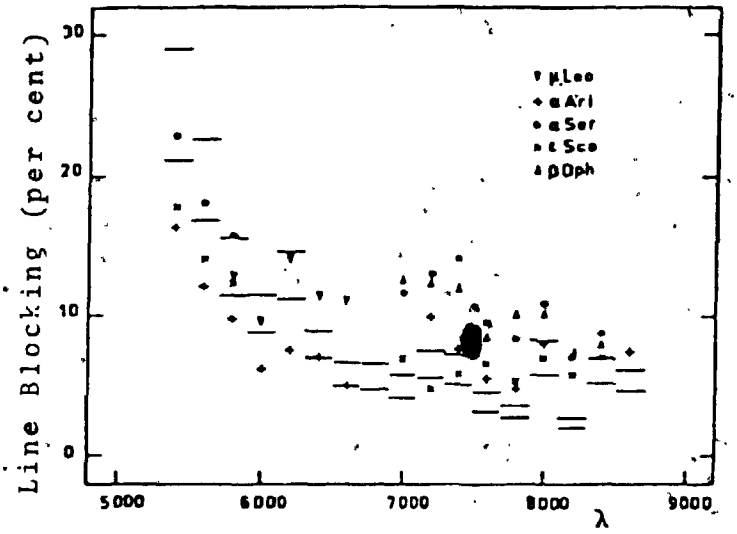

Fig.1.1. Wavelength distribution of line blocking coefficients in five K2 III stars. Notice that α Ser and β Oph share the behavior of the SMR prototype μ Leo in having higher line blocking than the normal stars α Ari and ε Sco. This figure has been taken from van Paradijs (1976).

blocking fractions and as will be shown in Chap.IV they have identical Te, log g values. What is even more interesting is that they also have identical K line profiles (cf. Chap.II) . So, the conclusion that β Oph is a SMR star is inescapable.

In addition to providing a comparison of the SMR and normal stars, the above investigation can offer important information on the late type stars in general. For example, the value of T_{min} is an important datum for stars with a chromospheric temperature rise. Ayres et al. (1976) have presented some evidence that in K type stars the T_{min}/Te ratio is close to 0.73 and is smaller than the ratio $\simeq 0.78$ predicted by the lineblanketed radiative equilibrium (RE) models of Carbon & Gingerich (1969). It will be interesting to see if the same conclusion applies to our program stars. Also, on the basis of simple dimensional arguments, Ayres, Linsky & Shine (1975) have shown that the K1 width-luminosity relation can be understood if the continuum optical depth $\tau_c(T_{min})$ of the temperature minimum is roughly independent of g in the late type stars. It will be interesting to see if this assumption is applicable to our program stars.

1.3. CHAPTER OUTLINE

This thesis is structured as follows. In Chap.II we discuss the observations of the Ca II K line profiles. In Chap. III we give a brief account of Ayres' (1975) LTE-PCS line

formation theory for the K wing and discuss some of the practical difficulties in applying this theory to the K Giants. In Chap.IV we derive the continuum models by matching the observed continua of the program stars with the theoretical ones, and also derive the Ca abundance by matching Anderson's (1974) Ca II λ8498 profiles with the theoretical profiles synthesized with these continuum models. In Chap.V we apply the theory contained in Chap.III to the Sun and Arcturus and confirm that our results are consistent with those obtained by Ayres (1975) and Ayres & Linsky (1975). We then proceed to derive upper photospheric temperature models for the program stars, using the observations and the background information contained in Chaps.II & IV respectively. Finally, in Chap.VI we discuss the astrophysical implications of the results obtained in Chap.V, summarise the conclusions and make some suggestions for future work.

CHAPTER II

OBSERVATIONS

In this chapter we describe the observation and reduction procedures of the Ca II K line in our program stars.

2.1. SELECTION OF STARS

The selection of stars was guided by the following practical considerations:

a) They should be brighter than the third magnitude so that a complete scan of the K wing and the reference window can be obtained on a given night of 7-9 hours duration. This is also the limiting magnitude set by the dark count rate of the instrument.

b) They should be observable in summer when the best observing weather prevails.

c) They should have observed energy distributions, line blocking coefficients and Ca II λ8498 profiles. These data are available for many of our stars, and whenever an item or two is missing for one or more stars, we have found a way (as will be described in later chapters) to get around this deficiency.

2.2. OBSERVING PROCEDURE

All the observations were made with a photoelectric line scanner built by Gray (1971) at the Coudé focus of the 48 inch telescope of the University of Western Ontario Observatory. The Coude system is fed by a f/30.9 beam from the telescope which is brought to a focus at the entrance slit outside the

Coude room. A 6.96m focal length mirror collimates this beam while a 204X254mm two part mosaic grating with 600 lines/mm disperses it. It is then brought to a focus outside the Coudé room by a 10.7m focal length camera, where the exit slit-photomultiplier assembly is located. The dispersion at the K line is 0.954Å/mm and the resolution is set by the sizes of the entrance and exit slits which are matched. The scanning is done by moving the exit slit-photomultiplier assembly on a precision screw table manufactured by the Gaertner Scientific Corporation. To account for the seeing fluctuations, extinction etc., a second fixed photomultiplier monitors an adjacent portion of the spectrum so that the instrument can be used in a ratioing mode. Hereafter, we refer to the scanning detector assembly as the " Profile Channel", and the fixed monitoring assembly as the "Reference Channel". The photons in both channels are counted by commercial pulse amplifiers, discriminators and scalars. More specifically, we employ thermoelectrically cooled ITT FW-130 photomultipliers with S-20 cathodes, SSR 1120 amplifier discriminators and Dana 8010 scalars. The method of operation is to count a certain fixed number of photons in the reference channel (usually 10^4 in our case) and record the corresponding number in the profile channel during this interval. The reduction is then straightforward, the flux ratio between the two channels being given by the ratio of the total number of photons counted less the dark count. The dark count rate in the profile channel is 1-2 per sec., while it is 20-70 per sec. in the

reference channel, depending upon the ambient temperature near the cold boxes at night.

2.3. RESOLUTION DATA

Our measurement of a line profile consists of the K wing in the range $-2\text{Å} < \Delta\lambda < 7.5\text{Å}$, and the window centred on $\lambda 3950.8$. We use a resolution of 0.5Å for the K wing and 0.2Å for the window. These rather low resolutions were chosen to extend the capability of the instrument to reach our (faint?) program stars without biasing or losing the physical information contained in the profiles. The 0.5Å resolution of course smears out the central emission peaks, but we decided to sacrifice the chromospheric information contained in them at the cost of extending our observations to faint stars, as we are only interested in the upper photospheric $T(\bar{\tau})$ models in this thesis. As we shall show in Chap.V, the profile beyond K1 is unbiased by our low resolution and is adequate to derive the upper photospheric $T(\bar{\tau})$ models. Had we restricted ourselves to 0.1Å resolution, Arcturus is the only program star we could have measured, and then only incompletely on a night of 8 hours duration, So, we must compromise. Because of the narrowness (0.3Å) of the window and the strong absorption lines flanking it, we have chosen a higher (0.2Å) resolution to measure the window. This is again chosen to be most efficient in photon counts without biasing the physical information. Usage of different resolutions in different parts of the profile presents the important problem of tying the two parts together, because the instrumental profiles

have different absolute areas in both cases. So, we have to calibrate these areas, which are determined by entrance and exit slit settings. We decided the best way to do this is to calibrate them relatively using an incandescent light source. To this end, our procedure consisted of the following steps:

a) Set the entrance and exit slits at 250μ and 500μ respectively to give 0.5Å resolution and obtain a scan of the K wing in the range $-2\text{Å} < \Delta\lambda < 7.5\text{Å}$.

b) Now, centre an incandescent light bulb fed by a constant voltage power supply in front of the entrance slit and record its brightness. A diffuser is placed between the light source and slit so that the latter is illuminated uniformly.

c) Change the slits to 100μ and 200μ respectively to give 0.2Å resolution and remeasure the light bulb. The previous measurement (in b) divided by this one is equivalent to the ratio of the instrumental profile areas corresponding to 0.5Å and 0.2Å resolutions.

d) Remove the light bulb from the optical path and obtain a complete scan of the window with 0.2Å resolution.

The need for this calibration arises because we wish to normalise the K wing profile to the window. Because of the absence of well defined continuum near the K line, we normalise the wing profile to the highest point in the wing itself. This poses no problem in comparing theory with observations, as the theoretical profiles can be similarly normalised.

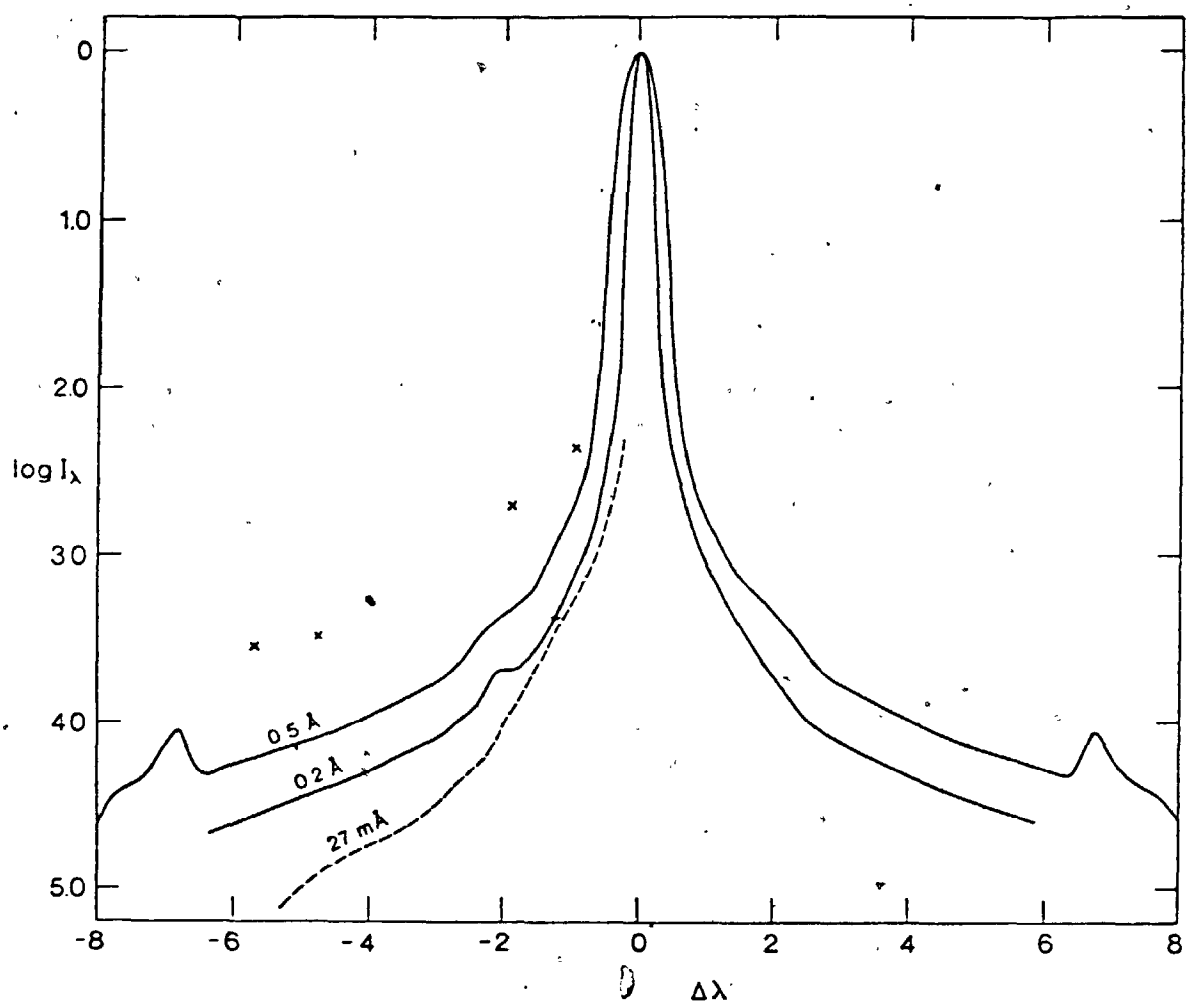

Fig.2.1. Instrumental profiles. Our 0.5Å and 0.2Å instrumental profiles are shown by solid lines. Part of the blue wing of Griffin's 27mÅ 3rd order instrumental profile is shown by a dashed line. The positions of the peaks of the ghosts in this profile are indicated by crosses.

Whenever a switch is made between the wing and window measurements during the night a calibration is obtained. Several such measurements made in the course of the night agreed to better than 2%. So, $\lesssim$2% can be accepted as the error associated with the above calibration process.

Normalization of the profile to the window proceeds as follows. The wing is sampled at every 0.25mm ($\sim$0.24Å) and the window at 0.1mm ($\sim$0.1Å). At each of these points the ratio ρ between the stellar counts in the profile and reference channels is formed. Normalization to the window then follows by dividing all the ρs by the ρ corresponding to the window and the slit width ratio determined above. Wavelength calibration is provided either by observing Vega or locating the centre of the window or both. When using Vega, the K line centre in the program star is located by applying a differential wavelength shift corresponding to the differences in the radial velocities and components of the Earth's orbital and axial motions in the direction of the two stars.

The instrumental profiles at both resolutions were measured using the λ4046Å line in a ^{198}Hg lamp. They are displayed in Fig.2.1.

2.4. ERRORS

Errors arise from two sources: a) Photometric errors from statistical fluctuations in the photon events; b) Systematic errors from the drifts in the sensitivity of the instrument as the temperature drops during the night. First, we consider the photometric errors. Fluctuations in the photon events

arise from variations in the stellar photon arrival rate and dark count rate (the sky background being negligible at the Coude' focus). If S is the stellar photon count rate (per second) and D is the dark count rate, and t is the integration time so that N=St is the total number of stellar photons counted, the relative standard error ε_ρ in the measured ratio ρ is given by

$$\varepsilon_\rho \simeq \varepsilon_p = \left(\frac{1 + D/S}{N}\right)^{\frac{1}{2}} \qquad (2.1)^*$$

If $D/S \ll 1$, Eq.2.1 reduces to $\varepsilon_\rho = N^{-\frac{1}{2}}$; on the contrary, if $D/S \sim 1$, the full expression 2.1 should be considered in calculating ε_ρ. In this case we can still reduce ε_ρ by increasing t or by adding many integrations together. We have followed the latter procedure for all our stars. The inner 3Å portion of the K line is so deep that the D/S ratio is a large fraction of unity for stars fainter than Arcturus. This necessitates the usage of the full expression 2.1 to evaluate ε_ρ. For simplicity, however, we replace it by $\varepsilon_\rho = 1.2N^{-\frac{1}{2}}$, which gives an approximate estimate of ε_ρ. The values thus obtained are in close agreement with Eq.2.1 in the inner wings, but are slightly larger in the far wings. Typical values of ε_ρ for Arcturus at λλ 3934.4Å, 3936.5Å, 3940.0Å and 3950.8Å are

---

* Eq.2.1 strictly applies to a single channel instrument. In case of a dual channel ratioing system such as ours, the relative standard error ε_ρ in the measured ratio ρ is given by

$$\varepsilon_\rho = (\varepsilon_p^2 + \varepsilon_R^2)^{\frac{1}{2}} \qquad (2.1a)$$

where ε_p and ε_R are the relative standard errors in the profile and reference channels. However, for all practical purposes $\varepsilon_R \ll \varepsilon_p$, so that $\varepsilon_\rho \simeq \varepsilon_p$ is a good approximation.

respectively 1.5%,0.9%,0.5%, and 0.5%; corresponding values for other stars are 3.3%,2.4%,1.5% and 1.6% at the respective wavelengths. So, we can expect the maximum cumulative relative standard photometric errors* in the normalized (to window) flux profiles to be $\sim$1.6% in case of Arcturus and $\sim$3.5% in other stars. As we shall see in the next section, this is the order of the internal consistency between the different nights' data of a single star.

As for the second source of error, the sensitivity of the detectors depends upon the ambient temperature near the cold boxes at night. Even though the line scanner is a ratioing system, the ratios may drift with time as the night cools, because the individual photomultipliers have different sensitivity drifts. However, this problem was not felt on many nights. Only on four nights was the drift bothersome. In order to trace the drift we monitor a high point in the wing (near λ3940Å) every 20 minutes and plot the ratios obtained against time. Usually this plot is a straight line parallel to the time axis. When this is not the case, we fit a polynomial through the points to obtain an analytical representation of the drift. All the observed ratios will then be corrected using this polynomial. In practice, this procedure works quite satisfactorily. An example is provided by the two sets of data obtained on 8th and 11th June, 1976 for Arcturus. The former

*When we normalize the K wing to the window, we have to consider a similar expression to Eq.2.1a, with ε_R replaced by the error in the ρ corresponding to the window. We refer to this error (in the normalized profile) as the cumulative relative standard error.

set is driftfree while the latter set is affected by one of the largest recorded drifts*. However, good agreement (within the photometric errors) between the two sets can be obtained after correcting the latter set for the drift according to the above procedure. This is illustrated in Fig.2.2g, where the triangles and crosses represent the two sets of data.

2.5. DISCUSSION OF INDIVIDUAL STARS

Table 2.1 lists the program stars together with the dates of observation. On each night we have also listed the star to dark count ratio S/D at four representative points in the profile, namely at $\lambda\lambda$3934.4Å, 3936.5Å, 3940.0Å, and 3950.8Å. The quality of each night can be judged from these entries. All stars fainter than Arcturus have similar errors as we have attempted to reduce ϵ_ρ by adding several integrations together in cases of low S/D. The observations are of course more accurate for Arcturus because of its brightness. It was not possible to measure the window on some nights. Normalization of the profile on such nights was effected by means of the window measurements obtained on other nights. We displayed the observations of the individual stars in Figs.2.2a-g.

A good idea of the accuracy and repeatability of the measurements and reliability of the slit width calibration can be had by looking at Figs.2.2a-g. It is seen that different sets of data of a single star show good agreement. This implies

---

* The ratio of the drift monitoring point on this night smoothly increased by a factor of 1.06 in the course of 3.5 hours of observing time.

that the repeatability is good and slit width calibration is reliable. To throw more light on the latter, we especially refer to Figs.2.2b,c,f, which contain the normalised profiles of ε Cyg, α Ser and α Ari. For ε Cyg independent calibrations were obtained on 30/7/76 (filled triangles), 10/8/76 (filled circles) and 29/9/76 (crosses); for α Ser one calibration was obtained by Gray on 4/6/76 (triangles) and the other by the author on 3/6/76 (circles); for α Ari two independent calibrations were obtained on 13/9/76 (circles) and 29/9/76 (squares). It is seen that the independently calibrated and normalised profiles of a given star agree within $\sim$2%, the error associated with the calibration process. However, some points on 30/7/76 in ε Cyg deviate more than this amount as that night was of poor photometric quality. Likewise, the last three points on 3/6/76 in α Ser (circles) deviate more, as proper drift correction for these points could not be made. But for these exceptions, the agreement between different sets of the independently calibrated and normalised profiles is very good. Thus, the typical relative standard errors (including calibration and photometry) in the normalised profiles are $\sim$4.5% in stars fainter than Arcturus, and are $\sim$2% in Arcturus. These values are estimated from the internal scatter in the data plotted in Figs.2.2a-g, and are about 1.3 times larger than the theoretical estimates obtained in §2.3.

TABLE 2.1

OBSERVING CONDITIONS

Date	Star to dark ratio at λ3934.4	λ3936.5	λ3940.0	λ3950.8	Typical percentage error[1] at λ3934.4	λ3936.5	λ3940.0	λ3950.8
1. β Gem, K0 III, m_V=1.16, B-V=1.02, R-I=0.50								
8/4/76	5	14	34	-	3.0	1.8	1.2	-
9/4/76	17	24	26	-	1.6	1.0	1.5	-
18/5/76	-	-	28	38	-	-	1.6	1.1
2. ε Cyg, K0 III, m_V=2.46, B-V=1.03, R-I=0.56								
9/7/76[D]	7	27	33	-	3.8	2.2	1.6	-
12/7/76	11	23	64	-	3.5	2.2	1.4	-
13/7/76	12	33	95	-	3.6	2.4	1.6	-
30/7/76	-	17	25	8	-	2.6	1.6	1.8
10/8/76	14	35	85	19	3.2	2.2	1.5	1.4
29/9/76	21	64	135	24	3.2	2.5	1.7	1.7
3. α Ser, K2 III, m_V=2.65, B-V=1.17, R-I=0.56								
3/6/76	5	10	8	11	2.8	1.8	1.6	1.4
4/6/76*	5	12	30	10	3.0	2.0	1.3	1.4
5/6/76[D]	5	17	29	-	2.5	1.5	1.0	-
4. β Oph[2], K2 III, m_V=2.77, B-V=1.16, R-I=0.57								
7/6/76*	4	16	32	9	3.5	2.2	1.5	1.5
5. κ Oph, K2 III, m_V=3.18, B-V=1.15, R-I=0.62								
8/7/76*[D]	3	8	16	-	3.3	2.0	1.2	-
12/7/76	2.5	7	12	-	4.0	2.2	1.8	-
9/8/76	-	-	17	5	-	-	1.9	2.2

(Table 2.1 continued)

6. α Ari, K2 III, m_V=2.00, B-V=1.15, R-I=0.62

31/7/76	-	16	50	-	-	2.4	1.4	-
8/9/76	13	48	90	-	3.2	2.4	1.4	-
13/9/76	14	32	66	22	3.3	2.6	1.5	1.5
29/9/76	20	50	80	28	3.3	2.4	1.3	1.4

7. α Boo, K2 III, m_V=-0.06, B-V=1.23, R-I=0.65

8/6/76	55	63	180	-	1.2	0.9	0.5	-
11/6/76[D]	30	53	180	65	1.2	0.9	0.5	0.5

---

* Observed by D.F.Gray; D indicates that instrumental drift was present.

1. This is the relative error in the measured ratio ρ, calculated according to the relation $\varepsilon_\rho = 1.2N^{-\frac{1}{2}}$.

2. Window at λ3954.3A was measured for this star. Hence the entries in the 5th and 9th columns refer to this window instead of the one at λ3950.8A.

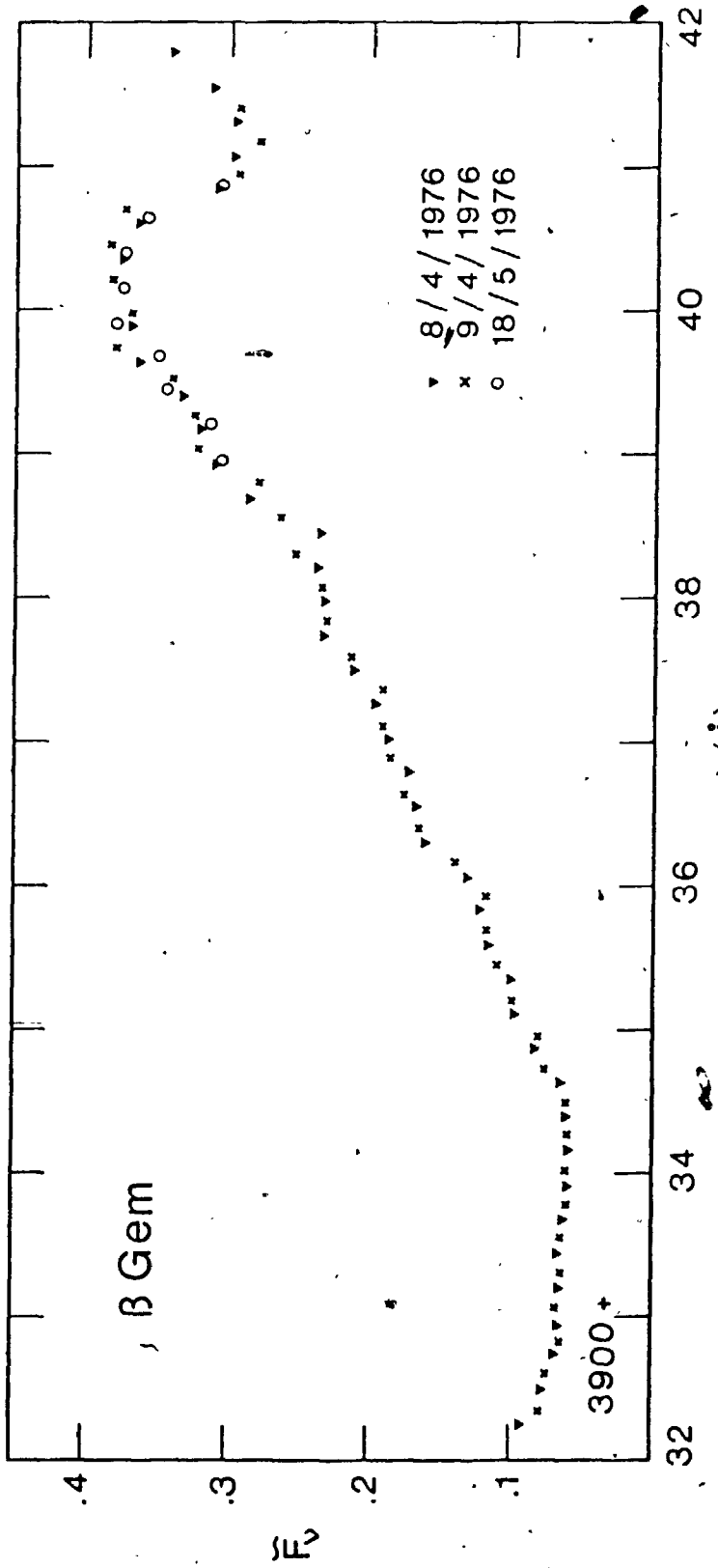

Fig.2.2a. Ca II K line observations of β Gem

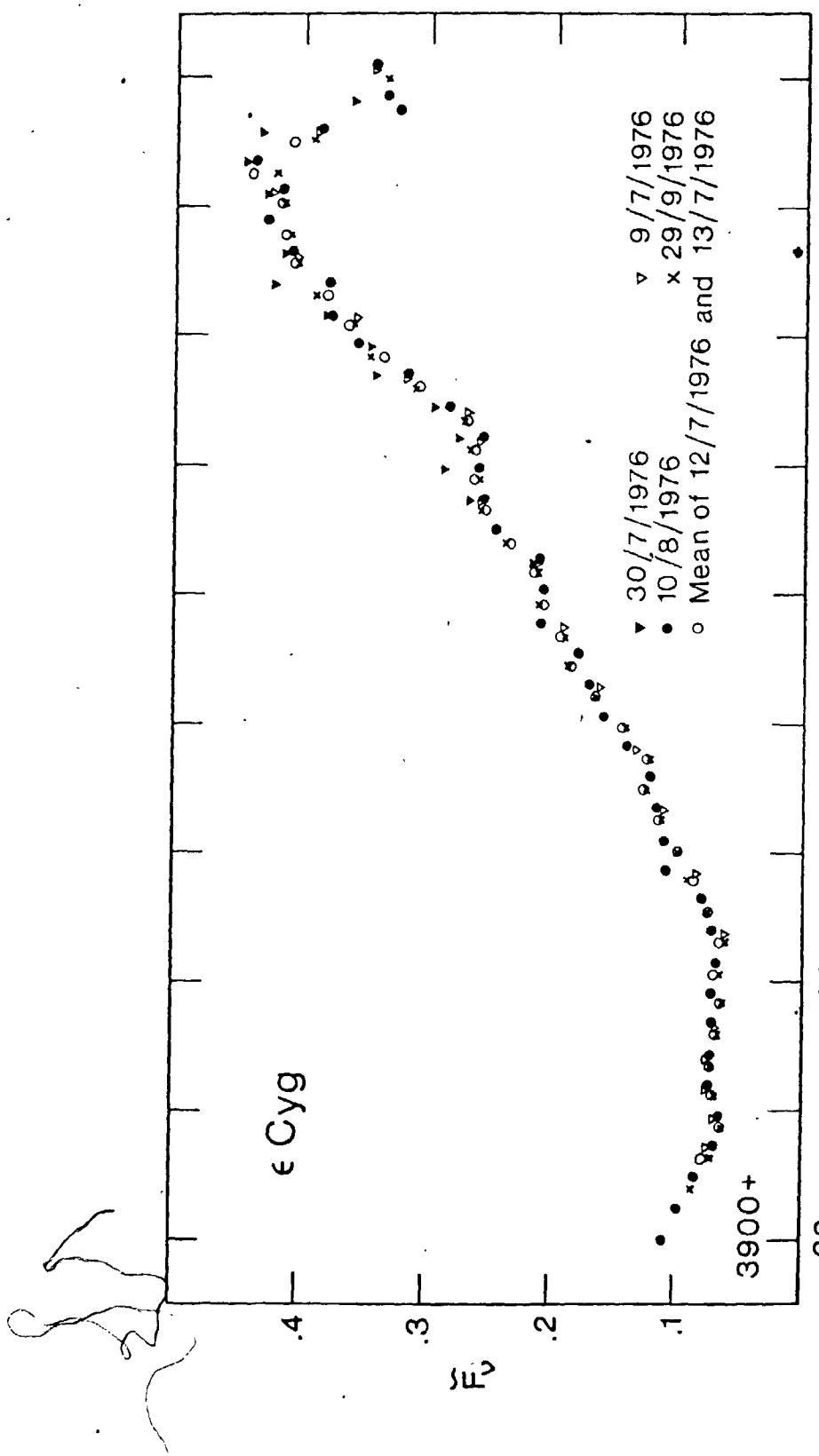

Fig.2.2b. Ca II K line observations of ε Cyg

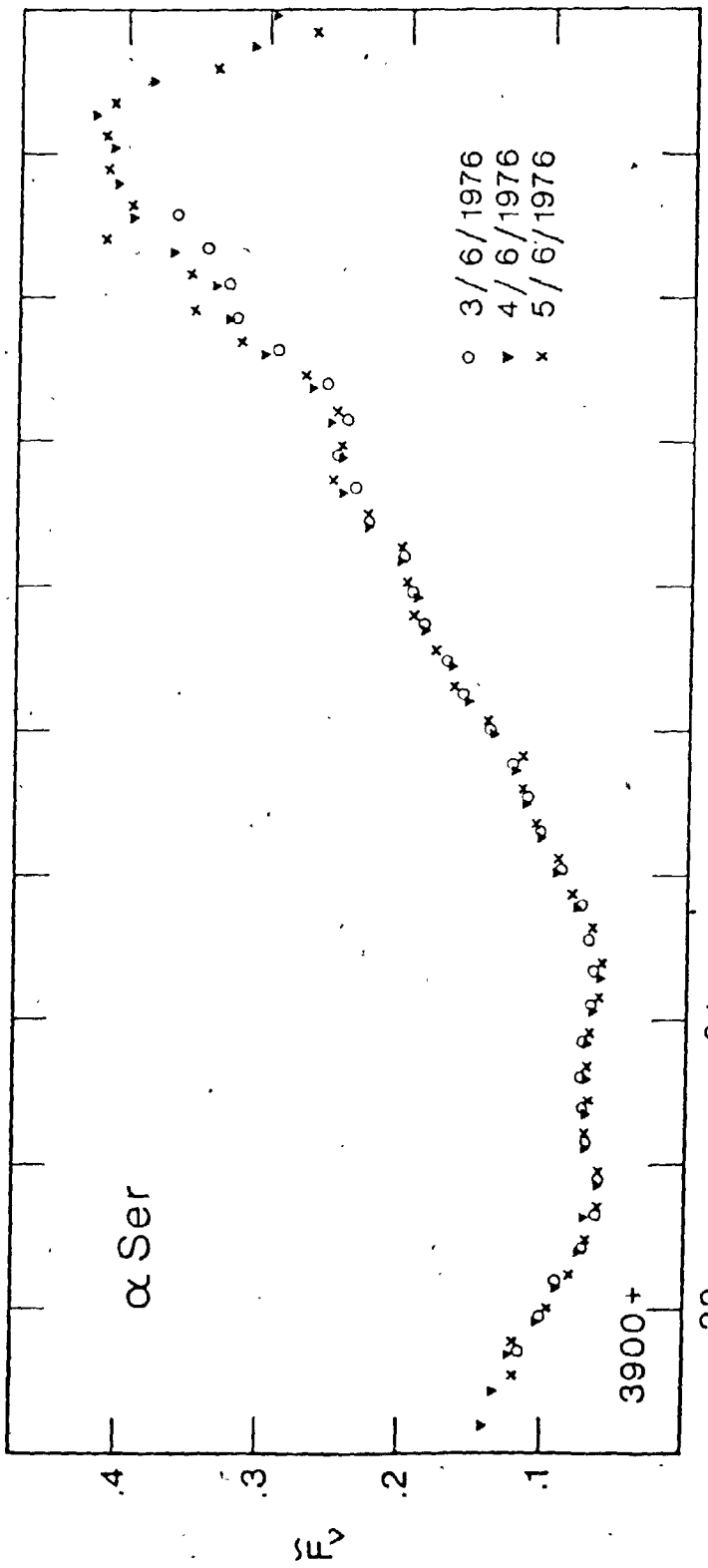

Fig.2.2c. Ca II K line observations of α Ser

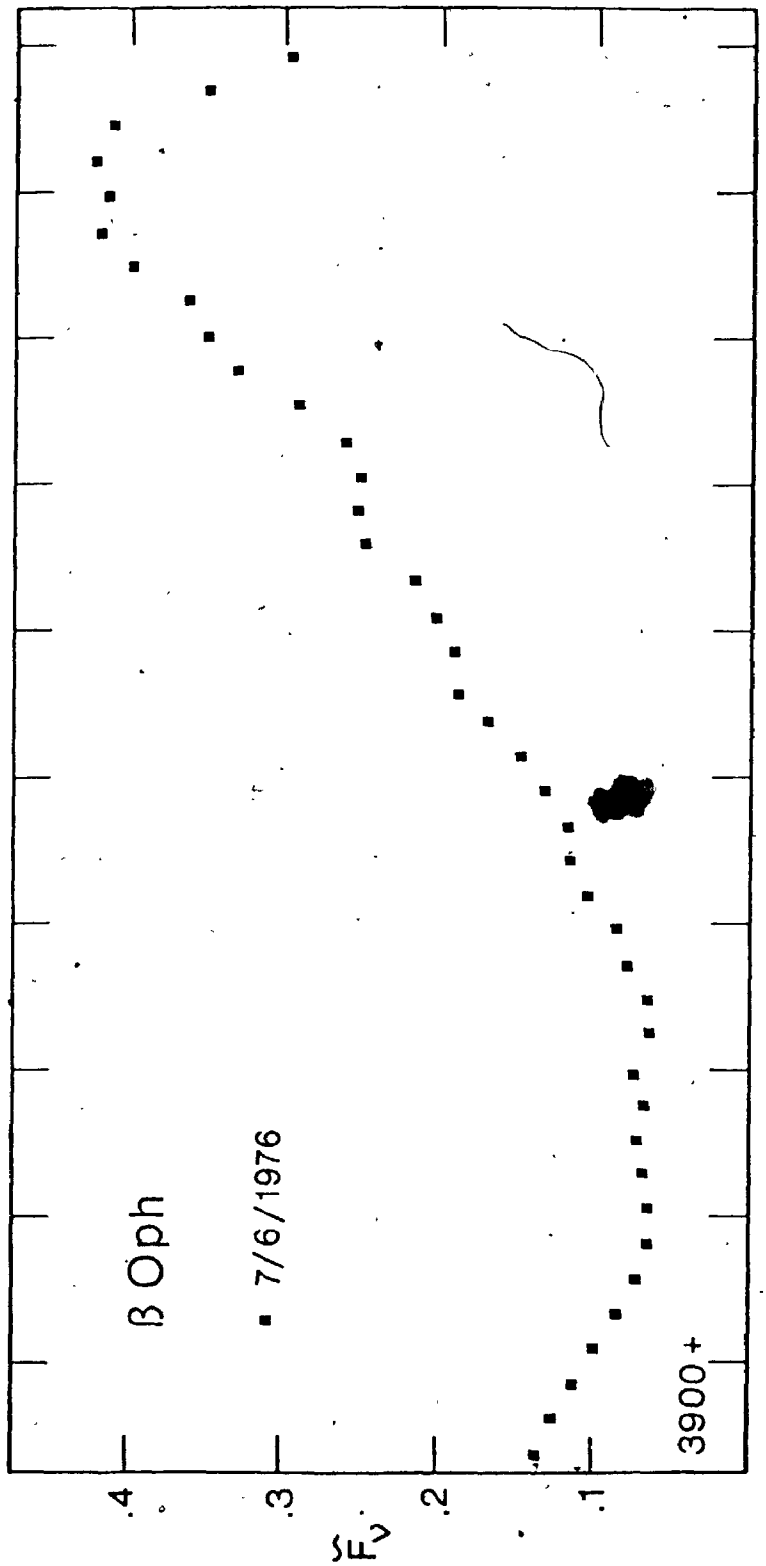

Fig.2.2d. Ca II K line observations of β Oph

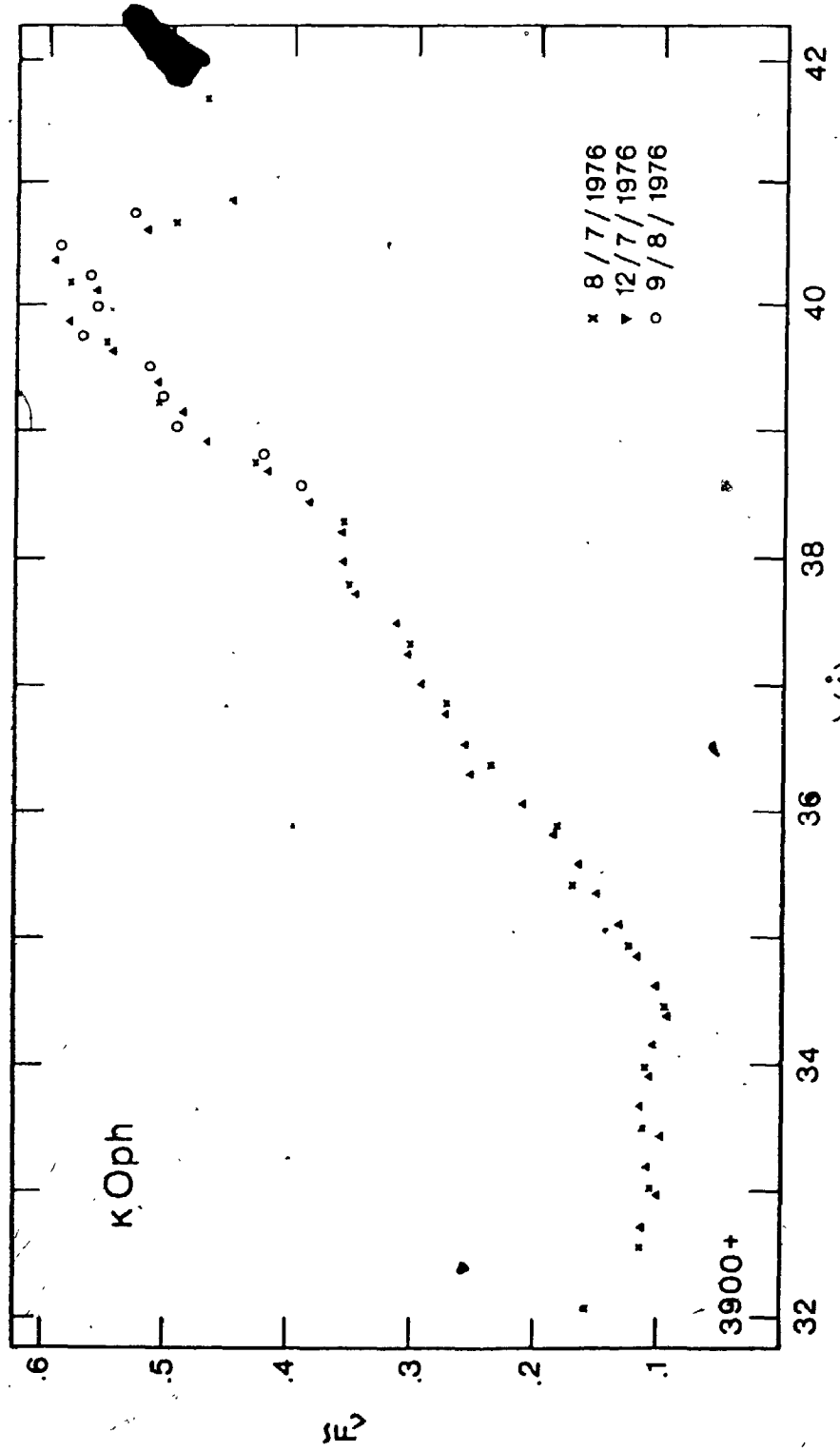

Fig.2.2e. Ca II K line observations of κ Oph

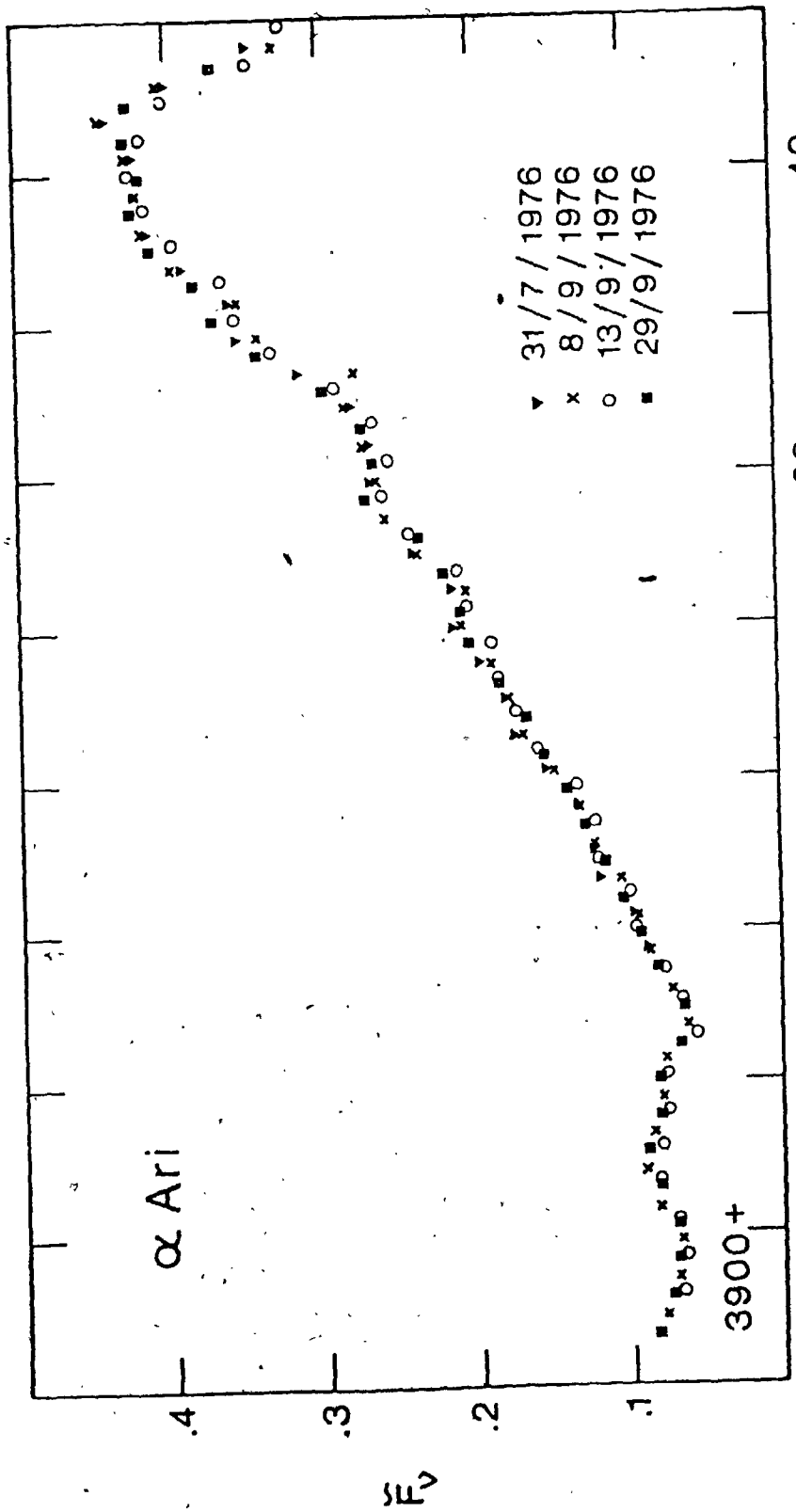

Fig.2.2f. Ca II K line observations of α Ari

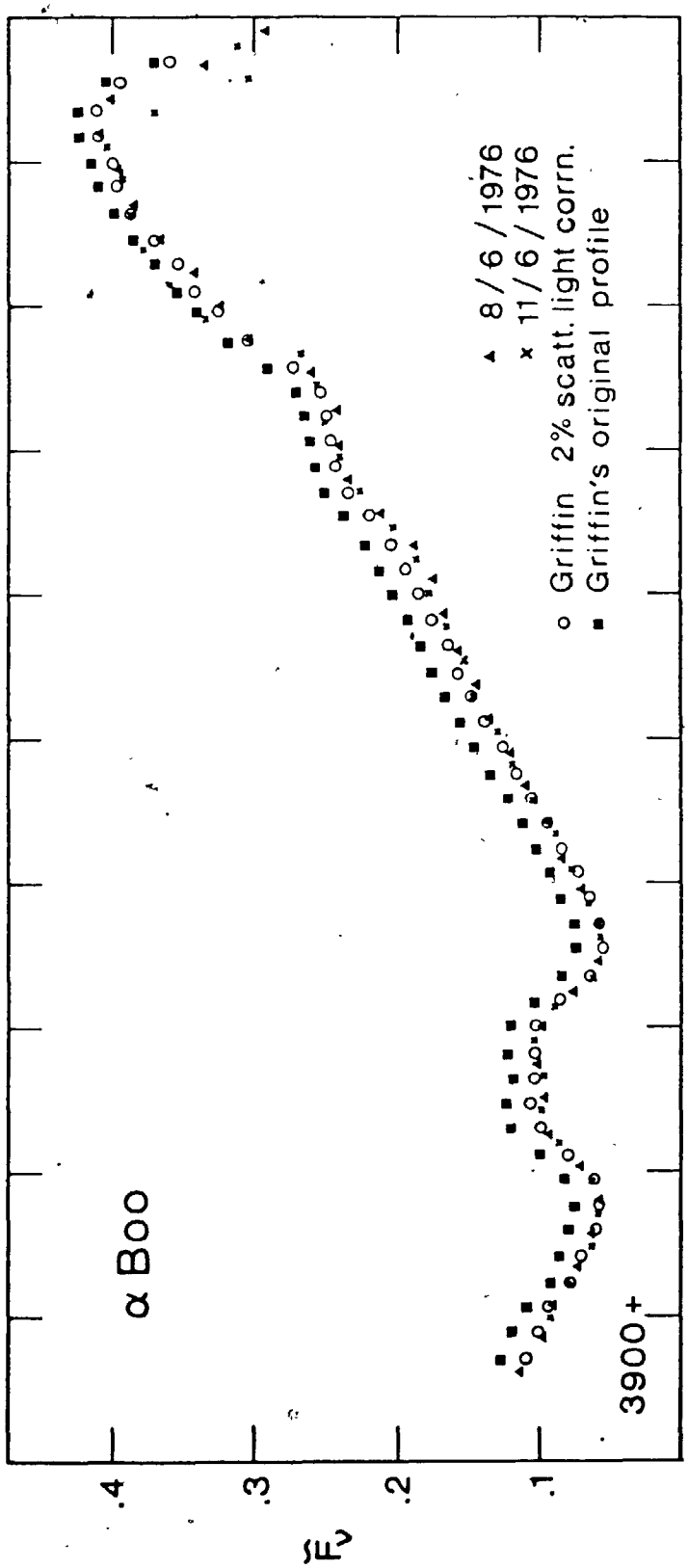

Fig.2.2g. Ca II K line observations of Arcturus. Squares represent Griffin's atlas profile convolved with our instrumental profiles and normalised to the window at λ3950.8Å. Circles represent the same profile after correcting for 2% scattered light. Triangles and crosses represent our own low resolution observations.

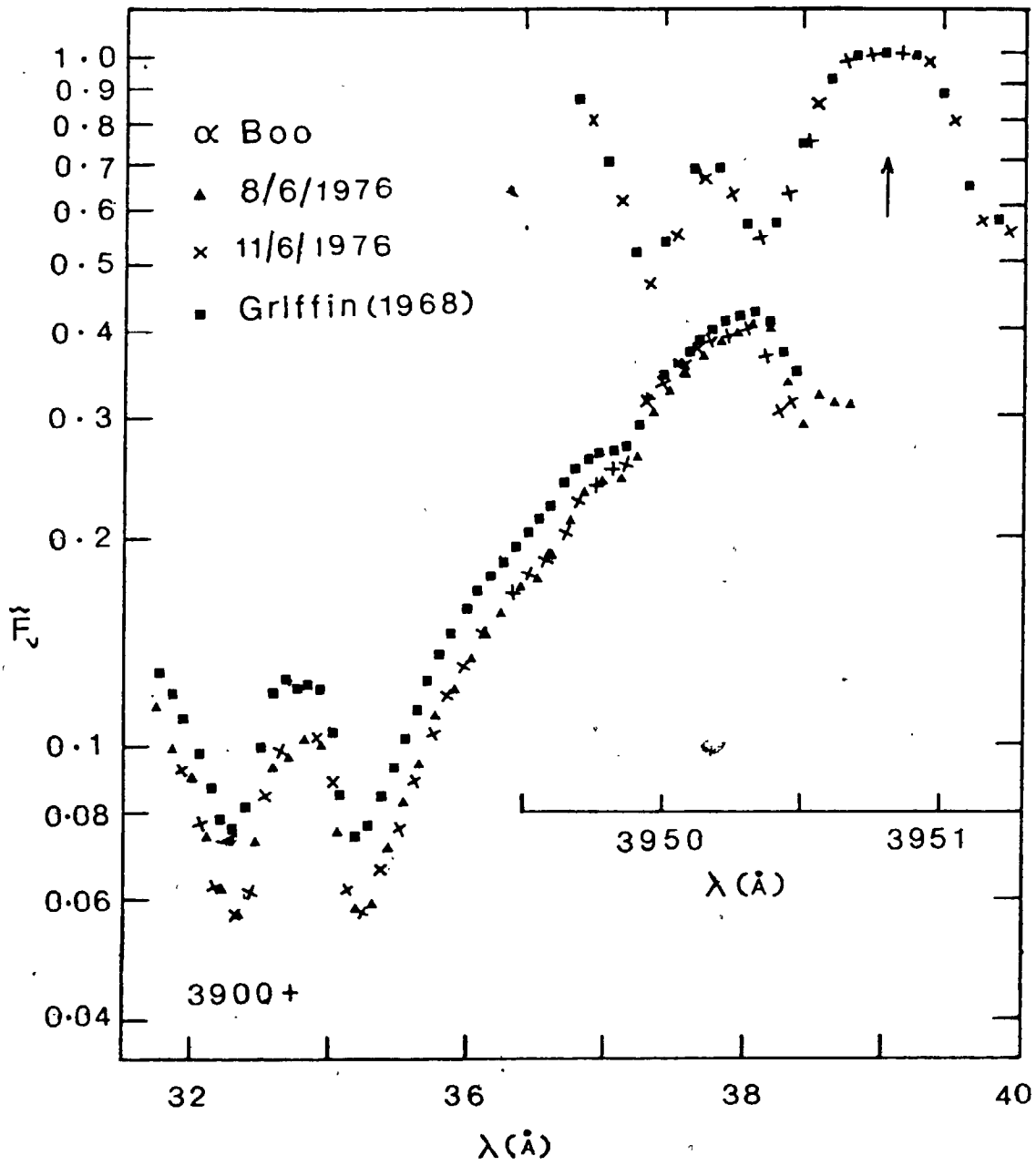

Fig.2.2h. Replot of Fig.2.2g on a logarithmic grid paper to clearly show correspondence between Griffin's low resolution uncorrected (for scattered light) profile and our observations at high residual intensities, but discordance at low residual intensities. Arrow locates the centre of the window at λ3950.8Å.

2.6. COMPARISON OF OUR ARCTURUS OBSERVATIONS WITH GRIFFIN'S ARCTURUS ATLAS PROFILE

Arcturus has been included in this program as a check on our observational and computational procedures. So, it is interesting to compare our observations with Griffin's (1968) Arcturus atlas profile. Griffin's profile was measured with a resolution of 27mÅ, which is several times higher than our 0.5Å and 0.2Å resolutions. So, in order to effect the comparison, it is necessary to convolve Griffin's profile with our our instrumental profiles shown in Fig.2.1. Accordingly, we have digitized the relevant portions of the atlas and convolved them with these instrumental profiles. The normalized low resolution profile thus obtained is shown by squares in Fig.2.2g. It may be mentioned here that the broad wings of the instrumental profiles (cf.Fig.2.1) have negligible effect ($<0.3\%$) on the convolved profile. This has been verified by convolutions made with and without the inclusion of the wings fainter than 10^{-3} times the peak intensity in the instrumental profiles.

In Fig.2.2g Griffin's profile (squares) lies systematically above ours. The fractional difference between the two profiles is inversely proportional to the local intensity, ranging from $\sim$4% (of the local intensity in Griffin's profile) at λ3940.0Å to $\sim$26% at λ3934.5Å. This is better illustrated by the logarithmic plot in Fig.2.2h, wherein the window profiles, which show little disagreement, are also plotted. Because there is a good agreement in the window, it is

possible that the disagreement in the wing might arise from errors in the slit width calibration and the window height. In the last section we have seen that the error from these sources is about 2%. Even if it is greater than this (say 4%), its effect is to scale the whole wing up or down by the corresponding amount. In other words, such a systematic effect is not dependent upon the intensity, and is uniformly the same at all points in the wing. So, it can not explain the observed systematic difference, even though it may partly contribute to it. On the other hand, consider what happens if Griffin's observations were affected by "scattered light" of amount s. If $F(\lambda)$ is the measured flux, $F_0(\lambda)$ is the true flux (i.e., without scattered light), $\tilde{F}(\lambda)$ is the normalized flux, and λ_{st} is the wavelength (λ3950.8) of the window, we have

$$\tilde{F}(\lambda) = \frac{F(\lambda)}{F(\lambda_{st})} = \frac{F_0(\lambda)+s}{F_0(\lambda_{st})+s} = \frac{F_0(\lambda)}{F_0(\lambda_{st})} \cdot \frac{1+s/F_0(\lambda)}{1+s/F_0(\lambda_{st})} .$$

If $s/F_0(\lambda) << 1$ as in the window, $\tilde{F}(\lambda)=F_0(\lambda)/F_0(\lambda_{st})$. I.e., if s is small, the normalized window is not affected. On the other hand, if $s/F_0(\lambda)$ is a large fraction of unity, as in the core and near wings of the K line, $\tilde{F}(\lambda) > F_0(\lambda)/F_0(\lambda_{st})$. So, the effect of the scattered light is to introduce inverse intensity dependent relative errors in the normalised flux profiles. This is exactly the nature of the discrepancy found between Griffin's and our observations. Now, we can ask if it is possible to remove this discrepancy by correcting Griffin's

data for an appropriate value of s. By trial and error we have found that this can be achieved by assuming s=2% (of the continuum normalised to 1), and very good agreement between the two sets of data can be obtained. This is illustrated by circles in Fig.2.2g, which correspond to the squares corrected for the 2% scattered light. In view of this near perfect agreement, we conclude that the apparent discrepancy between the two sets of data is caused by the presence of ~2% scattered light in Griffin's data.

Having concluded that Griffin's data are affected by ~2% scattered light, let us investigate the source of this stray light. As shown by the dashed line in Fig.2.1, Griffin's third-order instrumental profile has broad wings, even though these are considerably fainter than the wings of our instrumental profiles beyond $\Delta\lambda=2$Å. Griffin's instrumental profile also contains several ghosts, whose intensities rise up to 4 times the wing intensities of our 0.5Å instrumental profile. As verified already, the broad wings have negligible effect on the convolved profile. However, this can not be true of the ghosts which rise several times above the wing. They introduce stray light into the spectrum in proportion to their total area compared to the area of the main peak. Griffin estimates that ghosts contribute ~0.5% stray light in the second order. In the third order the contribution may be greater, as their intensities are 3.3 times higher. So, it seems that good part of the ~2% scattered light is contributed by the ghosts.

The observations contained in this chapter form the main body of the data, which when interpreted by proper theory yield the upper photospheric $T(\bar{\tau})$ models. Obviously, the accuracy of these models rests on the accuracy of these observations. So, it is heartening to see that our observations show good internal consistency and repeatability, which assure their quality.

CHAPTER III

THEORY

In this chapter we briefly describe the LTE-PCS formulation of Ayres (1975) for the K wing formation and discuss some of the difficulties encountered in the application of this theory to K giants.

3.1. RELEVANCE OF Ca II K WING FOR THE DERIVATION OF THE UPPER PHOTOSPHERIC $T(\bar{\tau})$ DISTRIBUTION

There are three ways of deriving a stellar $T(\bar{\tau})$ distribution. These are: a) Measurement of the continuum flux over a wide range of wavelengths; b) Measurement of limb darkening; c) Synthesis of a strong line like Ca II K, which is formed over a wide range of continuum optical depths.

Continuum energy measurements require observing and calibrating a large number of spectral band passes. This procedure is prone to uncertainty, especially in the extreme ultraviolet and infrared regions, where ground based observations are not possible; and these are just the data needed to derive an upper photospheric $T(\bar{\tau})$ model. Interpretation of the continuum measurements by a theoretical model requires accurate atomic data for many continuous absorbers and proper handling of any NLTE effects that may affect these absorption processes.

Reliable limb darkening data can only be obtained for the Sun, which only provides the $T(\bar{\tau})$ distribution of the deeper photospheric layers. More specifically, limb darkening data

are capable of yielding temperatures only in the optical depth range $-1.3 < \log \bar{\tau} < 0.7$ (cf. Böhm, 1961; Mihalas, 1970). So, this method is unsuitable to derive the temperature model of the upper photosphere ($-4.0 < \log \bar{\tau} < -1.0$), in which we are primarily interested in this thesis.

The K line synthesis method is preferable to the above two methods in some respects. As shown in Fig.3.1, taken from Shine's (1973) thesis, the K wing is formed in the upper photosphere, and this makes the K wing more suitable than the limb darkening data to derive an upper photospheric $T(\bar{\tau})$ model. Since only a small wavelength band (10-15Å) has to be measured and calibrated, potentially better accuracy over that of the continuum method can be expected. However, the K line synthesis method is not without difficulties. For example, damping constants and the stellar Ca abundance, A_{Ca}, must be well known. To compare observations with the theory, absolute flux calibrations of the observed profile in ergs cm^{-2} sec^{-1} hz^{-1} must be available. This is a nontrivial problem because it requires accurate knowledge of the stellar radius and distance. For Procyon and Arcturus, whose distances and radii are well known because of their proximity, Ayres, Linsky & Shine (1974), and Ayres & Linsky (1975) have obtained such calibrations with an estimated error of $\sim$30%. This error is a cumulative effect of the errors in the apparent flux measured at the Earth, errors in line blocking corrections applied to this measurement, and errors in radius and distance. For more distant stars this calibration becomes

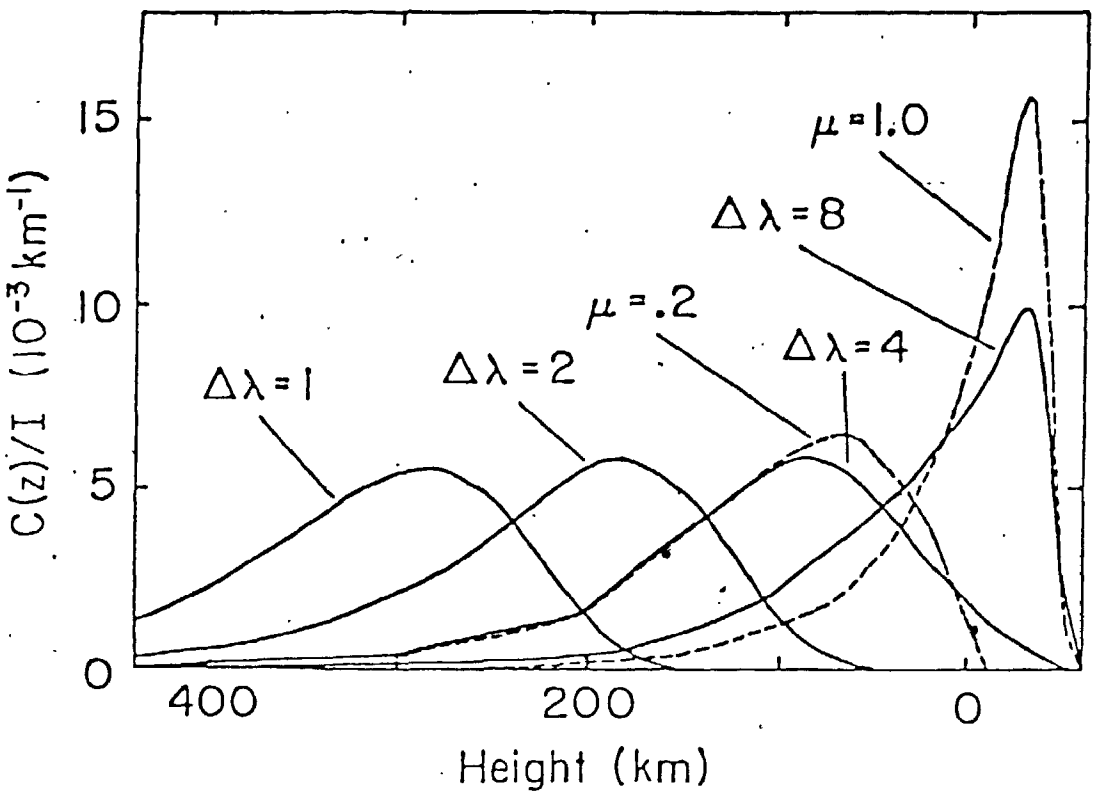

Fig.3.1. Contribution functions vs. height for the Ca II K line at disk centre of the Sun for several displacements from line centre as indicated (solid lines) and for the continuum at λ5000Å at μ=1 and at μ=0.2 (broken lines). This figure has been taken from Shine's(1973) thesis.

increasingly uncertain as the errors in distances and radii rapidly increase. Therefore, the applicability of this calibration method is limited to a few nearby stars, whose distances and radii are well determined.

We can avoid dependence upon the radius and distance by turning to model atmospheres for calibration. In this case, one predicts the flux in the window centred on λ3951Å from an accurate line blanketed RE model and calibrates the rest of the profile with respect to this window. This method assumes that the $T(\bar{\tau})$ distribution of the deeper optical continnum forming layers ($-1.0 < 10g\ \bar{\tau} < 0.0$) is well determined, hence the window flux originating in these layers is correctly estimated. This is a reasonable assumption because the $T(\bar{\tau})$ distribution of the deeper layers can be reliably fixed by a comparison of the theoretical and observed Paschen continuum slopes. Good accuracy in this procedure can be expected because the Paschen continuum slope can be measured fairly accurately in late type stars. Once this $T(\bar{\tau})$ distribution is fixed, the K line calibration appears to be straightforward. But, there are problems in practice. For example, the observed utraviolet continuum in late type stars is systematically depressed with respect to the theoretical continuum (cf.Fig.3.6), necessitating inclusion of an "Opacity Enhancement Factor", or E_c for short, in computations in order to force agreement between the theory and observation. This problem will be discussed in more detail in §3.3, where we will also consider the dependence of E_c upon the adopted

$T(\bar{\tau})$ distribution for the deeper layers, gravity, and A_{Ca}. It turns out that the dependence on A_{Ca} is very important, necessitating an accurate determination of A_{Ca}. So, it appears that the accuracy of the calibration based on model atmospheres depends mainly upon the accuracy of the $T(\bar{\tau})$ distribution for the deeper layers and of A_{Ca}. In this thesis we pay special attention to the determination of these quantities. In Chap.IV we determine accurate $T(\bar{\tau})$ distributions for the deeper layers by fitting Paschen continua and values of A_{Ca} by fitting far wings of Ca II λ8498 line profiles observed by Anderson (1974) in our stars. We expect these determinations ensure the accuracy of our calibration.

Two quantities that affect the K line upper photospheric $T(\bar{\tau})$ models through their effect on the line absorption coefficient are A_{Ca} and damping constants. Of these, the A_{Ca} can be reliably estimated from the λ8498 line wings, while the radiation damping constant, Γ_R, is well determined and the Stark broadening is unimportant for our stars. On the other hand, the van der Waals damping constant, Γ_6, is not well known; the classical Unsöld (1955) formula underestimates this quantity considerably (Holweger,1972). Thus it is necessary to derive an empirical "van der Waals Enhancement Factor", E_6, from well calibrated solar K line profiles. This will be done in §3.2. This procedure rests on the assumption that the solar $T(\bar{\tau})$ model, Ca abundance, and absolute intensity calibration are well known, so that E_6 can be determined by forcing agreement between observations and theory.

As this E_6 will be used in the K line synthesis of all other program stars, the upper photospheric $T(\bar{\tau})$ models thus derived are relative to the particular $T(\bar{\tau})$ model, A_{Ca}, and absolute calibration used for the Sun.

In any case, the K line synthesis seems to be the most convenient way of deriving the upper photospheric and lower chromospheric $T(\bar{\tau})$ models for the late type stars at present. Far infrared and far ultraviolet continuum measurements, which contain the same information are not available for these stars, while the limb darkening is not measureable. So, the immediate accessibility of the K line to the ground based observer makes it ideal for the derivation of the upper photospheric and lower chromospheric temperature models.

3.2. FORMATION OF Ca II K WING— AYRES' LTE-PCS FORMULATION

The Ca II K line is formed over a large range of continuum optical depths, which makes it a good probe for the physical conditions in the upper photospheres and lower chromospheres of the late type stars. In particular, in the Sun K1 is formed at the temperature minimum ($\log \bar{\tau} \simeq -3.5$), K2 in the lower chromosphere ($\log \bar{\tau} \simeq -4.5$) and K3 in the intermediate chromosphere ($\log \bar{\tau} \simeq -5.6$). Here, following the usual notation, K1, K2 and K3 respectively refer to the flux minimum in the inner wing, the emission peak, and the central minimum in a typically centrally reversed K line profile. In this thesis we are interested in the K wing ($\Delta\lambda > \Delta\lambda_{K1}$) only, which is formed between the temperature minimum and the optical continuum forming layers ($\log \bar{\tau} \simeq 0.0$).

Ayres has formulated a LTE-PCS theory of the K wing formation which we briefly describe in the following.

a) ASSUMPTIONS

In his theory, Ayres makes several assumptions which are outlined below:

a-1. Assume a 5 level Ca II ion as shown in Fig.3.2. The K line is coupled to H through the ground state 4^2S, while it is coupled to the infrared (IR) λ8498 and λ8542 lines through the upper level 4^2P. We also assume that the continuum transitions (both radiative and collisional) from these 5 levels are in detailed balance. These continuua are located shortward of λλ1044Å, 1219Å and 1420Å for ionization from 4^2S, 3^2D and 4^2P respectively. In G and K type stars these continua are thermalised well above the temperature minimum (Linsky,1968; Ayres,1975), hence detailed balance is a good approximation at the K wing frequencies.

a-2. Neglect stimulated emissions. This is a good approximation as stimulated emissions play a negligible role in the stars we are considering.

a-3. K wing is formed in LTE. This is a reasonable approximation because the line centre optical depths at K1 are comparable or greater than the thermalization lengths in the solar type stars and K giants (Linsky,1968, Linsky & Ayres, 1973). If we assume complete noncoherence in the scattering process (NCS hereafter), the line source function S_ν is given by

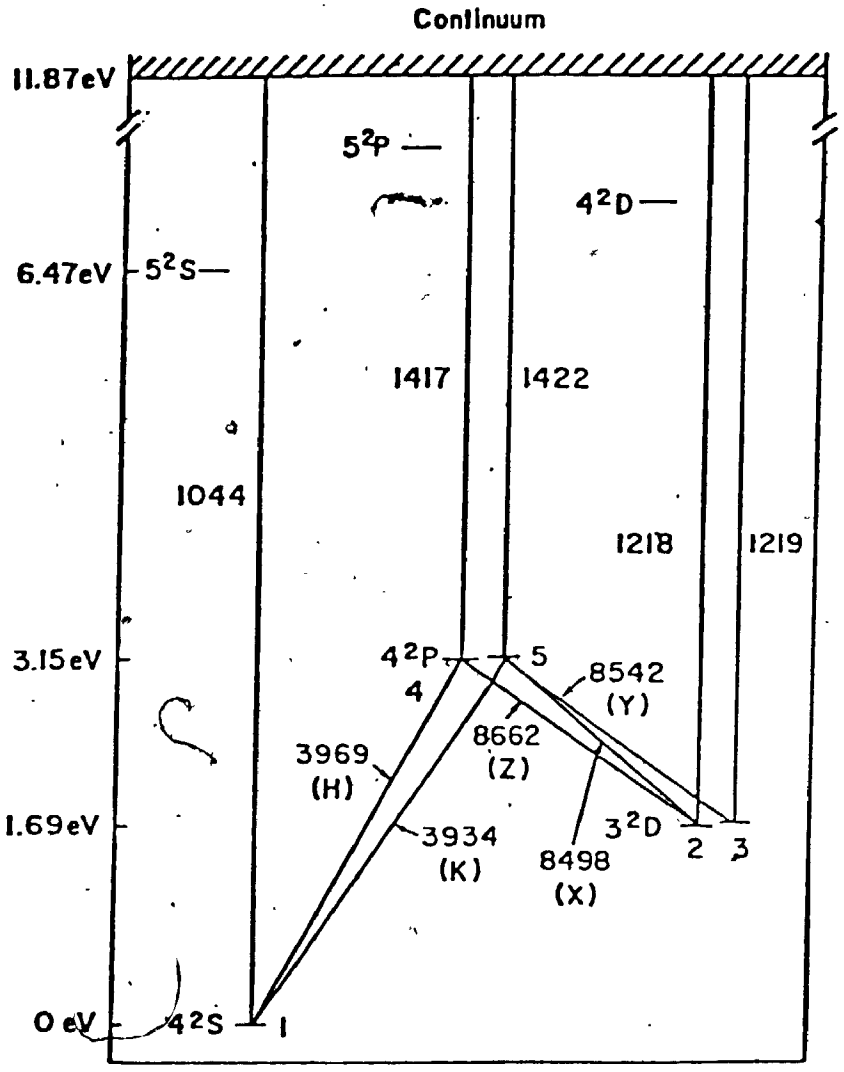

Fig.3.2. Energy level diagram of a 5 level Ca II atom.

$$S_\nu = B_\nu = (2h\nu^3/c^2)e^{-h\nu/kT} \qquad (3.1)$$

a-4. Partial coherency effects in the line scattering process (hereafter PCS for brevity) are not negligible. This implies that the emission profile is different from the absorption profile, so that a LTE-PCS source function is given by

$$S_\nu = \beta_\nu B_\nu = (2h\nu^3/c^2)\psi_\nu/\phi_\nu \, e^{-h\nu/kT} \qquad (3.2)$$

where ψ_ν and ϕ_ν are the emission and absorption profiles, and $\beta_\nu = \psi_\nu/\phi_\nu$. The essence of the problem is then to determine β_ν, because if we know β_ν we know the source function.

Recent work by Milky & Mihalas (1974) and Shine, Milkey & Mihalas (1975a,b) has highlighted the importance of PCS in the formation of Mg II h & k and Ca II H & K resonance lines in the late type stars. More specifically, inclusion of PCS correctly reproduces the observed centre-to-limb behavior of K1(k1), K2(k2) and H1(h1), H2(h2) features of the Ca II (Mg II) lines both in wavelength and intensity in the case of the Sun.

In a resonance line transition, the lower level is extremely sharp, while the upper level is broadened by radiation and collision damping. In an isolated system where collisions are absent the emission and absorption profiles are identical in the rest frame of the atom, as complete coherence exists between the absorbed and emitted photons. In this case, the emission profile is a Lorentzian with the radiation damping width Γ_R. When the collisions are important, the emission profile is still a Lorentzian

with a total width of $\Gamma_R+\Gamma_c$, where Γ_c is the collision damping width. However, this situation is markedly different from the previous one, because the emission is no longer completely coherent in the atom's frame. Collisions introduce partial redistribution by shuffling the electrons in the upper state before they radiatively decay. In fact, if collisions dominate NCS will be realized. When transformed to the laboratory frame, it can be shown that NCS prevails in the Doppler core of the line, while PCS prevails in the inner wings (Jefferies & White, 1960). In this case, in the inner wing sufficiently away from the Doppler core, i.e., for $\Delta\lambda>10\Delta\lambda_D$, the angle averaged redistribution function, $R(\nu,\nu')$, in the observer's frame can be approximated by a linear combination of a purely coherent part and a purely noncoherent part, given by

$$R(\nu,\nu') = (1-\alpha)\,\delta(\nu-\nu') + \alpha\,\phi_\nu\phi_{\nu'}, \qquad (3.3)$$

where $R(\nu,\nu')$ represents the probability that a photon of frequency ν is emitted following the absorption of a photon of frequency ν', ϕ_ν and $\phi_{\nu'}$ are the normalised absorption profiles, $\delta(\nu-\nu')$ is the normalised Dirac delta function, and α is the NCS probability (or the complete redistribution probability), given by

$$\alpha = \Gamma_c/(\Gamma_c + \Gamma_R) = (\Gamma_6 + \Gamma_4)/(\Gamma_6 + \Gamma_4 + \Gamma_R) \qquad (3.4)$$

where Γ_6 and Γ_4 are the usual van der Waals and Stark broadening parameters. In case of Ca II K, ν always refers to the K line, while ν' can refer either to K or to the IR lines.

The first term in Eq.3.3 refers to a purely coherent part, while the second term refers to a purely noncoherent part.

In the upper photosphere where the inner wing ($\Delta\lambda < 5\text{Å}$) of Ca II K is formed, the radiation damping dominates over the collisional damping. Fig.3.3 illustrates this situation in the case of the Sun and a log g=2.5, T_e=4650K model atmosphere, typical of the K giants considered in this thesis. Because of this, the first term in Eq.3.3 far outweighs the second term in the inner wings and the source function becomes strongly frequency dependent. This can be understood as follows. Since $\Gamma_R >> \Gamma_C$, the emission is mostly coherent in the atom's frame. This strong coherency is maintained when we transform to the laboratory frame also, because the absorbing atoms are nearly at rest as there are very few atoms with velocities large enough to have their central absorption peak shifted to the inner wing frequencies. In the far wings ($\Delta\lambda > 5\text{Å}$), however, collisions become increasingly important and NCS becomes a good approximation.

a-5. All the broadening is provided by levels 4 and 5. This implies that the damping widths for the resonance and subordinate lines which share the common upper level are identical. This is a reasonable approximation as the metastable levels 2 and 3 are relatively sharp, while level 1 is the ground level.

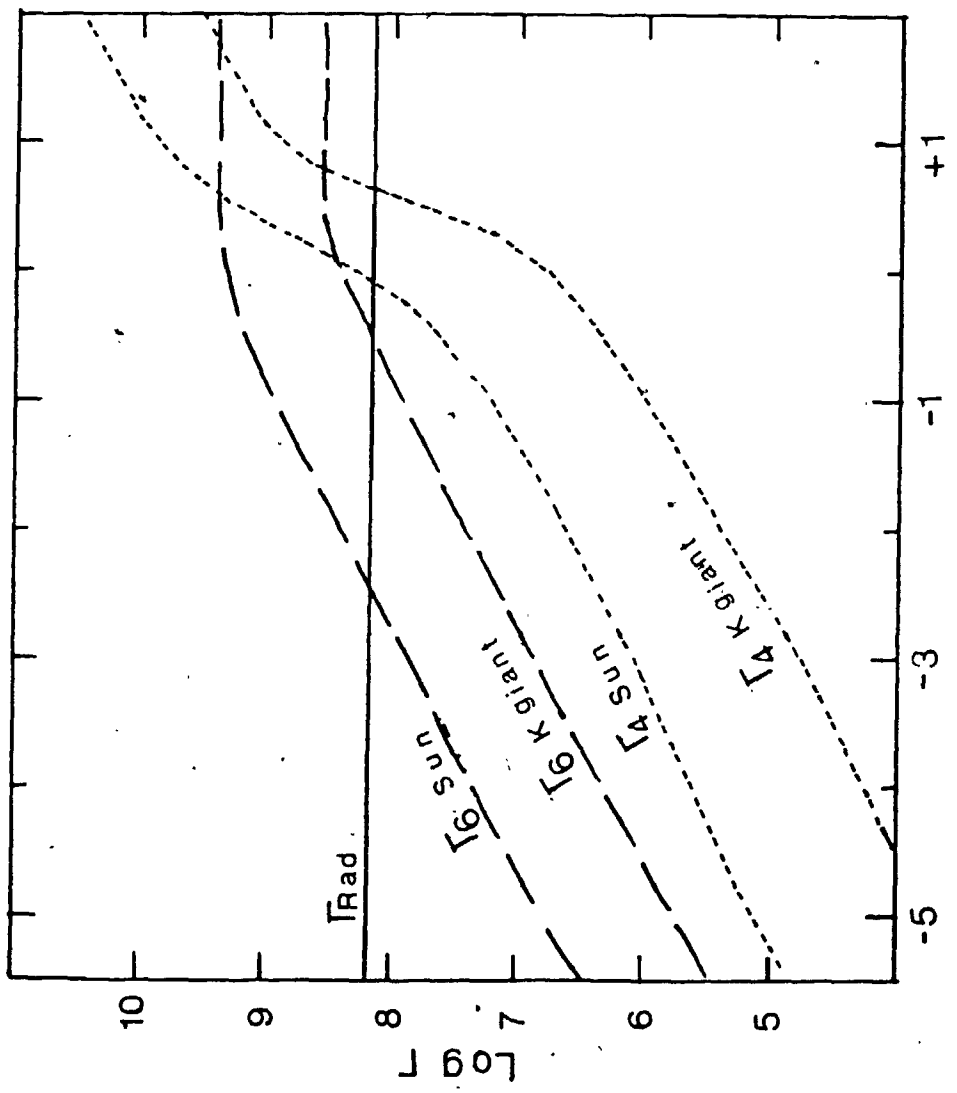

Fig.3.3. Plot of damping widths in the Sun and in a K giant with T_e=4650K, log g=2.5

b) DERIVATION OF β_ν

An expression for β_ν can now be derived by considering its effect on level populations. In LTE the total population of a level is given by the combined Saha-Boltzmann equation. Let n5* be the total LTE population of level 5. Now we can subdivide this broadened level into discrete frequency sub-states whose populations are given by

$$n5(\nu)\, d\nu = n5^*\, \phi_\nu\, d\nu \qquad \text{in NCS} \qquad (3.5)$$

$$n5(\nu)\, d\nu = n5^*\, \beta_\nu \phi_\nu\, d\nu \qquad \text{in PCS} \qquad (3.6)$$

where $n5(\nu)\, d\nu$ is the population of a frequency substate band $d\nu$. Thus β_ν can be interpreted as a departure coefficient from NCS. Notice that Eqs.3.5 & 3.6 are subject to the normalisation conditions

$$\int_{-\infty}^{+\infty} n(\nu)\, d\nu = n5^* \int_{-\infty}^{+\infty} \phi_\nu\, d\nu = n5^* \qquad (3.7)$$

$$\int_{-\infty}^{+\infty} n(\nu)\, d\nu = n5^* \int_{-\infty}^{+\infty} \beta_\nu \phi_\nu\, d\nu = n5^*. \qquad (3.8)$$

So, it is clear that to derive β_ν we must write down substate by substate statistical equilibrium equations involving levels 1-5. But before doing so, we should consider the fact that only a fraction of the total number of n5* will branch out into the 5-1 (i.e., K line) transition. This is accomplished by partitioning level 5 into sublevels 5_ℓ (ℓ=1,3) according to the fraction of the excited atoms which spontaneously decay by emitting photons through a 5-ℓ transition. Thus we replace Eq.3.6 by

$$n5_1(\nu)d\nu = n5_1\beta_\nu\phi_\nu d\nu = n5^* \delta 5_1\beta_\nu\phi_\nu d\nu \qquad (3.9)$$

where the 5→1 branching ratio, $\delta 5_1$, is given by

$$\delta 5_1 = A5_1/\sum_{\ell=1,5} A5\ell$$

Here $A5\ell$ are the usual spontaneous emission coefficients. Ayres writes down the statistical equilibrium equation for $n5_1$ level population, and after some reduction obtains

$$\beta_\nu = \frac{B^{-1}}{(1+a+\varepsilon)} \{(1-\alpha)J_\nu + B(\alpha+\varepsilon) + \sum_{\ell=2,3} a5\ell \left[(1-\alpha)J_\nu^\ell/B^\ell + \alpha\right]B\} \qquad \ldots\ldots (3.10)$$

where J_ν and J_ν^ℓ represent the mean intensities in the wings of the K and IR(ℓ=2,3) lines, and the frequency variation of the corresponding Planck functions B_ν and B_ν^ℓ over the width of the absorption profile is neglected. In addition, a and ε are defined by

$$a = \sum_{\ell=2,3} A5\ell/A51 \quad , \text{ and } \quad \varepsilon = \sum_{\ell=1,4} C5\ell/A51 \ .$$

where $C5\ell$ are the collisional excitation rates. The monochromatic line source function S_ν is then obtained by simply substituting Eq.3.10 into Eq.3.2, which reduces to

$$S_\nu = (1-\tilde{\alpha})J_\nu + \tilde{\alpha}\tilde{B}_\nu \qquad (3.11)$$

where the modified incoherence fraction, $\tilde{\alpha}$, is given by

$$\tilde{\alpha} = (a+\alpha+\varepsilon)/(1+a+\varepsilon) \qquad (3.12)$$

and the monochromatic source term $\tilde{B}_\nu$ is given by

$$\tilde{B}_\nu = B\left[\frac{\alpha+\varepsilon+\sum_{\ell=2,3} a5\ell\{\alpha+(1-\alpha)J_\nu^\ell/B^\ell\}}{\alpha+\varepsilon+a}\right] \qquad (3.13)$$

which reduces to B in NCS (α=1). Eq.3.11 is in the form of a simple partial coherent scattering source function, although $\tilde{\alpha}\tilde{B}_\nu$ can substantially depart from $\tilde{\alpha}B$ at those depths where α differs from unity and J_ν^ℓ differs substantially from B^ℓ. In the upper photosphere $\alpha<<1$ and $J_\nu^\ell > B^\ell$. Hence the effect of the term coupling IR radiation fields is to pump $\tilde{B}_\nu$ above B in the upper atmosphere.

So far we have not considered the H line, which has overlapping wings with the K line ($\lambda_H-\lambda_K$=34.81Å). When we include this and the background continuous opacities, the total monochromatic source function at a given depth becomes

$$S_\nu^t = (1-\tilde{\alpha}_t)J_\nu + \tilde{\alpha}_t \tilde{B}_\nu^t \qquad (3.14)$$

where

$$\tilde{\alpha}_t = (\kappa_\nu^H \tilde{\alpha}^H + \kappa_\nu^K \tilde{\alpha}^K + \kappa_\nu^c \varepsilon_c)/\kappa_\nu^t$$

$$\tilde{B}_\nu^t = (\kappa_\nu^H \tilde{B}_\nu^H + \kappa_\nu^K \tilde{B}_\nu^K + \kappa_\nu^c B)/\kappa_\nu^t$$

$$\kappa_\nu^t = \kappa_\nu^H + \kappa_\nu^K + \kappa_\nu^c$$

$$\kappa_\nu^c = \sigma_\nu^c + k_\nu^c \qquad \text{and} \qquad \varepsilon_c = k_\nu^c/\kappa_\nu^c$$

Here $\kappa_\nu^H, \kappa_\nu^K, \kappa_\nu^c$ are the H & K and continuum opacities, while k_ν^c & σ_ν^c are the pure absorption and scattering components. At the K wing frequencies of our interest the corresponding H wing is formed deep in the photosphere where the density is so high that $\tilde{\alpha}^H \approx 1$ and $\tilde{B}_\nu^H \approx B_\nu$ is a good approximation.

Computationally we proceed as follows. Given a continuum model with a specified $T(\bar{\tau})$ distribution, gas and electron pressures and background continuous opacities, and also given

the Ca abundance and appropriate atomic parameters, we solve the Ca II ionization-excitation equilibrium in LTE and then calculate the infrared radiation fields J_ν^ℓ (ℓ=2,3) which enter the Eq.3.13 for the monochromatic source term $\tilde{B}_\nu$. For the range of νs we are interested in here, the corresponding IR radiation fields originate in the far wings of the IR lines where the source function is continuum controlled. In addition, Shine et al. (1975b) have shown that PCS effects are negligible in the IR lines. Therefore, we can assume that $S_\nu^\ell = B^\ell$, neglecting the frequency variation of the Planck function over the width of the absorption profile. Once we have made this assumption, it is straight forward to compute J_ν^ℓ using the familiar integral expression for the mean intensity. Having thus computed J_ν^ℓ/B^ℓ which enters Eq.3.13, we are in a position to obtain $\tilde{B}_\nu$, as α, ε, and $\tilde{\alpha}$ can be obtained from the input continuum model. We can then solve for $\tilde{\alpha}_t$ and B_ν^t, which enter Eq.3.14 for the total source function S_ν^t. In this equation J_ν is still unknown, which can be obtained by solving the second order form of the transfer equation by Feautrier method as described by Mihalas (1970). In particular, we use up to 95 depth steps and four angle quadrature points. Having obtained J_ν, we know S_ν^t completely, so that the emergent central intensity or flux can be calculated using the expressions:

$$I_\nu = \int_0^\infty S_\nu(\tau_\nu) e^{-\tau_\nu} d\tau_\nu \quad ; \text{ and}$$

$$F_\nu = 2\pi \int_0^\infty S_\nu^t(\tilde{\tau}_\nu) E2(\tau_\nu) d\tau_\nu$$

c) MORE COMPUTATIONAL DETAILS

We take all the atomic parameters, viz. spontaneous and collision rate coefficients and oscillator strengths from Shine & Linsky (1973). From the same source we also have a Γ_R=1.5E8 for K and the IR lines at λ8498A and λ8542A, while for H and the IR line at λ8662A we have a Γ_R=1.48E8. Γ_R is depth independent. Shine & Linsky also give the following expression for Γ_4, which is assumed to be the same for all the 5 lines.

$$\Gamma_4 = 3.0E\text{-}6\ N_e \qquad (3.15)$$

where N_e is the electron density. To calculate van der Waals broadening we adopt from Gray (1976)

$$\Gamma_6 = 10^{(19.6+0.4\log C_6(H)+\log P_g+0.7\log T)} \qquad (3.16)$$

where P_g is the gas pressure and T is the temperature. $C_6(H)$ is the van der Waals interaction constant for H, which is given by

$$C_6(H) = 0.3E\text{-}30\{(I-\chi-\chi_\lambda)^{-2} - (I-\chi)^{-2}\} \qquad (3.17)$$

where I is the ionization potential and χ is the excitation potential of the lower level of the atom of interest. χλ is the line photon energy in electron volts. Since Eq. 3.17 is only an approximation, we derive an empirical multiplicative correction factor to $C_6(H)$ by synthesizing the solar K wing profile. This correction factor is referred to as the "van der Waals Enhancement Factor", and hereafter will be denoted by E_6.

The rationale behind using the solar K line profile to derive E_6 has been explained in §3.1. The total damping width is given by

$$\Gamma = \Gamma_R + \Gamma_4 + \Gamma_6 \ . \qquad (3.18)$$

Knowing Γ and its components and the collisional and spontaneous rates we can obtain $\tilde{\alpha}^K$ at each depth in the atmosphere. To derive $\tilde{\alpha}^t$ and B_ν^t we have to know the line and continuum opacities too. The line absorption coefficient is given by

$$\kappa_\nu^{line} = \frac{\pi e^2}{mc} N(\text{Ca II}) f H(a,u)/\Delta\nu_D \qquad (3.19)$$

where e and m are electron charge and mass, f is the oscillator strength, N(Ca II) is the number of Ca II atoms per gram capable of absorbing the line, $\Delta\nu_D$ is the Doppler width in frequency units, H(a,u) is the usual Voigt function with $u=\Delta\nu/\Delta\nu_D$ and $a=\Gamma/4\pi\Delta\nu_D$. The continuum opacities k_ν^c and σ_ν^c are calculated by our model atmosphere program and read into the line synthesis program.

3.3. DETERMINATION OF E_6

As mentioned earlier, it is necessary to determine E_6 using the solar K line profile. The value of E_6 thus determined is dependent upon the $T(\bar{\tau})$ model, A_{Ca}, and the absolute intensity calibration used for the Sun. Here we determine E_6 for two solar temperature models, namely, the LTE line blanketed RE model of Kurucz (1974; KREo hereafter) and the Harvard-Smithsonian Reference Model for the Sun derived by Gingerich et al. (1971, abbreviated as HSRA hereafter).

We adopt an A_{Ca}=2.14E-6 relative to H (Withbroe, 1971); the same value was used by Ayres (1975), Ayres & Linsky (1976), and Shine & Linsky (1974). We use the disc centre K line observations of White & Suemoto (1968), supplemented by Shine's (1973) data for $\Delta\lambda<2\AA$. We place these observations on an absolute scale by means of Houtgast's (1970) measurements in the λ3954Å window. The resulting intensity profile is displayed in Figs.3.4 & 3.5 by squares and circles respectively. This absolute calibration has an uncertainty of ~8% (Houtgast, 1970). In Figs.3.4 & 3.5 we have shown the theoretical profiles synthesized using various values of E6 and the KREo and HSRA $T(\tau)$ models respectively. It is seen that E_6s of 1.2 & 1.45 give satisfactory fits for these two temperature models, respectively. The residual disagreement shortward of λ3938Å is due to the prevalance of the RCS effects in the solar upper photosphere. It is interesting to compare these values of E_6 with the values derived by Ayres and his associates. Thus, Ayres (1975) obtains an E_6=1.1 for KREo, while Shine & Linsky obtain an E_6=1.6 for HSRA. We feel that our values are in good agreement with these, the small differences being attributable to the different formulations used to calculate Γ_6 and to small differences in the pressure structures of the continuum models used to synthesize the K line. Finally, we note that the expected 0.1 dex uncertainty in the solar Ca abundance gives rise to a similar uncertainty in the derived values of E_6.

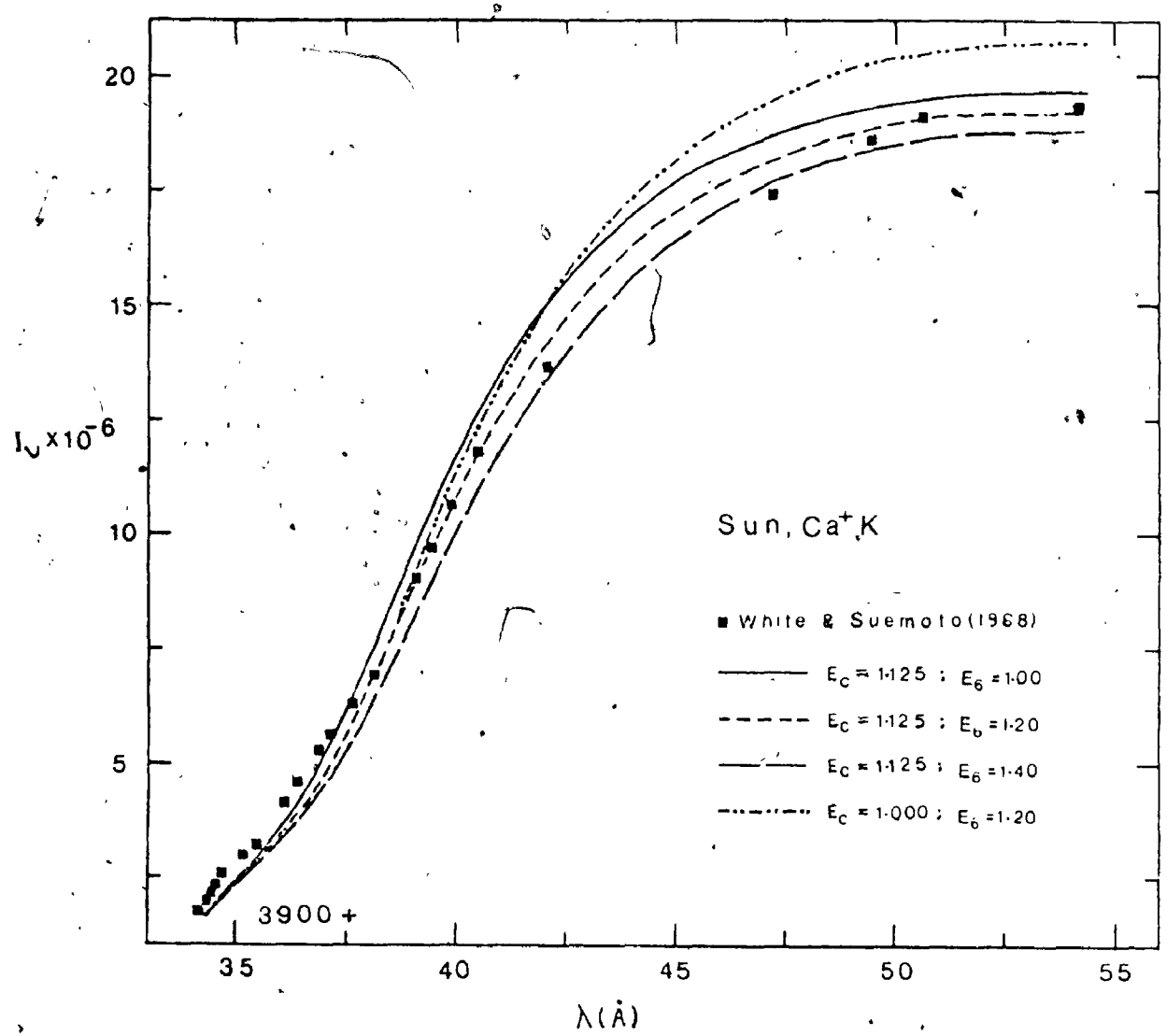

Fig.3.4. Determination of E_6 for the K line. White & Suemoto's observations (squares) are fitted with the theoretical profiles synthesized with the KREo $T(\bar{\tau})$ model and various values of E_6. An A_{Ca}=2.14E-6 is used in all the calculations.

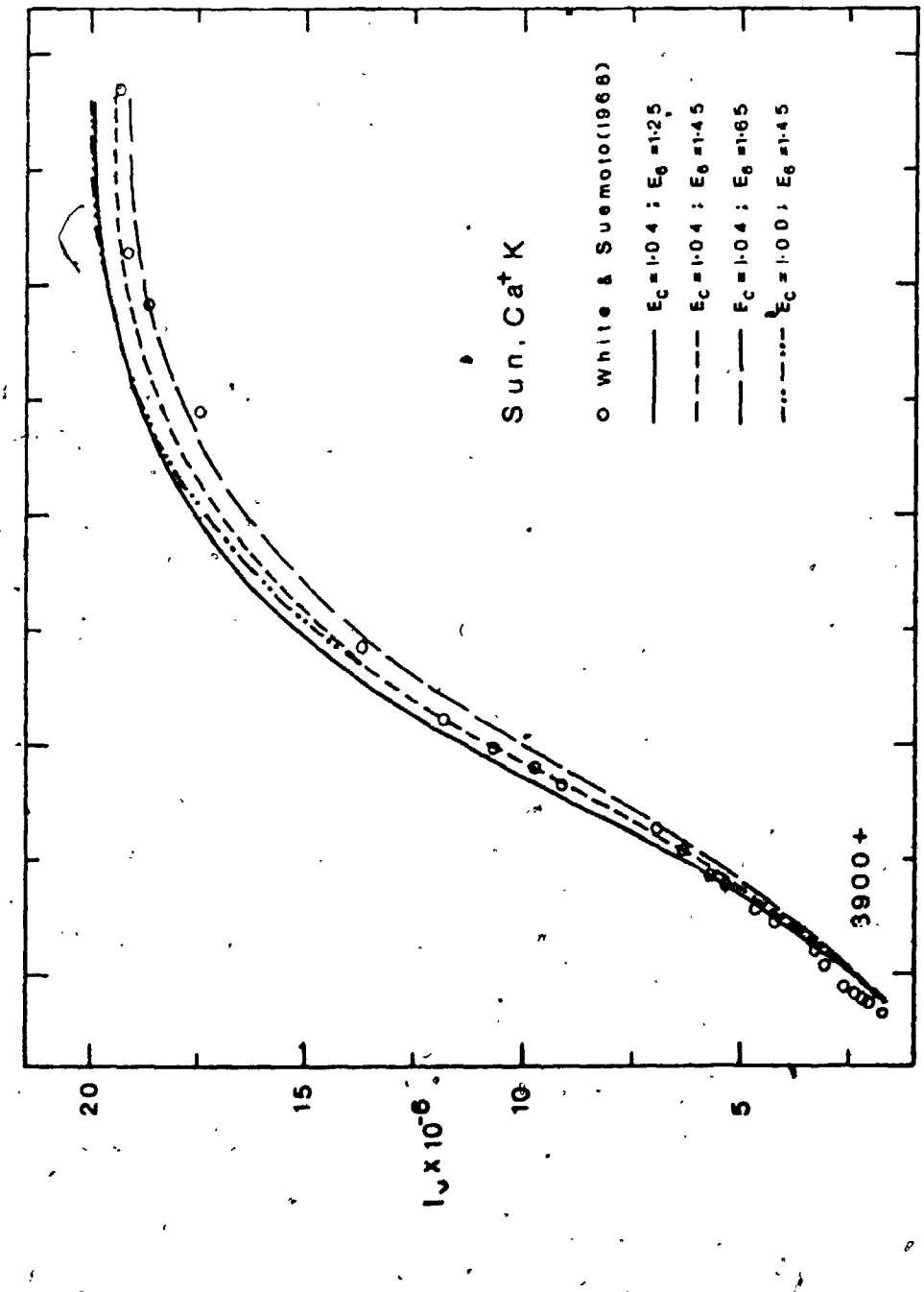

Fig.3.5. Determination of E6 for the K line. White & Suemoto's observations (circles) are fitted with the theoretical profiles synthesized with the HSRA T(τ) model and various values of E6. An A_{Ca}=2.14E-6 is used in all the calculations.

3.4. MISSING OPACITY

In late type stars there is a large discrepancy between the theoretical and observed continuum fluxes in the ultraviolet. For example, Gingerich et al. (1971) note that at λ4000Å the HSRA predicts 7% higher intensity than that measured by Labs & Neckel (1962). This discrepancy increases with decreasing wavelength and decreasing effective temperature (cf.Fig.4.1a, where the observed continuum fluxes of Arcturus are compared with a theoretical model). A consequence of this is that the theoretical fluxes in the far wings ($\Delta\lambda$ >5Å) and the windows at λλ3951Å & 3954Å, where the continuous opacity dominates over the line opacity, are overestimated. This behavior, illustrated by dot-dashed lines in Figs.3.4 & 3.5, was also noticed by Shine (1973). Increasing the Γ or A_{Ca} will not help because the increase needed is so large that a strong disagreement is caused in the inner wings ($\Delta\lambda$< 5Å) where the line opacity is greater than the continuous opacity. The inference is that we are dealing with some kind of "missing opacity", which affects the far wings most but has little effect on the inner wings. The presence of such a missing opacity was also advocated by Lites (1973) in a study of the solar Iron lines shortward of λ4070Å. Lites has simply scaled up the overall continuous opacity at these wavelengths between 20-100% to match the theoretical wing intensities with the observations. We adopt a similar procedure and introduce an "Opacity Enhancement Factor", or E_c for short, which scales up the total continuous opacity at the frequency

of the window so as to force agreement between the observations and theory in the far wings. Examples of determination of E_c for the Sun using the KREe and HSRA models are given in Figs.3.4 & 3.5 respectively. In these Figs. the dot-dashed lines represent the K line profiles synthesized without incorporating the continuous opacity enhancements (i.e., E_c=1). These profiles are systematically brighter than the observations because of the "missing opacity". So, in order to force agreement between the observation and the theory, we introduce continuous opacity enhancements (E_cs) of 1.04 and 1.13 respectively in case of the HSRA and KREe models. The profiles thus synthesized are shown by short-dashed lines in Figs.3.4 and 3.5. The E_cs for these two temperature models differ because of small differences in their temperature structures. Besides these differences, the A_{Ca} and g used in line synthesis also influence the choice of E_c. Since we have held the A_{Ca} and g fixed in our computations, the difference in E_cs entirely arises from differences in the temperature structures. For K giants we derive much larger values of E_c than the Sun (cf.Chap.V), because of larger discrepancy in the observed and computed ultraviolet continuum fluxes in these stars. E_c plays a crucial role in comparing the observed normalised (to window) profile with the theory, because of its effect on the theoretical window flux with respect to which the rest of the theoretical profile has to be normalised. So, it is very important to investigate how the choice of the $T(\bar{\tau})$ model, A_{Ca} and g affect the choice of E_c. The next three sections are

devoted to this discussion.

a) DEPENDENCE OF E_c ON A_{Ca}

For simplicity, we assume that the line is formed in pure absorption and in LTE and neglect the frequency dependence of the continuous opacity over the width of the line. Thus we write

$$\kappa_\nu^c = \kappa_{\bar{\nu}}^c = E_c \bar{\kappa}_{\bar{\nu}}^c \qquad (3.20)$$

where $\bar{\kappa}_{\bar{\nu}}^c$ and $\kappa_{\bar{\nu}}^c$ are the original (unenhanced) and enhanced continuous absorption coefficients at the frequency $\bar{\nu}$ of the window. If we also assume: 1) The ratio, η_ν, of the line to continuous absorption coefficient is independent of depth; 2) the source function, B_ν, is linearly expandable on the continuum optical depth scale, we can approximately write (Mihalas, 1970)

$$R_\nu = \left(1+\frac{b/a\sqrt{3}}{1+\eta_\nu}\right) \Big/ \left(1+b/a\sqrt{3}\right) \qquad (3.21)$$

where R_ν is the residual intensity of the line, $\eta_\nu = \kappa_\nu^K/\kappa_{\bar{\nu}}^c$ and a and b are constants. In our case we do not have R_ν, but $\tilde{F}_\nu$, the emergent flux normalised to the window. However, for a qualitative discussion of the dependence of $\tilde{F}_\nu$ on η_ν, we can still use Eq.3.21 to a rough approximation. Thus we write

$$\tilde{F}_\nu \sim c1+c2/(1+\eta_\nu) \qquad (3.22)$$

where

$$c1=(1+b/a\sqrt{3})^{-1} \quad \& \quad c2=c1\,b/a\sqrt{3} \qquad (3.23)$$

Now, a change in A_{Ca} affects $\tilde{F}_\nu$ through its effect on η_ν. In general we can write

$$d\eta_\nu = \frac{d\kappa_\nu^K}{\kappa_{\bar{\nu}}^c} - \eta_\nu \frac{d\kappa_{\bar{\nu}}^c}{\kappa_{\bar{\nu}}^c} \qquad (3.24)$$

A change in A_{Ca} changes the line absorption coefficient κ_ν^K by amount $d\kappa_\nu^K$, while leaving the continuous absorption coefficient $\kappa_{\bar{\nu}}^c$ unaffected. But to preserve $\tilde{F}_\nu$ in case of changing κ_ν^K, we must alter $\kappa_{\bar{\nu}}^c$ such that $d\eta_\nu \equiv 0$. This condition gives rise to the relation

$$d\kappa_{\bar{\nu}}^c = \bar{\kappa}_{\bar{\nu}}^c \, dE_c = d\kappa_\nu^K/\eta_\nu = \text{const. } dA_{Ca} \qquad (3.25)$$

where dE_c and dA_{Ca} are the changes in E_c and A_{Ca} respectively. Thus it is clear that an overestimate of A_{Ca} leads to a corresponding overestimate of E_c and vice versa. E_c has only a small effect on the absolute fluxes of the inner wings, because $\kappa_\nu^K >> \kappa_{\bar{\nu}}^c$ in the inner wings (cf. Fig. 5.8). On the other hand, the normalised flux profile is sensitively dependent upon E_c, since the effect of E_c is to scale the entire $\tilde{F}_\nu$ profile up or down by altering the window flux. This behavior is illustrated in Fig. 5.9, where we changed A_{Ca} but adjusted E_c such that the profiles agree in the far wings. It is therefore clear that we must know A_{Ca} correctly, otherwise we will introduce errors in the normalisation of the theoretical profiles, hence in the derived upper photospheric temperature models.

b) DEPENDENCE OF E_c ON THE $T(\bar{\tau})$ DISTRIBUTION OF THE DEEPER LAYERS

Since the far wings of the K line upon which the determination of E_c is based are formed in the deeper optical continuum forming layers ($-1.0 < \log \bar{\tau} < 0.0$), the $T(\bar{\tau})$ distribution relevant to this discussion pertains to these layers. This $T(\bar{\tau})$ distribution is derived by comparing the observed and computed Paschen continuum slopes and has an uncertainty of $\sim$2% at T=5000K. This uncertainty in T is such that N(Ca II) and N_H are negligibly affected, while the N_e is slightly affected. Gray (1976) has derived a $P_e(T)$ relation given by

$$P_e \simeq \text{const. } e^{\Omega T} \tag{3.26}$$

where Ω=0.0011/deg. The temperature dependence of κ_ν^K in the line wings is given by

$$\kappa_\nu^K = C1\Gamma_R + C2T^{0.3} \tag{3.27}$$

where C1 and C2 are constants. If $\Gamma_R \ll \Gamma_6$, i.e., if the temperature dependent term in Eq.3.27 dominates, we have

$$d\kappa_\nu^K/\kappa_\nu^K = 0.3\ dT/T\ . \tag{3.28}$$

Thus, a 2% change in T results in a 0.6% change in κ_ν^K. On the other hand, if $\Gamma_R \gg \Gamma_6$, κ_ν^K is independent of T. The reality lies in between, hence Eq.3.28 represents the maximum possible change in κ_ν^K for a given change in T. The temperature dependence of the H^- opacity, on the other hand, is given by

$$\kappa_\nu^{H^-} = \text{const. } T^{-2.5} P_e e^{8730/T} \quad . \qquad (3.29)$$

Replacing P_e by Eq.3.26 and differentiating, we have

$$\frac{d\kappa_\nu^{H^-}}{dT} \frac{1}{\kappa_\nu^{H^-}} = 0.0011 - \frac{2.5}{T}\left(1 + \frac{3481}{T}\right). \qquad (3.30)$$

The right hand side of Eq.3.30 is positive or negative depending upon whether $T \gtrless 4170K$. Hence for a given dT (dT positive) $\kappa_\nu^{H^-}$ increases in the layers hotter than 4170K and decreases in the layers cooler than 4170K. In many of our stars the window flux originates in layers hotter than 4170K. Therefore $\kappa_\nu^{H^-}$ changes in direct proportion to dT. Now assuming that $\tilde{\kappa}_{\bar{\nu}}^{c} \doteq \kappa_{\bar{\nu}}^{H^-}$, and rewriting Eq.3.24 we have

$$d\eta_\nu = \frac{d\kappa_{\bar{\nu}}^{K}}{E_c \kappa_{\bar{\nu}}^{H^-}} - \eta_\nu \frac{d\kappa_{\bar{\nu}}^{H^-}}{E_c \kappa_{\bar{\nu}}^{H^-}} \quad . \qquad (3.31)$$

If we wish to preserve $\tilde{F}_\nu$ in the case of a changing T, we must have $d\eta_\nu = 0$. This condition gives rise to the result

$$E_c = (d\kappa_\nu^K / \kappa_\nu^K) \Big/ (d\kappa_{\bar{\nu}}^{H^-} / \kappa_{\bar{\nu}}^{H^-}) \quad . \qquad (3.32)$$

Thus, for a given dT/T, $E_c \gtrless 1$ depending upon whether $d\kappa_\nu^K/\kappa_\nu^K \gtrless d\kappa_{\bar{\nu}}^{H^-} / \kappa_{\bar{\nu}}^{H^-}$. This behavior is illustrated by the E_cs of 1.04 and 1.13 derived above for the HSRA and KREe models, respectively. The HSRA model is about 140K hotter than KREe in layers $-1.0 < \log \bar{\tau} < 0.0$, where most of the window flux originates. This enhancement in T causes fractional enhancements of $\sim$0.85% and $\sim$4% in κ_ν^K and $\kappa_{\bar{\nu}}^{H^-}$ respectively. Since $\kappa_{\bar{\nu}}^{H^-}$ increases faster than κ_ν^K in this case, we have to use a smaller E_c in HSRA compared to KREe model.

c) DEPENDENCE OF E_c ON g

A change in g affects the κ_ν^K mainly through the dependence of Γ_6 on P_g, while it affects κ_ν^c through the dependence of the H^- opacity on P_e. We do not consider the effect on Γ_4 here, because $\Gamma_4 << \Gamma_6$ at most depths in our stars. Holding all the physical variables insensitive to a change in g constant, we have

$$\kappa_\nu^K \propto \Gamma_R + \text{const. } P_g; \text{ and } \kappa_\nu^c \propto E_c P_e.$$

Hence, $$\eta_\nu = \text{const.}\Gamma_R/E_c P_e + \text{const. } P_g/E_c P_e.$$

Now, using the $P_g(g)$ and $P_e(g)$ relations of Gray(1976), viz. the relations $P_g \propto g^{2/3}$ and $P_e \propto g^{1/3}$, we have

$$\eta_\nu = \text{const.}(\Gamma_R/E_c)g^{-1/3} + \text{const.}(g^{1/3})/E_c \qquad (3.33)$$

Therefore, η_ν decreases or increases with g depending upon which of the two terms on the right hand side of Eq.3.33 dominates. It turns out that the first term dominates in our stars, so that

$$\eta_\nu \propto \text{const.}(\Gamma_R/E_c)g^{-1/3}.$$

Suppose that the adopted value of g differs from the actual (correct) value by a factor R1 such that g(adopted)=R1g(actual). In this case, to force agreement between the observed and computed far wing profiles, we must alter E_c such that

$$E_c \propto R1^{-1/3}.$$

Thus, the gravity dependence of E_c is much weaker than the dependence on A_{Ca}, sufficing it to know g within a factor of 2. The second term on the right-hand side of Eq.3.33 further

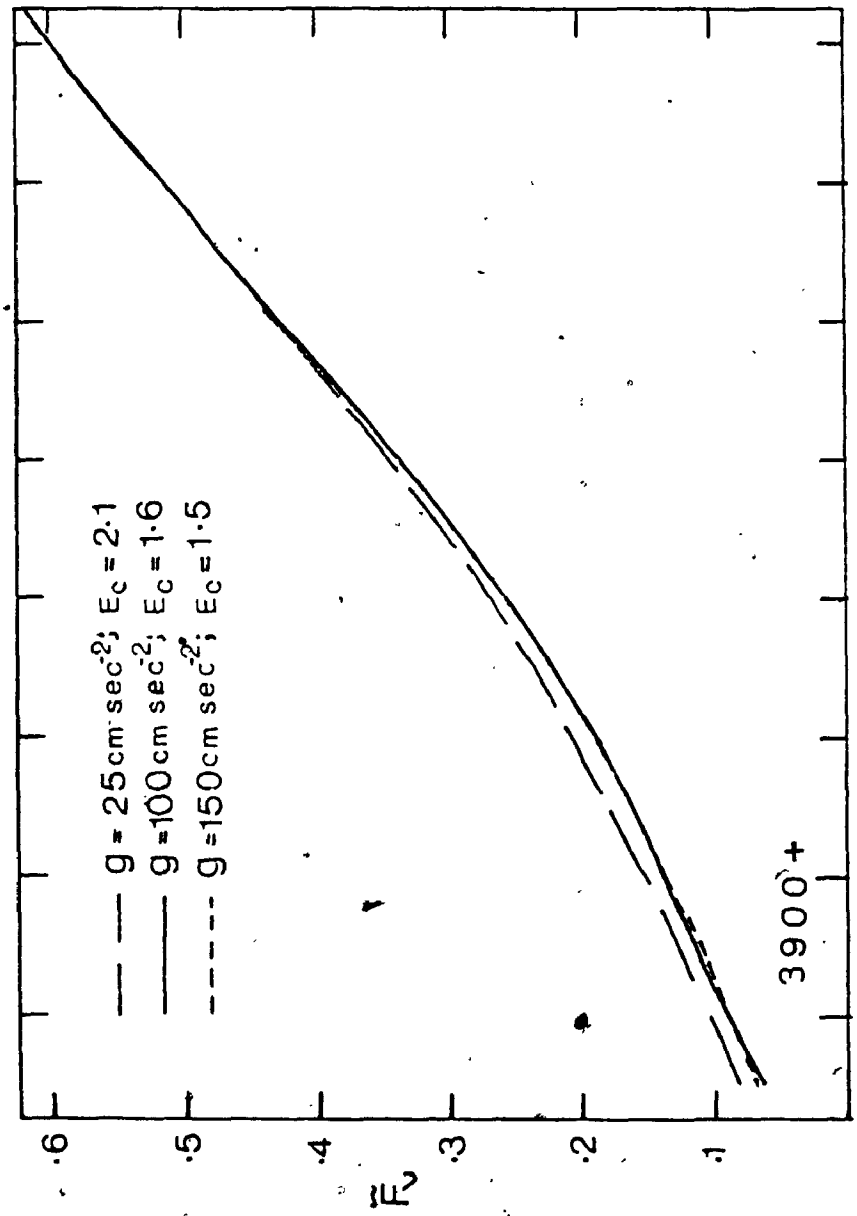

Fig.3.6. Dependence of E_c upon g. The $T(\bar{r})$ distribution is that of Arcturus. In each case the E_c has been adjusted so as to force agreement between the different K wing profiles in the "usable" far wing segment between λλ3939.5Å-3940.5Å.

weakens this dependence because of its reverse proportinality to g compared to the first term. In Fig.3.6 we have shown some numerical calculations, where we have varied g but adjusted E_c such that there is agreement in the far wings.

In these sections we have emphasized the importance of using the correct basic input data, namely the $T(\bar{\tau})$ distribution for the deeper layers, A_{Ca} and g, to avoid errors in E_c and hence in the derived upper photospheric temperature models. These input data will be derived in the next chapter. Using these data in combination with the theory outlined in the earlier sections of this chapter, we will derive the upper photospheric $T(\bar{\tau})$ models in Chap.V.

CHAPTER IV

CONTINUUM MODELS AND CALCIUM ABUNDANCES

In this chapter we derive the $T(\bar{\tau})$ distribution of the continuum forming layers and the Ca abundance A_{Ca} for the program stars.

4.1. MODEL ATMOSPHERES

The model atmosphere program was written by D.F.Gray with the addition of a few modifications incorporated in the opacity routines by the author. This program makes the usual assumptions of a plane parallel homogeneous atmosphere in a steady state, hydrostatic equilibrium and LTE ionization equilibrium. Since no flux constancy is imposed the $T(\bar{\tau})$ distribution is not calculated by the model, rather it is an input datum usually taken from the literature such as the model atmosphere tabulations of the late type stars by Bell et al. (1976). Given the $T(\bar{\tau})$ distribution, chemical composition and the gravity g, the purpose of the program is to calculate the emergent flux or the central intensity through the expressions:

$$F_\nu = 2\pi \int_0^\infty B_\nu(T)\, E_2(\tau_\nu)\, d\tau_\nu \qquad (4.1)$$

$$I_\nu = \int_0^\infty B_\nu(T)\, e^{-\tau_\nu}\, d\tau_\nu \qquad (4.2)$$

where τ_ν, the optical depth at frequency ν is given by

$$\tau_\nu = \int_0^{\bar{\tau}} (\kappa_\nu^c / \kappa_c)\, d\bar{\tau} \qquad (4.3)$$

where κ_ν^c and κ_c are the mass absorption coefficients at

ν and the frequency corresponding to the standard wavelength $\lambda = 5000\text{Å}$. The essence of the problem then lies in determining τ_ν, because if τ_ν is known and $B_\nu(T)$ is given we can solve Eqs.4.1 and 4.2. To obtain τ_ν we have to know the opacities, which depend upon the electron pressure, P_e, and T. If we can guess the run of the gas pressure $P_g(\tau)$, we can iteratively solve the relation

$$P_g = P_e + P_{ions} + P_{neutrals} \tag{4.4}$$

for P_e. Now we can compute κ_c. Since we have only guessed $P_g(\bar{\tau})$, it is essential that we obtain an improved estimate of this quantity by solving the hydrostatic equation in the form

$$P_g^{\frac{1}{2}}\, dP_g = P_g^{\frac{1}{2}}\, g/\kappa_c \; d\bar{\tau} \tag{4.5}$$

which leads to

$$P_g = \left[3/2\; g \int_0^{\bar{\tau}} \left(P_g^{\frac{1}{2}}/\kappa_c\right) dt\right]^{2/3} \tag{4.6}$$

or in terms of logarithmic optical depth

$$P_g = \left[3/2\; g \int_{-\infty}^{\log \bar{\tau}} \{(t\, P_g^{\frac{1}{2}})/(\kappa_c \log e)\}\, d\log t\right]^{2/3}$$

Using this improved value of $P_g(\bar{\tau})$ we once again solve Eq.4.4 for P_e and therefrom obtain a new $P_g(\bar{\tau})$ relation and repeat this process until convergence is achieved. Thus we would establish $P_g(\bar{\tau})$, $P_e(\bar{\tau})$ and $\kappa_c(\bar{\tau})$ relations, while the $T(\bar{\tau})$ relation is assumed to be known. We then calculate $\tau_\nu(\bar{\tau})$ and finally obtain the flux or the central intensity

from Eqs.4.1 and 4.2.

Unless otherwise stated all the models use the solar chemical composition (Withbroe, 1971) given in table 4.1. The opacity sources include H bound free (bf) and free free (ff) absorption, He^- ff absorption, H_2^+ molecular absorption and the continuous absorption due to all the metals listed in table 4.1. The same metal composition is used in the calculation of Pe. In addition to the opacity sources mentioned above, we also include electron scattering and Rayleigh scattering due to H_2.

For H, Mg and Si we have used the continuous opacity routines provided by Carbon & Gingerich (1969). A hydrogenic approximation was used for all other metals beyond λ4000Å. Below λ4000Å we have used the quantum defect cross sections of either Peach (1969) or Travis & Matsushima (1968). Of the metals considered, only Fe, Mg, Si, Ca, Na and K are significant absorbers; others are included for completeness. In any case, as H^- absorption dominates the other sources by one to several orders of magnitude at the visual and near infrared wavelengths, the uncertainties in other opacities have insignificant effect on the emergent flux. For H^-, He^- and H_2^+ we have used the polynomial approximations of Gray (1976), who has also provided the expressions for electron and Rayleigh scattering. An idea of the accuracy of our opacity routines can be obtained from the fact that we can reproduce the HSRA model intensities (Gingerich et al.,1971) to better than 0.6% between 0.36μ

But, this is an overestimate as the random observational errors in individual points cause negative and positive shifts with equal probability, thus leaving the mean observed energy distribution only slightly (<< 7%) altered. Hence, we believe that the observational errors introduce no more than 20K uncertainty in the derived T_es. However, there is a ±50K uncertainty in fitting the models to the observations. i.e., the theoretical models differing by ±50K in T_e from the best fitting model also match the observed Paschen continuum slope fairly well. So, we estimate that the T_es derived above are uncertain by ∿ 70K. In view of this uncertainty, it is interesting to compare these values with with the others. Table 4.2 provides such a comparison, where we have listed our results together with the T_es derived by Williams (1971, 1972) from R-I colors and by Oinas (1974) from a procedure similar to ours. The values agree within the quoted uncertainty.

TABLE 4.2. RESULTS

Star	Spectrum	Log g	T_e	T_e(W)	T_e(O)	A_{Ca}
β Gem	K0 III	2.8	4750	4793	-	3.5E-6
ε Cyg	K0 III	2.8	4750	4672	-	2.7E-6
α Ser	K2 III	2.5	4650	4521	4560	-
β Oph	K2 III	2.5	4650	4551	-	4.4E-6
κ Oph	K2 III	2.3*	4600*	4553	-	-
α Ari	K2 III	2.5	4450	4480	4500	2.2E-6
α Boo	K2 III	1.7	4250	4338	4250	1.0E-6

* Adopted from Peterson (1976); T_e(W) & T_e(O) respectively refer to the T_es derived by Williams (1971,1972) & Oinas(1974).

within a factor of 2.

4.4. INITIAL $T(\bar{\tau})$ DISTRIBUTIONS

We take all the initial $T(\bar{\tau})$ distributions from the line blanketed RE model tabulations of Bell et al. (1976). Since their spacing of 500K in T_e is too coarse for our purposes, we interpolate between their models at intervals of 50K. The gravity dependence of the $T(\bar{\tau})$ distributions is very weak, sufficing it to choose a model with a log g within ±0.5 of the estimated log g.

4.5. $T(\bar{\tau})$ DISTRIBUTIONS FOR THE INDIVIDUAL STARS

Aided by the theory and the above observational data, we are in a position to obtain the $T(\bar{\tau})$ distributions of the deeper optical continuum forming layers for our program stars. Below, we discuss the individual cases in some detail.

a) ARCTURUS

Blackwell et al. (1975) have published good deblanketed absolute flux measurements of Arcturus. Their line blocking data were taken from Griffin's (1968) atlas in the range 0.36μ to 0.825μ and from Connes' (1968) infrared spectrum in the range 1μ to 2.5μ. Edmonds (1973) provided the data at intermediate wavelengths. We also had access to the deblanketed scan of Oinas (1975), who once again used Griffin's atlas for deblanketing. These observations, placed on the absolute system of Hays & Latham (1975) are displayed in Fig.4.1a. Also drawn in this figure is the best fitting theoretical model with T_e=4250K and log g=1.7. The agreement

between the observations and theory is generally good except in the peak at 1.6μ and below 0.45μ . The peak at 1.6μ corresponds to the H^- opacity minimum and is formed in the deepest ($\log \bar{\tau}>0.5$) photospheric layers. The discrepancy in this peak therefore reflects the uncertainties in the temperature of the deeper layers in the adopted initial $T(\bar{\tau})$ model of Bell et al. (1976). These uncertainties arise from the uncertainties in the treatment of convection and from the incompleteness of the ultraviolet line blocking data. A similar discrepancy is also found in the Sun (cf. Figs.15 & 16 in Vernazza et al., 1976). However, the uncertainty in the $T(\bar{\tau})$ distribution of these layers is of little concern to the K line problem, as these layers contribute little flux at the K line wavelengths. The discrepancy below 0.45μ arises from the lack of real continuum in a K giant spectrum at these wavelengths (Griffin, 1968). Even the highest points in the spectrum at these wavelengths are significantly depressed by the crowding of the lines. Hence the observed points fall systematically below the theoretical line.

The log g=1.7 adopted above was taken from Ayres & Linsky (1975). On the other hand, Mackle et al. (1975) from an extensive spectroscopic analysis of Arcturus obtain a log g=0.9± 0.35 and T_e=4260±50K. Ayres & Linsky have argued that this log g is too low. In any case, this discussion is only of academic interest to us as we intend to use Arcturus to check the working of our line synthesis program rather than to obtain fundamental information about it.

Since we have to compare our results with those of Ayres & Linsky (1975), it is appropriate that we adopt their log g.

Following Griffin & Griffin (1967), we have used 1/3 solar metal abundances in our model calculations. The $T(\bar{\tau})$ distribution derived above is compared with the Mackle et al's $T(\bar{\tau})$ distribution in Fig.4.2. The agreement is good.

b)β Gem

The narrow band observations of ST, corrected for line absorption, are compared with the best fitting theoretical model with log g=2.8 and T_e=4750K in Fig.4.1b. The line blocking data for this star are given by Rodriguez (1969). But his values are systematically larger by ≈40% than the values obtained by VP, as judged by the data for η Cep (K0 IV), which is common to both these observers. Incidentally, Rodriguez's values for β Gem are almost identical to those for η Cep; therefore, for the sake of homogeneity (since we have taken all other line blocking data from VP), we have used the VP data for η Cep to deblanket β Gem. At the wavelengths where VP did not measure η Cep, we have adopted a mean of his values for the three K0 III stars, α Phe, θ Cen and αInd. Williams gives a log g=2.9 (g=800 cm sec^{-2}) for β Gem, while Griffin(1976) estimates a value of 2.5 (g=320 cm sec^{-2}). Griffin's value is probably too low because it is based on a very low mass (0.23M⊙) adopted for Arcturus. So, we give a low weight to his value and adopt a log g=2.8 (g=600cmsec^{-2}). Thus the best fitting model corresponds to T_e=4750K and log g=2.8.

c) ε Cyg

Fig.4.1c shows the narrow band observations of ST corrected for line absorption using the line blocking coefficients of VP. We adopt a log g=2.8 (g=600 cm sec-2) from Williams and derive a T_e=4750K. Thus ε Cyg and β Gem, which have the same spectral type also have the same T_e and log g values.

d) α Ser

The narrow band observations of ST corrected for line absorption using the line blocking coefficients of VP and Oinas are shown in Fig.4.1d. Williams gives a log g = 2.7 (g=500 cm sec^{-2}) while Griffin estimates a value between 2.4 and 2.7 for this star. We have adopted a value of 2.5 (g=320 cm sec^{-2}). The best fitting model thus derived corresponds to T_e=4650K and log g=2.5 and is drawn in Fig.4.1d.

e) β Oph

The ST scan corrected for line absorption and the best fitting model are shown in Fig.4.1e. Line blocking values are from VP; at the wavelengths where he did not measure this star, a mean of his values for α Ser and μ Leo was used. Williams gives a log g=2.7 (g=400 cm sec^{-2}) while Gustafsson et al. (1974) give a value of 2.4 (g=250 cm sec^{-2}). We adopt a log g=2.5 (g=320 cm sec^{-2}) and derive a T_e=4650K. These values are the same as for α Ser.

f) α Ari

The deblanketed scan of ST together with the best fitting model is shown in Fig.4.1f. The line blocking data are from VP and we have adopted a log g=2.5 (g=320 cm sec^{-2}) from Williams. We derive a T_e=4450K.

g) κ Oph

ST observations of κ Oph do not extend into infrared, making the comparison between the theory and observations rather uncertain. Also, no line blocking measurements are available for this star. However, this star has been the subject of extensive analysis by Peterson (1976), who derived an empirical $T(\bar{\tau})$ model with T_e=4600K and log g=2.3. Her model $T(\bar{\tau})$ distribution is very similar to the Bell et al.'s (1976) model with T_e=4550K and log g=2.25.

4.6. ERRORS

ST, who provide the bulk of energy distributions, estimate that their data are uncertain by ≃ 1.5%. The systematic errors in their data should be quite small as judged from the good agreement between their and Oinas' data for α Ser (cf. Fig.4.1d). On the other hand, VP estimates an internal probable error of ≃ 3% for his line blocking measurements, and mentions that his values are systematically smaller than Oinas' values by 2± 1% whenever there is duplication between the two. So, we conclude that the overall error in the measured points is ≲ 7%. At the T_e and g values we are considering, a ∿7% error in flux transforms into ∿ 35K error in T_e.

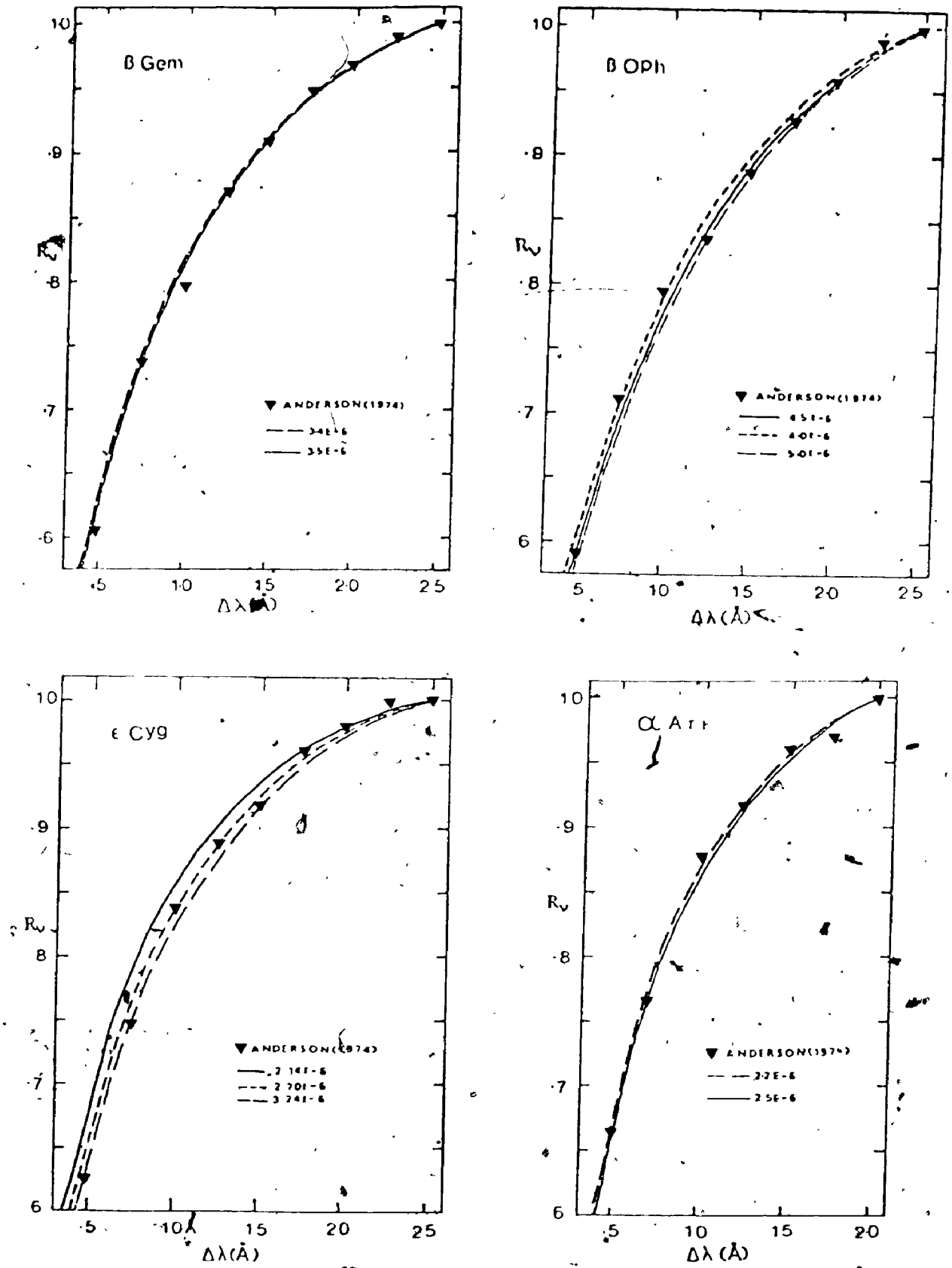

Figs. 4.3e-h. Determination of A_{Ca} for β Gem, ε Cyg, β Oph and α Ari. Anderson's Ca II λ8498 observations are shown by triangles. Theoretical profiles are labeled after the A_{Ca} used in the spectrum synthesis.

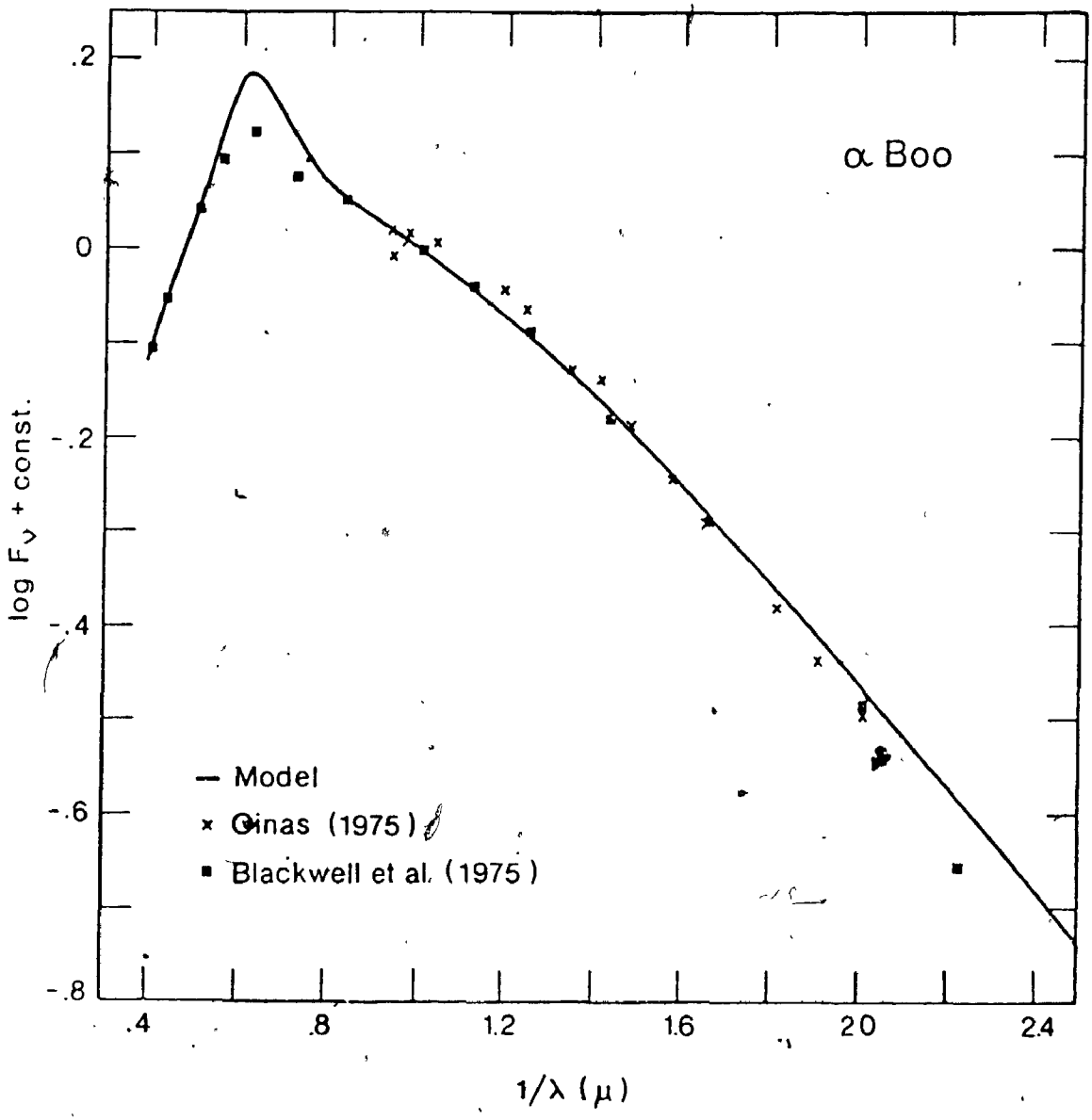

Fig.4.1a. Absolute energy distribution of Arcturus.

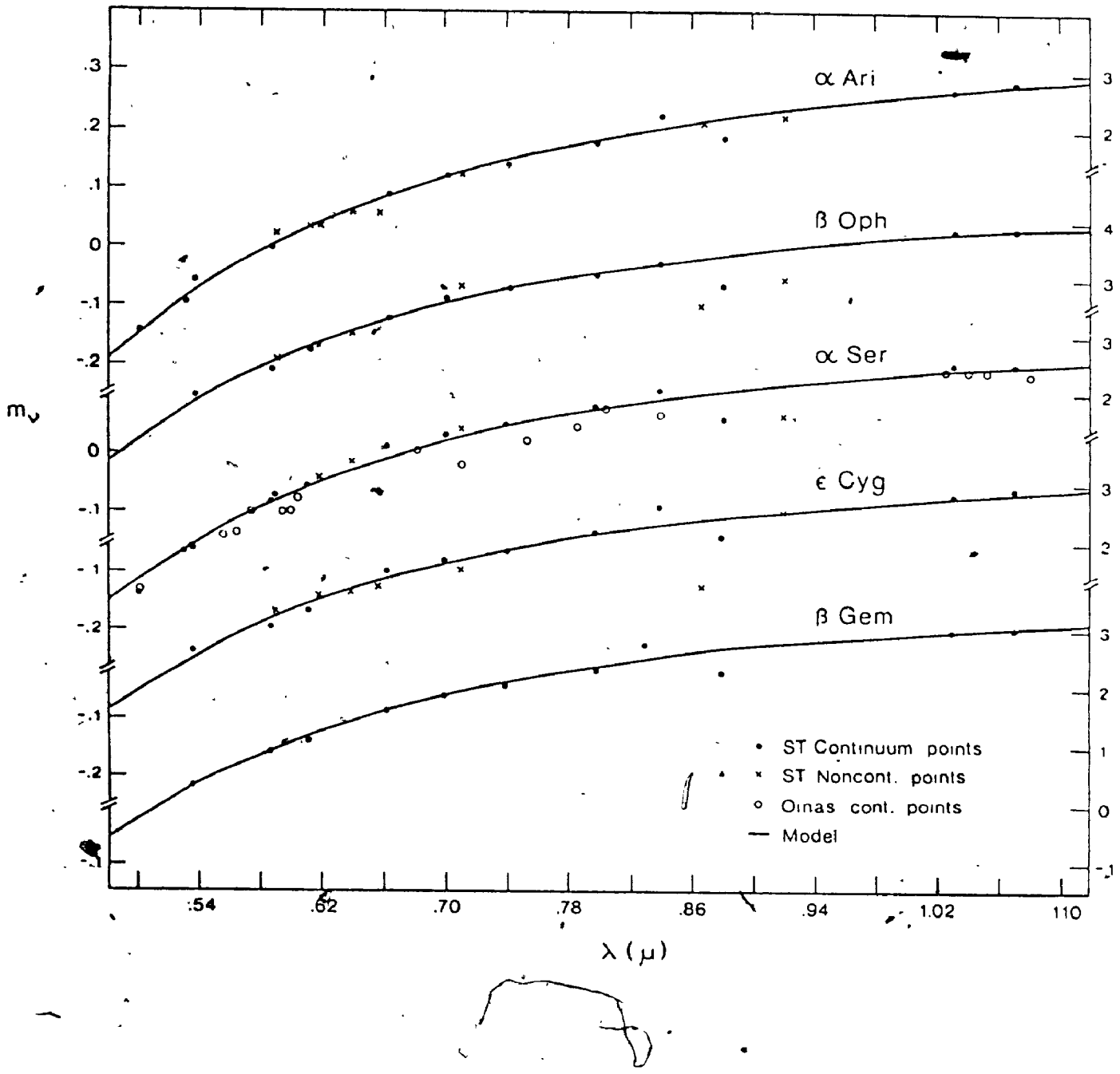

Figs.4.1b-f.

Absolute energy distributions of β Gem, ε Cyg, α Ser, β Oph and α Ari.

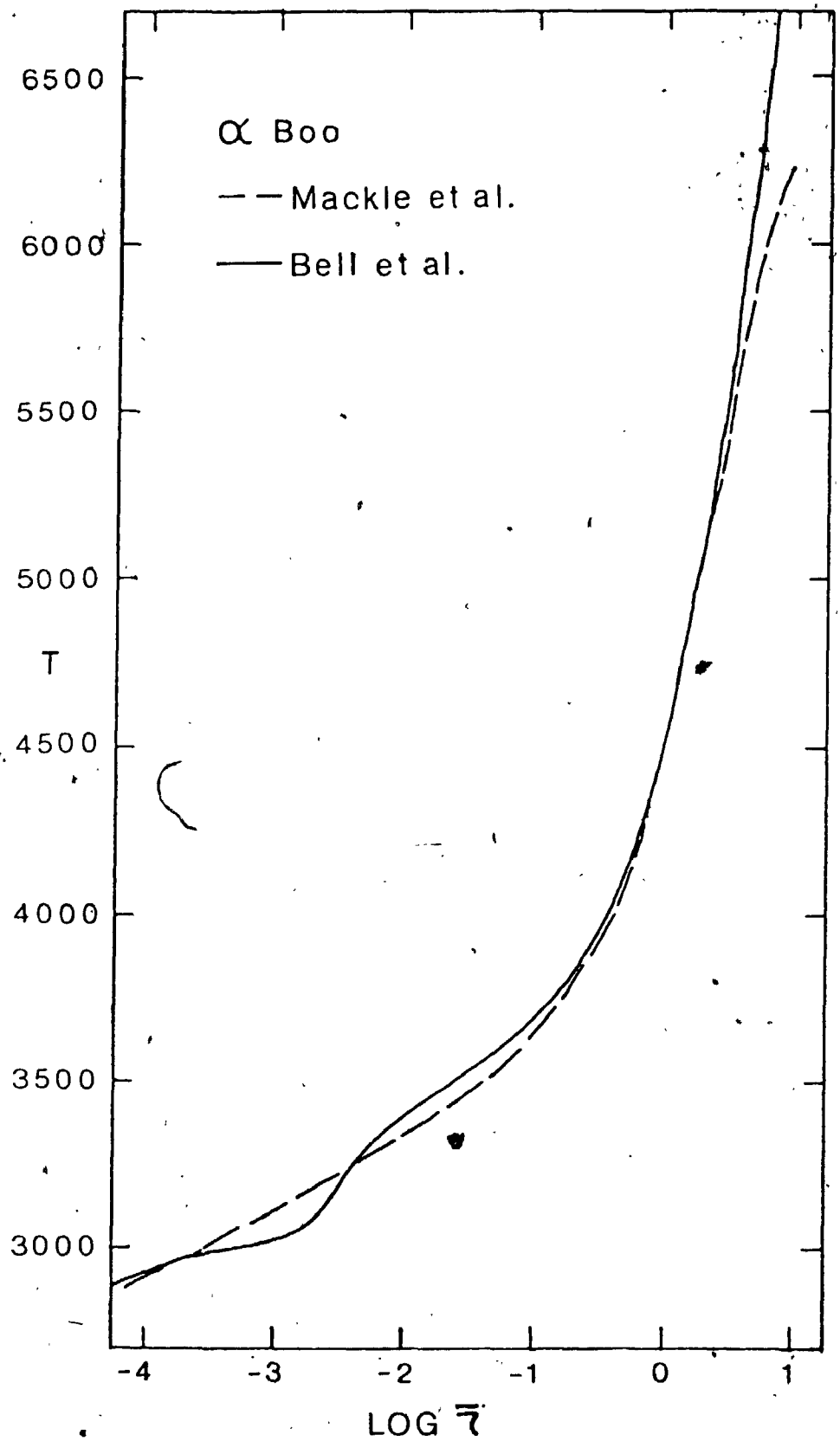

Fig.4.2. Comparison of our $T(\bar{\tau})$ distribution for the optical continuum forming layers in Arcturus (solid line) with the empirical $T(\bar{\tau})$ model of Mackle et al. (1976, dashed line).

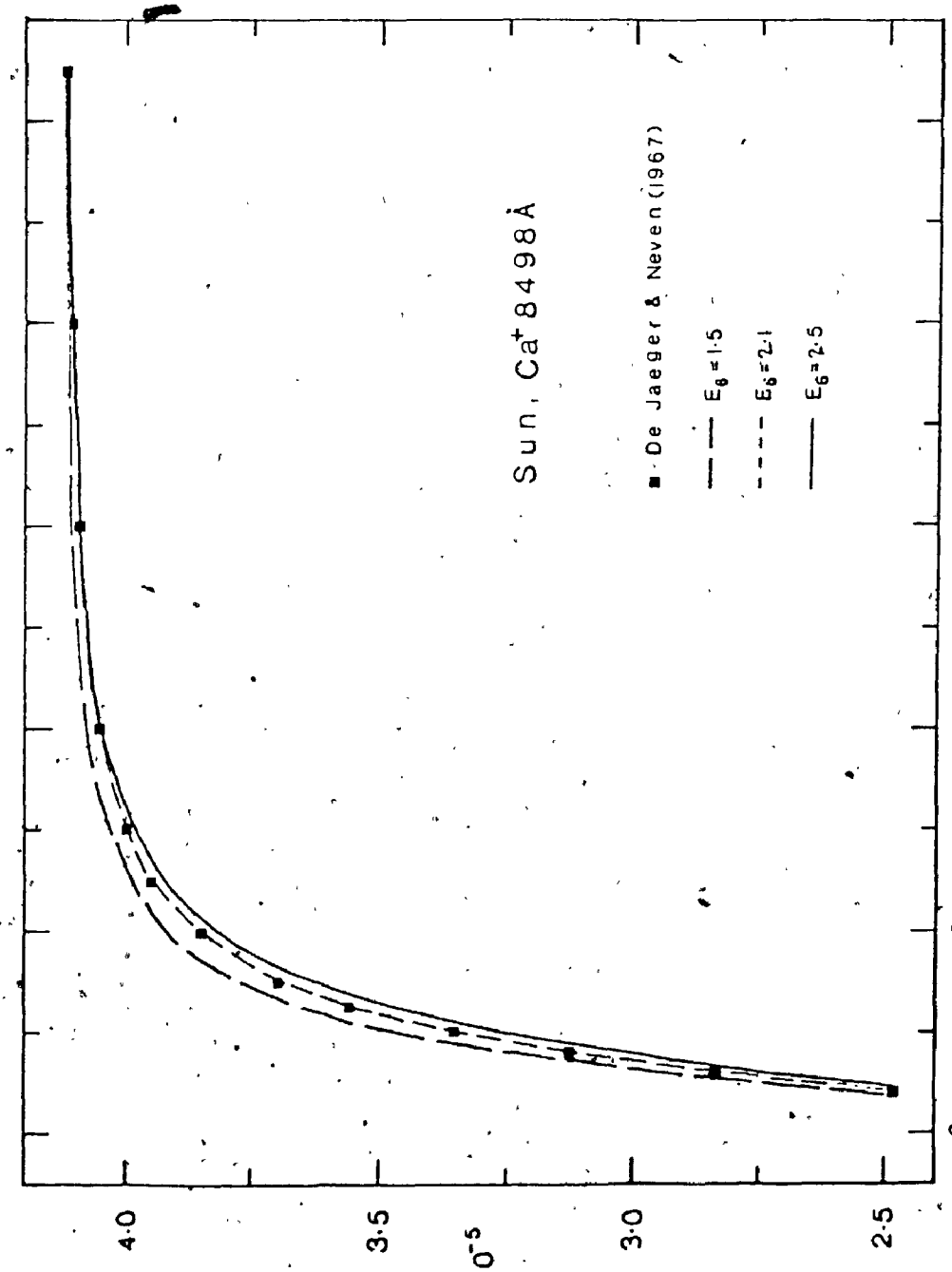

Fig.4.3a. Determination of van der Waals enhancement factor E_6 for Ca II λ8498. de Jager & Neven's disc centre solar λ8498 profile is shown by squares. Theoretical profiles are labeled after the E_6 used in line synthesis. E_6=2.1 gives the best fit.

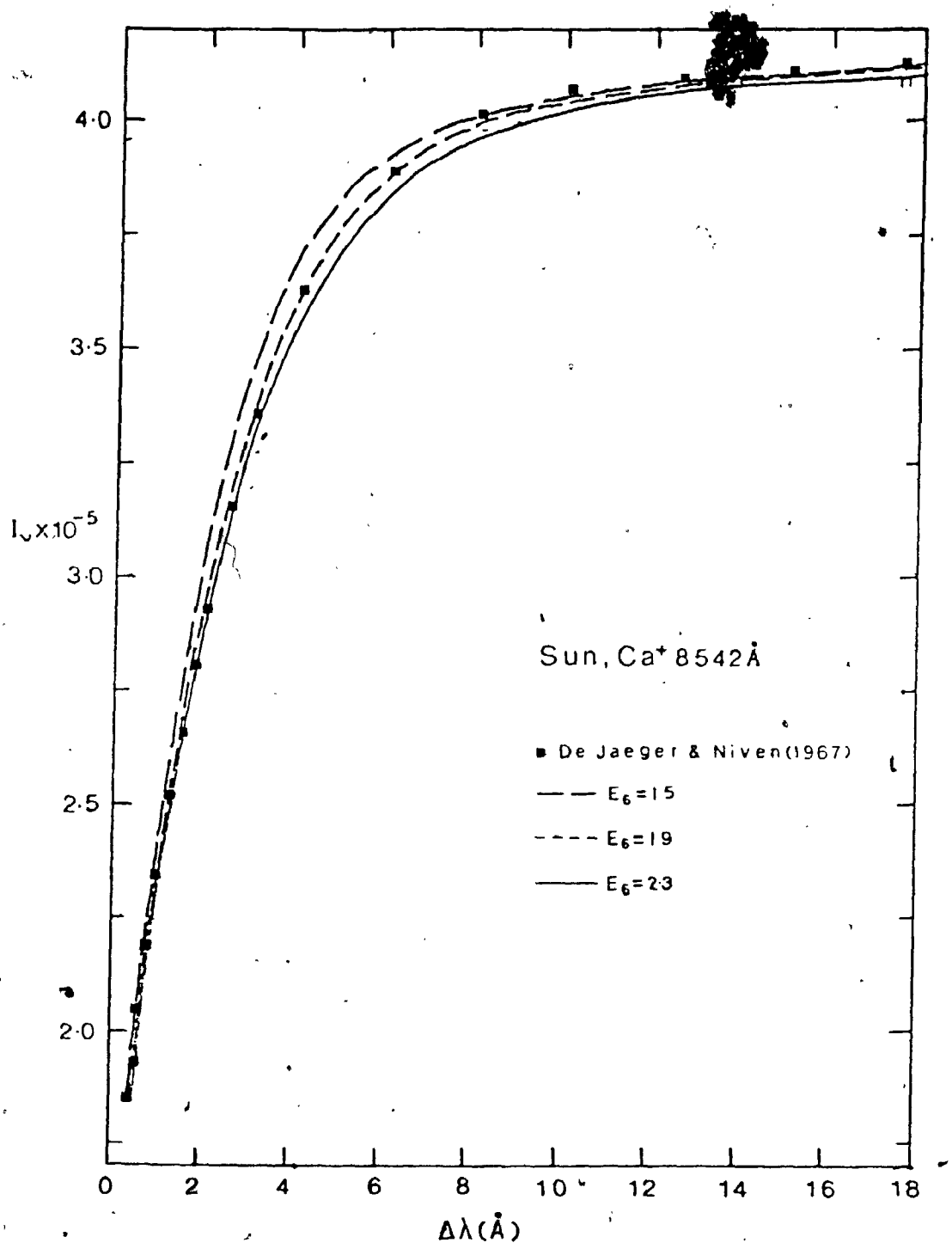

Fig.4.3b. Derivation of van der Waals enhancement factor for Ca II λ8542 line.de Jager & Neven's disk centre solar λ8542 profile is shown by squares. The theoretical profiles are labled after the enhancement factor E_6 used in the line synthesis. E_6=1.9 gives best fit to the observations.

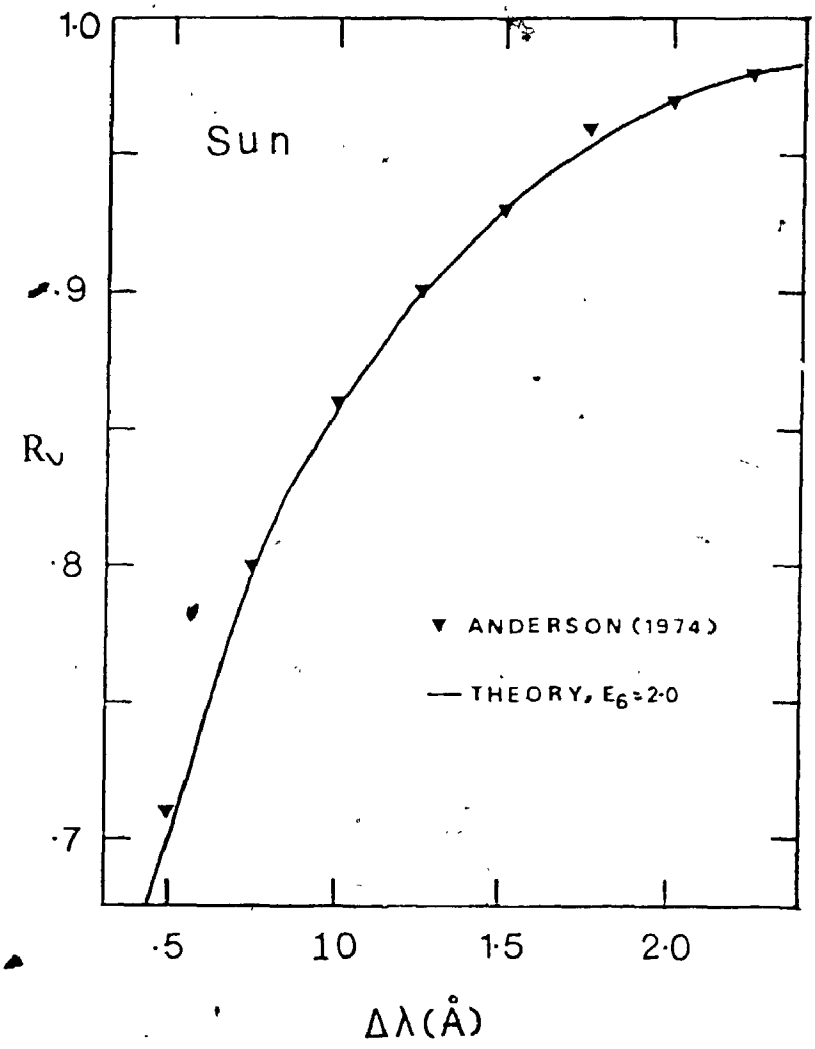

Fig.4.3c. Anderson's solar Ca II λ8498 profile is shown by triangles. The theoretical profile with E_6=2.0 is shown by a solid line.

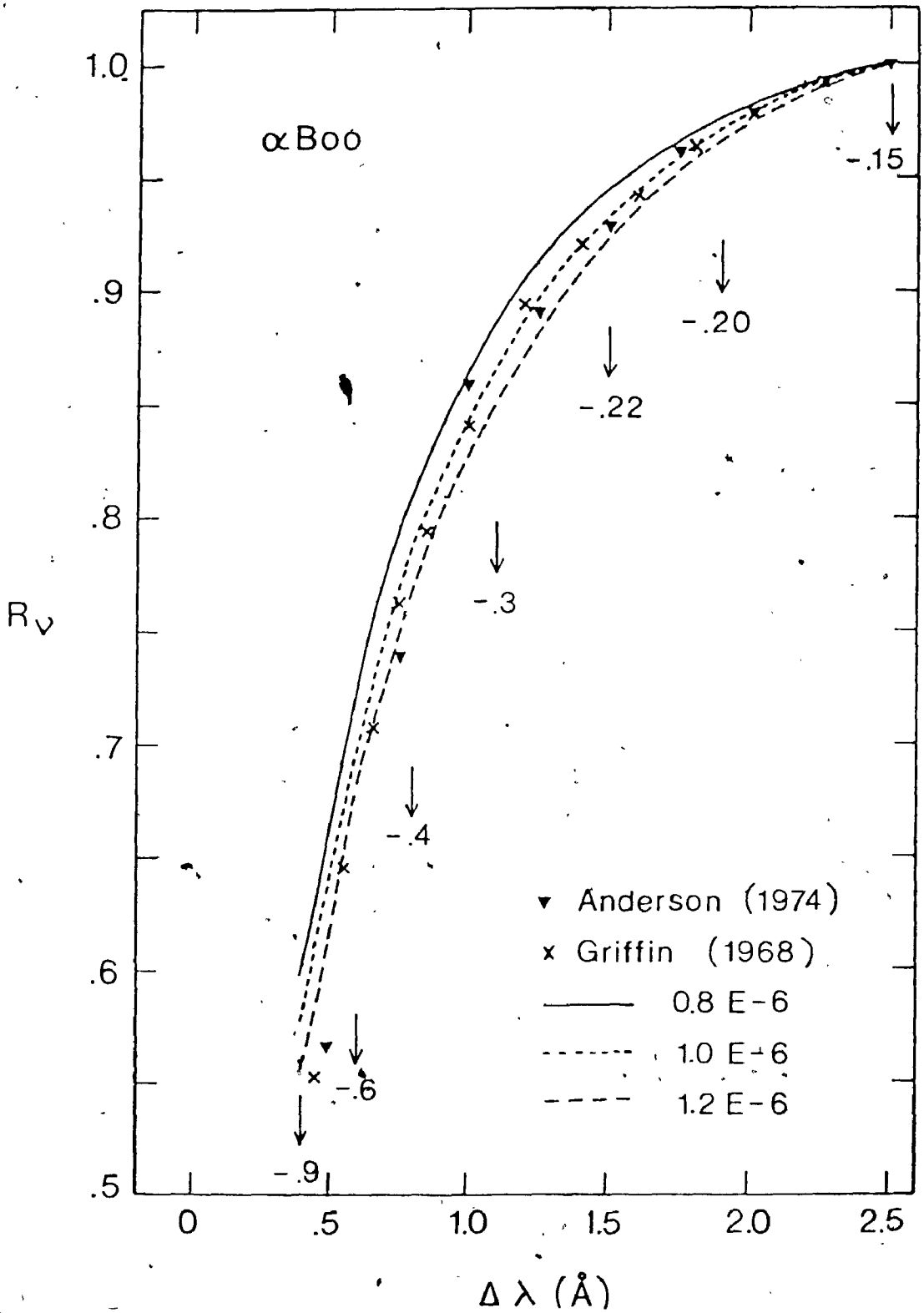

Fig. 4.3d. Determination of A_{Ca} for Arcturus. Anderson's and Griffin's observations Ca II λ8498 profile are shown respectively by triangles and crosses. Theoretical profiles are labeled after the A_{Ca} used in the line synthesis. The depth of formation of different parts of the profile are indicated by arrows.

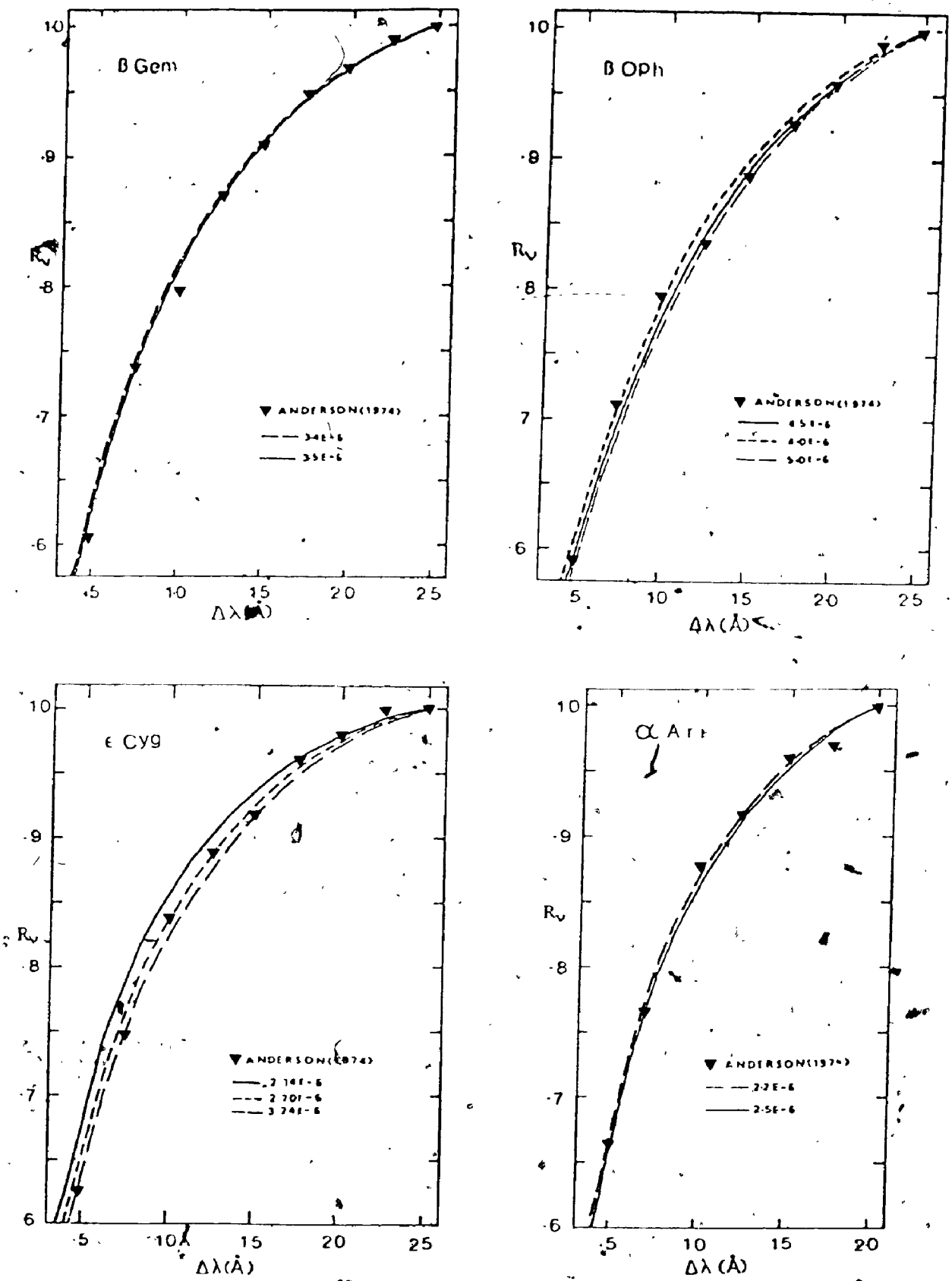

Figs. 4.3e-h. Determination of A_{Ca} for β Gem, ε Cyg, β Oph and α Ari. Anderson's Ca II λ8498 observations are shown by triangles. Theoretical profiles are labeled after the A_{Ca} used in the spectrum synthesis.

2 2

OF/DE

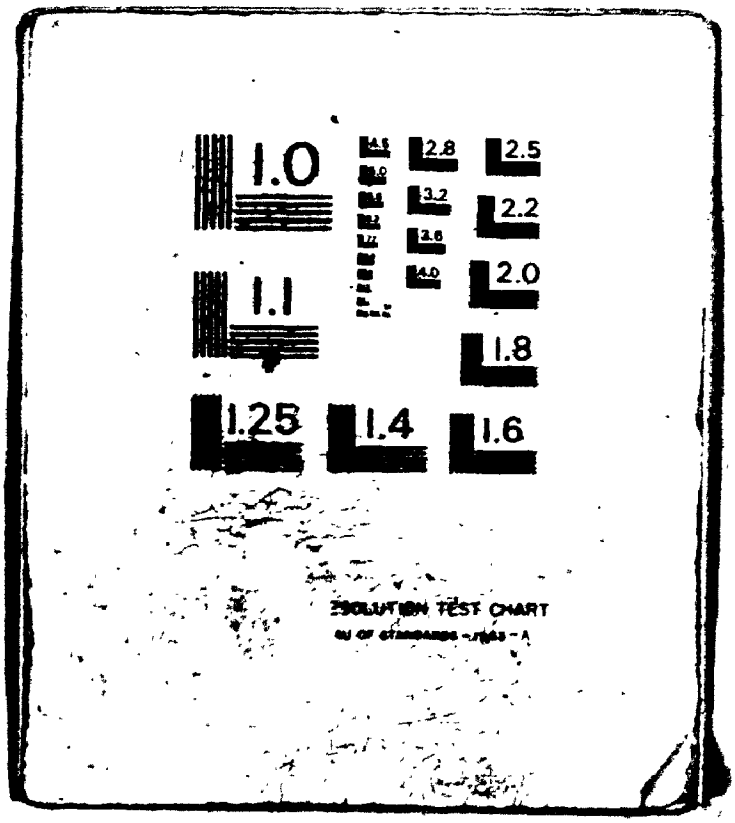

4.7. DETERMINATION OF A_{Ca}

In view of the discussion presented in the last chapter, the importance of deriving a Ca abundance consistent with the adopted continuum model can not be overemphasized. Here we use Anderson's (1974) Ca II λ8498 line profiles to derive the Ca abundance A_{Ca}. These line profiles were measured photoelectrically at a resolution of 0.28Å with the Washburn Observatory's 91cm reflector and have a quoted uncertainty of ~ 3%. Because of this high precision, they can be expected to yield reliable values of A_{Ca}. Moreover, the λ8498 wing ($\Delta\lambda$ >0.3Å) profile is entirely determined by the temperature distribution in the deeper layers ($-1.0 < \log\bar{\tau} < 0.0$) and is independent of the upper photospheric $T(\bar{\tau})$ model adopted for the star. This situation is illustrated in Fig.4.3d , wherein the arrows locate the $\bar{\tau}$ at which the contribution functions at different $\Delta\lambda$s are peaked in a model of Arcturus. However, Γ_6 for this line is not well known, and must be determined by an empirical calibration of the solar λ8498 profile, as has been done for the K line in the last chapter. For this purpose, we adopt the disk centre observations of de Jager & Neven (1967) and place them on the absolute intensity scale of Labs & Neckel (1968). These observations are shown by squares in Fig.4.3a. Also shown in this figure are the theoretical profiles synthesized with the HSRA model using an A_{Ca}=2.14E-6. Of the several such synthesized profiles corresponding to various van der Waals enhancement

factors, the one with an enhancement factor of 2.1 gives the best fit to the observations. The Ca II λ8498 and λ8542 lines arise from the same upper state and are expected to have equal van der Waals enhancement factors. So, it is interesting to derive an enhancement factor for the λ8542 line too. Fig.4.3b shows such an attempt. Hereagain, the squares represent de Jager & Neven's observations of the λ8542 profile placed on the absolute intensity scale of Labs & Neckel. Using the same continuum model and A_{Ca} as above, we have synthesized several theoretical profiles for various van der Waals enhancement factors. It is seen that an enhancement factor of 1.9 gives the best fit to the observations. This is in good agreement with Shine's (1973) value of 2 obtained with the same model. This is also in good agreement with 2.1 obtained above. Hereafter, we adopt a mean value of 2.0. This value reproduces Anderson's(1974) solar relative flux profile of λ8498 very well. This is shown in Fig.4.3c.

Using the above enhancement factor in combination with the continuum models derived in §4.5, we have varied A_{Ca} until we obtained good fits to Anderson's λ8498 profiles in our program stars. These calculations are shown in Figs. 4.3d–h respectively for αBoo, β Gem, ε Cyg, β Oph and α Ari. The values of A_{Ca} thus derived are listed in table 4.2. Unfortunately, α Ser and κ Oph were not observed by Anderson, so we can not derive their A_{Ca}s in the same manner. It is interesting to compare our values of A_{Ca}

with the ones determined from reliable curve of growth analyses. Thus, Griffin (1976), Mackle et al. (1975) and Oinas (1974) respectively derive A_{Ca} = 2.4±0.3E-6, 0.76±0.2E-6 and 2.6±0.35E-6 for β Gem, α Boo, α Ari. These values are to be contrasted respectively with A_{Ca}= 3.5E-6, 1.0E-6 and 2.2E-6 obtained for the same stars in the present analysis.

The continuum models and the Ca abundances derived in in this chapter constitute important background information upon which our upper photospheric $T(\bar{\tau})$ models will be based. The derivation of these models forms the subject matter of the next chapter.

CHAPTER V

TEMPERATURE ENHANCEMENT MODELS

Using the theory and background information contained in Chaps. III & IV we are in a position to derive the upper photospheric $T(\bar{\tau})$ models. Here our approach will be to adopt the $T(\bar{\tau})$ distribution derived from the continuum data as the "Basic Temperature Model" or BTM for short, but alter it in the upper photosphere ($\log \bar{\tau} < -1.0$) to force agreement between the observed and computed K line inner wing profiles. Such altered BTMs will hereafter be called the "Temperature Enhancement Models" or TEMs in short. An implication of this approach is to assume that the BTM correctly characterizes the $T(\bar{\tau})$ distribution of the deeper layers ($\log \bar{\tau} > -1.0$) where the far wing profile is formed, so that this profile can be synthesized using the BTM in combination with the theory outlined in Chap. III and relevant atomic data. However, we have seen in §3.4 that such computations overestimate the far wing flux unless an opacity enhancement factor E_c is incorporated. So, we include an E_c in our computations to guarantee agreement in the far wings. Thus, having fixed BTM, A_{Ca} and g, we attribute all the deviations in the far wings to the missing opacity. This is a reasonable procedure because other effects such as the partial coherency have negligible influence on the far wing formation. In summary, our approach to derive TEMs consists of the following steps:

a) Given the BTM, A_{Ca} and g, synthesize the K wing adjusting E_C until the observed and computed far wing profiles agree.

b) Even when agreement is obtained in the far wings, the theoretical inner wing profiles lie below the observed ones due to the importance of the partial coherency effects in the upper photosphere, coupled with the fact that the RE models (BTMs) that fit the optical continuum data are generally cooler in these layers. So, in order to force agreement raise the temperature in the shallower layers which gives TEM. This TEM is then believed to charecterise the temperature structure of the upper photosphere.

5.1. TEM FOR THE SUN

Our intent in deriving a TEM for the Sun is to check our computer program rather than to obtain fundamental information about the Sun. Here we use the K line observations of White & Suemoto (1968) and Shine (1973) placed on the absolute intensity scale of Houtgast (1970). These observations were described in Chap.III, where we have also determined E_6=1.2, E_C=1.13 for KREO and E_6=1.45, E_C=1.04 for HSRA. Given these and A_{Ca}=2.14E-6, our purpose here is to derive TEMs adopting KREO and HSRA as our BTMs. Figs.5.1 & 5.2 show such attempts. In both figures the dashed line is obtained with the BTM (i.e., with the original KREO and HSRA $T(\bar{\tau})$ models), which conspicuously deviates from the observations for $\Delta\lambda \lesssim 3$Å. So, in order to force agreement at these $\Delta\lambda$s we introduce the TEMs shown in Fig.5.3. These are

obtained by linearly (in log $\bar{\tau}$) enhancing the temperature between the points P1 and P2, where P1 corresponds to the log $\bar{\tau}$ at which the contribution function of the farthest deviating $\Delta\lambda$ is peaked, while P2 is usually located at the log $\bar{\tau}$ corresponding to the T_{min} (temperature minimum). Above P2 the temperature is kept at T_{min}. The profiles synthesized with the TEMs are in good agreement with the observations and are shown by solid lines in Figs.5.1 & 5.2. P1 is located at log $\bar{\tau}$ = -0.83, T = 5140K in KREo, and at log $\bar{\tau}$ = -1.1, T = 5080K in HSRA, and P2 at log $\bar{\tau}$ = -4.0, T = 4300K in both models. These TEMs are shown by solid lines Fig.5.3. The insert in this figure shows the TEMs at a higher resolution in T. The solid line in the insert shows the TEMs for both KREo and HSRA (which are identical for log $\bar{\tau}$<-1.1), while the dashed line represents the TEM (T_{min}= 4300) for KREo obtained by Ayres (1975), which best fits the inner wing in the range 0.6Å <$\Delta\lambda$< 3Å. We consider the agreement between ours and Ayres' TEMs to be very good, the differences being ∿20K at most. Hence, we conclude that our line synthesis routine can be trusted to give accurate results. However, our program stars are more like Arcturus in T_e and g than the Sun. As the partial coherency effects become more pronounced at the low gravities of these stars, it is important to confirm that our program handles these effects properly. To this end we analyse Arcturus and demonstrate that our results are in good agreement with those obtained by Ayres & Linsky (1975).

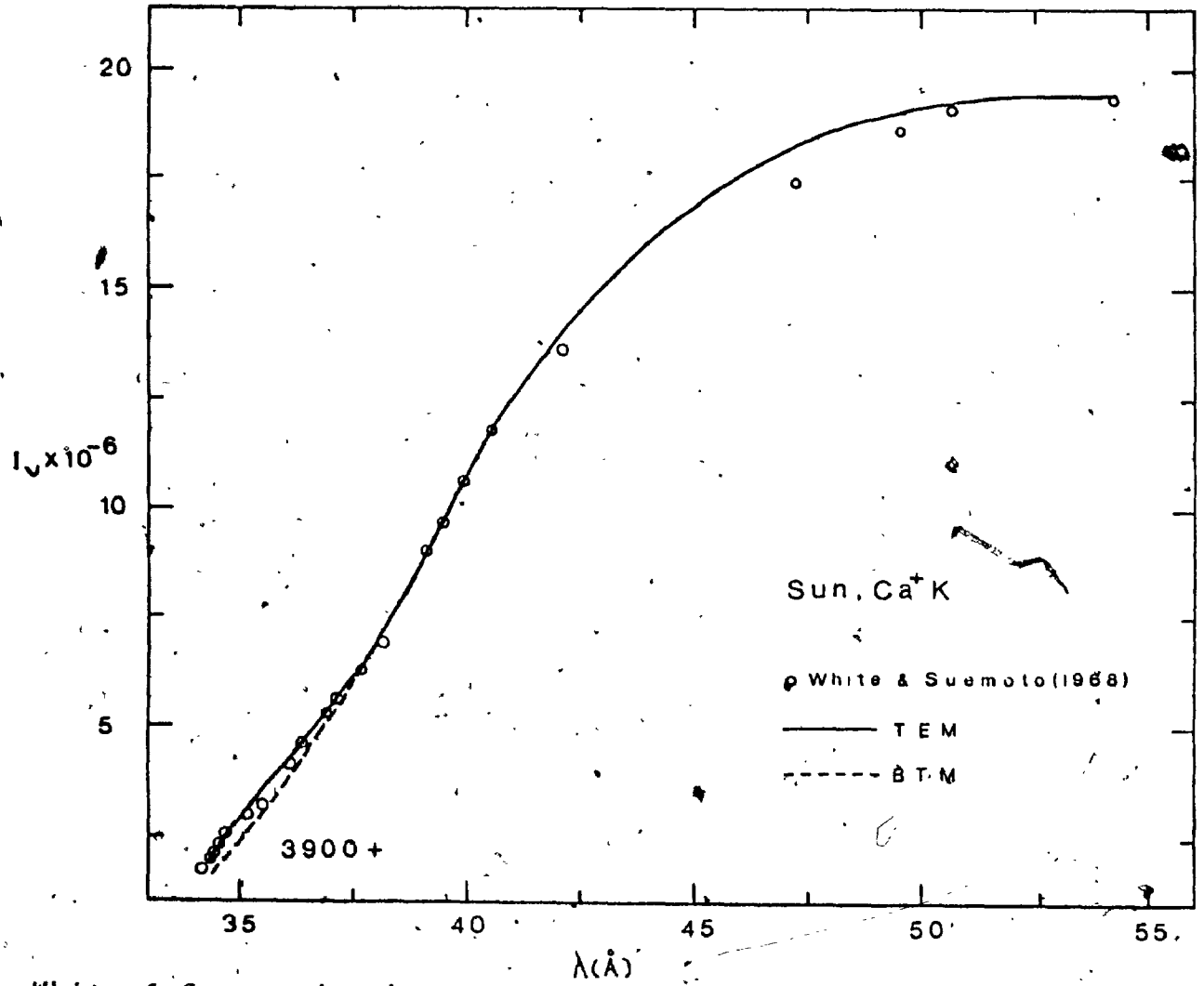

Fig.5.1. White & Suemoto's observations of the solar K line profile are shown by circles. The profiles synthesized with KREe and TEM(-0.83,5140; -4.0,4300) are shown by the dashed and solid lines respectively.

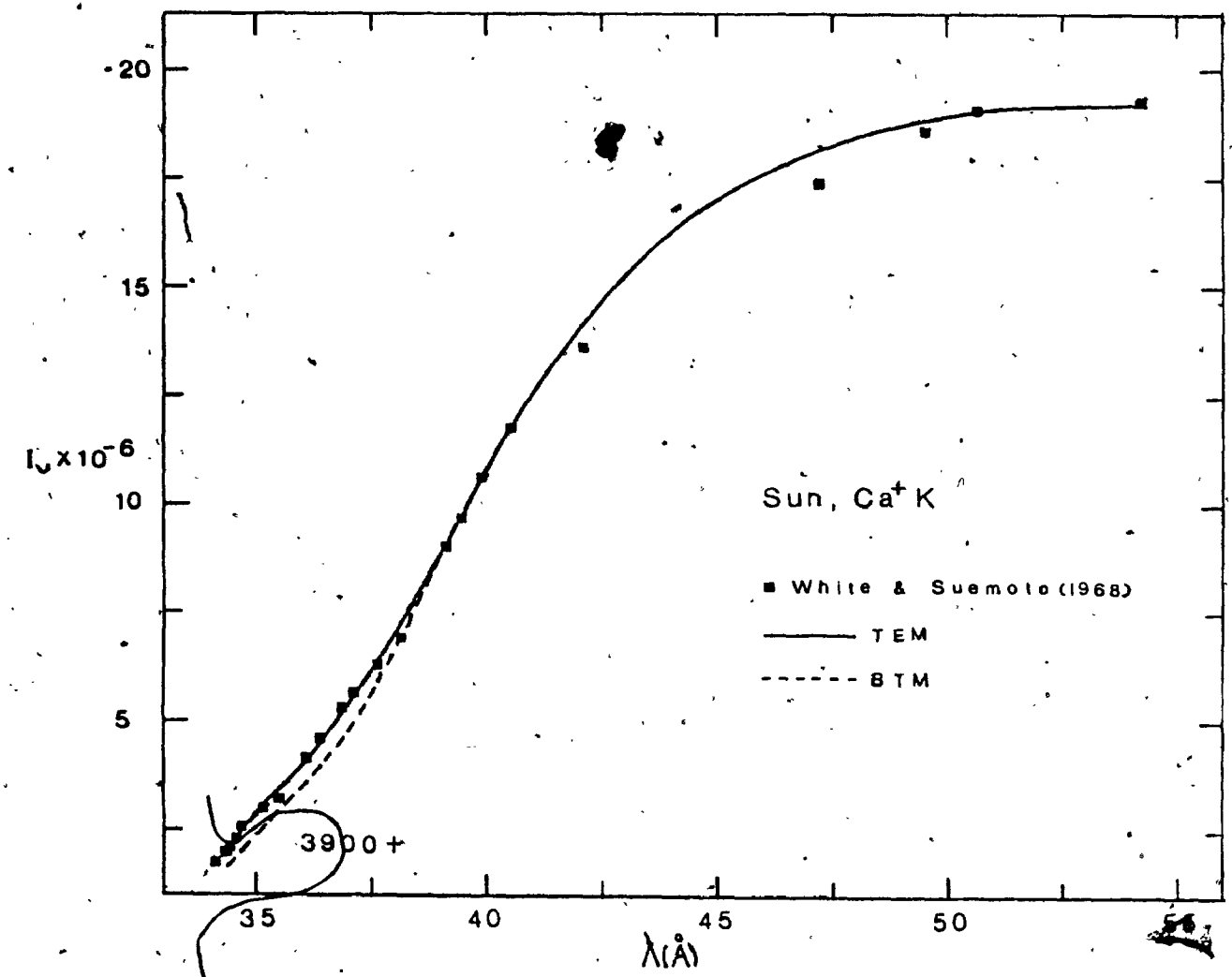

Fig.5.2. White & Suemoto's observations of the solar K line profile are shown by squares. The profiles synthesized with HSRA and TEM(-1.1,5080; -4.0,4300) are shown by dashed and solid lines respectively.

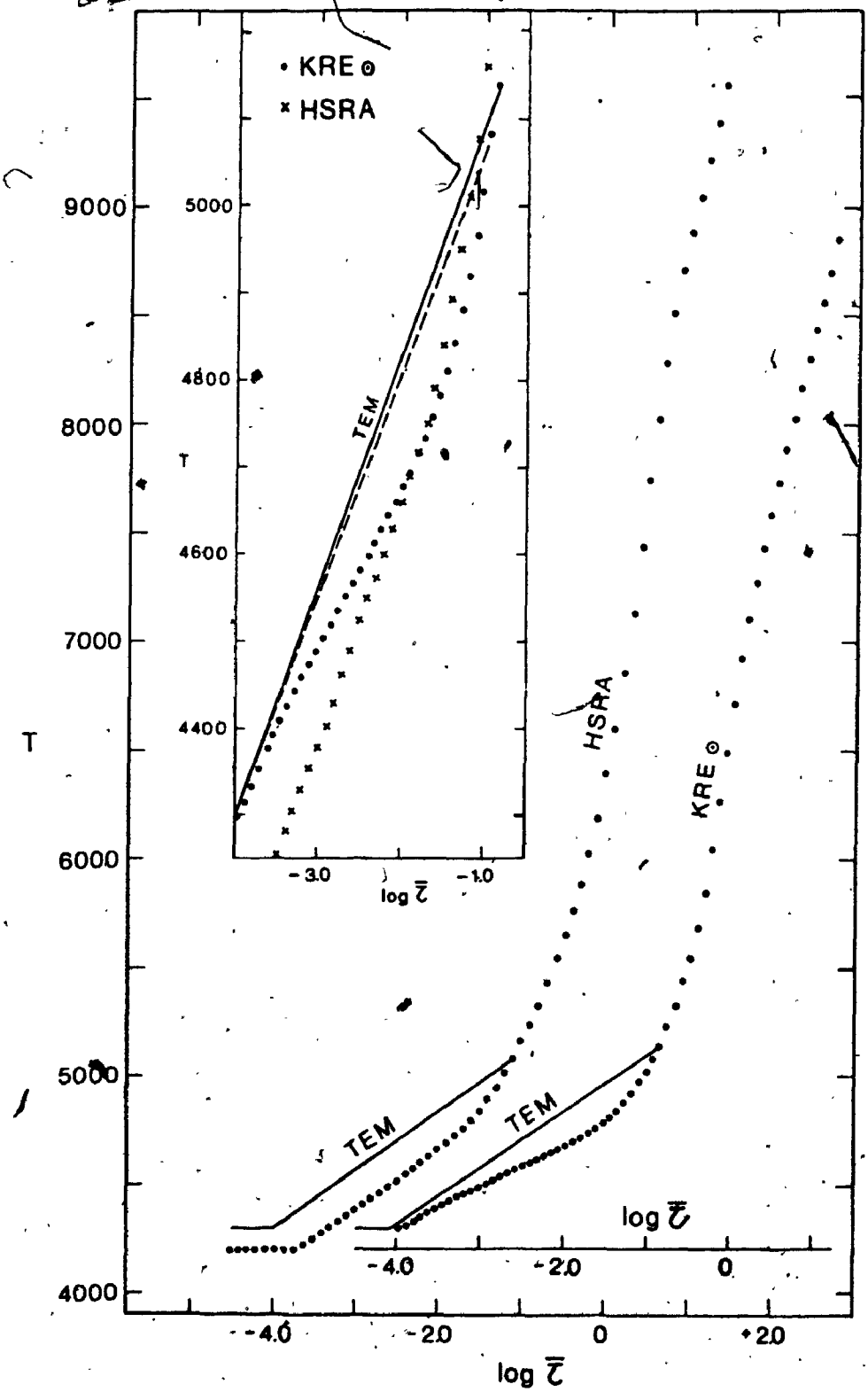

Fig.5.3. Temperature enhancement models for the Sun. Solid line represents our model, while Ayres model is shown by a dashed line.

5.2. TEM FOR ARCTURUS

Since we intend to compare our results with those obtained by Ayres & Linsky, it is worthwhile to summarise their results first. Ayres & Linsky have obtained an absolute flux calibration of Griffin's (1968) K line profile by correcting the apparent narrow band flux measurements of Willstrop (1964) in the vicinity of the K line for the effect of the geometrical dilution factor $(R^*/d^*)^2$ where R^* and d^* are the radius and distance of the star respectively. The estimated uncertainty in this calibration is $\sim$30%, which arises from errors in Willstrop's photometry, line blocking corrections, R^* and d^*. By relating the H & K wing absolute fluxes to T through the Eddington-Barbier relation, Ayres & Linsky have derived a NCS-TEM and also a PCS-TEM after correcting the NCS-TEM for partial coherency effects. These temperature models are shown in Fig.5.4, wherein the crosses represent the PCS-TEM while the circles and squares denote the NCS-TEMs obtained from the H & K wings respectively.

Our derivation of a PCS-TEM for Arcturus proceeds as follows. Using the brightness temperature $T_B(\Delta\lambda)$ given by Ayres & Linsky and the relation

$$F_\nu(\Delta\lambda) = \pi B_\nu(T_B(\Delta\lambda)) \qquad (5.1)$$

where $F_\nu(\Delta\lambda)$ denotes the absolute flux at $\Delta\lambda$, we place Griffin's Arcturus K line profile on the absolute scale of Ayres & Linsky. This profile is shown in Fig.5.5. This calibration gives an absolute flux, F_ν=2.12E-6 ergs cm^{-2} sec^{-1}hz^{-1}

in the window at λ3950.8Å. This value is about 1.7 times smaller than F_ν=3.536E-6 ergs cm^{-2} sec^{-1} hz^{-1} predicted by BTM*(Bell et al.,4250,1.7,0.33) that best fits the continuum data (cf. Chap.IV). We attribute this discrepancy to the missing opacity and introduce an E_c=1.96 such that the observed and computed window fluxes agree. The K line profile synthesized with the BTM incorporating this E_c and A_{Ca}=6.42E-7 (same as Ayres & Linsky's) is shown by a dashed line in Fig.5.5. This profile agrees well with the observations in the far wing, but systematically falls below the observations in the inner wing. Similar behavior was noticed in the case of the Sun (§5.1), but it is more pronounced in Arcturus because of its low gravity. We attribute this deviation to cooler temperatures in the BTM upper photosphere and introduce TEMs to force agreement in the inner wing. The best fitting three point (P1,P2,P3) TEM is shown by a dot-dashed line in Fig.5.4. In this model P1, P2 and P3 are respectively located at (-1.5, 3526K), (-3.5, 3275K) and (-4.0, 3160K), where the bracketed quantities represent log $\bar{\tau}$ and T at a given point P_i. This TEM has to be compared with Ayres & Linsky's PCS-TEM, shown by crosses in Fig.5.4. It is seen that the agreement between these two models is very good in the range -3.8 <log $\bar{\tau}$<-1.5, where the inner wing is formed. Also, the log $\bar{\tau}(T_{min})$=-3.8 and T_{min}=4210K in our model are in good accord with the corresponding values of -3.72 and 4200K in

* Hereafter we parameterise a BTM by specifying the source of the initial $T(\bar{\tau})$ distribution, T_e, log g, and metal content relative to the Sun.

Ayres & Linsky's model. Above T_{min}, our model differs from theirs in not incorporating the chromospheric temperature rise as we do not attempt to synthesize the K2 emission peaks. Noninclusion of this temperature rise has little effect on the derived TEMs, because as shown by Shine et al. (1975a) the K1 source function becomes decoupled from the core source function and monotonically decreases outward even in the presence of a chromospheric temperature rise. In other words, the K1 source function is insensitive to the chromospheric temperature rise. This is illustrated in Fig. 5.6, taken from their paper.

In conclusion, our upper photospheric $T(\bar{\tau})$ model for Arcturus is in very good agreement with a similar model obtained by Ayres & Linsky, hence our line synthesis routine can be trusted to give correct results for our program stars which are similar to Arcturus.

5.3. DETERMINATION OF E_c FROM RELATIVE FLUX PROFILES

Independent absolute flux calibrations of the observed K line profiles are not available for our program stars. So, we can not derive E_c by forcing agreement between the observed and computed absolute window fluxes as done above. Instead, we have to determine E_c by matching the observed and computed far wing relative flux profiles. Unfortunately, the entire far wing is not usable for this purpose as it is badly cut up by numerous intervening absorption lines beyond λ3940.5Å. So, our determination of E_c rests on the fit obtained for the "usable" far wing segment between λ3939-3940.2Å.

Fig.5.7 shows the determination of E_c for Arcturus according to this procedure. The squares in this figure represent Griffin's Arcturus atlas K line profile convolved with our 0.5Å and 0.2Å instrumental profiles and normalised to the window. The dashed line represents the theoretical profile synthesized with the BTM(Bell et al.,4250,1.7,0.33) together with A_{Ca}=6.42E-7 and E_c=1.98, which gives the best fit to the far wing segment between λ3939-3940.2Å. This E_c is practically identical to the value 1.96 obtained in §5.2 by matching the absolute fluxes in the window, and this identity completely justifies the above determination of E_c from the "usable" far wing segment. For completeness, we have also shown in Fig.5.7 the relative flux profile (solid line) synthesized with the TEM derived in §5.2. We recall that this TEM was derived to provide good fit to the inner wing of Griffin's high (27mÅ) resolution absolute flux profile shown in Fig.5.5. It is clear from Fig.5.7 that this TEM also provides a good fit (except at K1) to the inner wing of Griffin's low (0.5Å) resolution relative flux profile. This agreement implies: a) the TEMs derivable from our relative flux approach are consistent with those derived from the absolute flux calibrations of Ayres & Linsky; b) the low (0.5Å) resolution of our observations does not introduce any systematic errors in the derived TEMs except in the T_{min} region where the K1 feature is formed. The low resolution fills in the K1 minimum by the spill over flux from the adjacent regions, thus raising the K1 relative flux by ∿25%

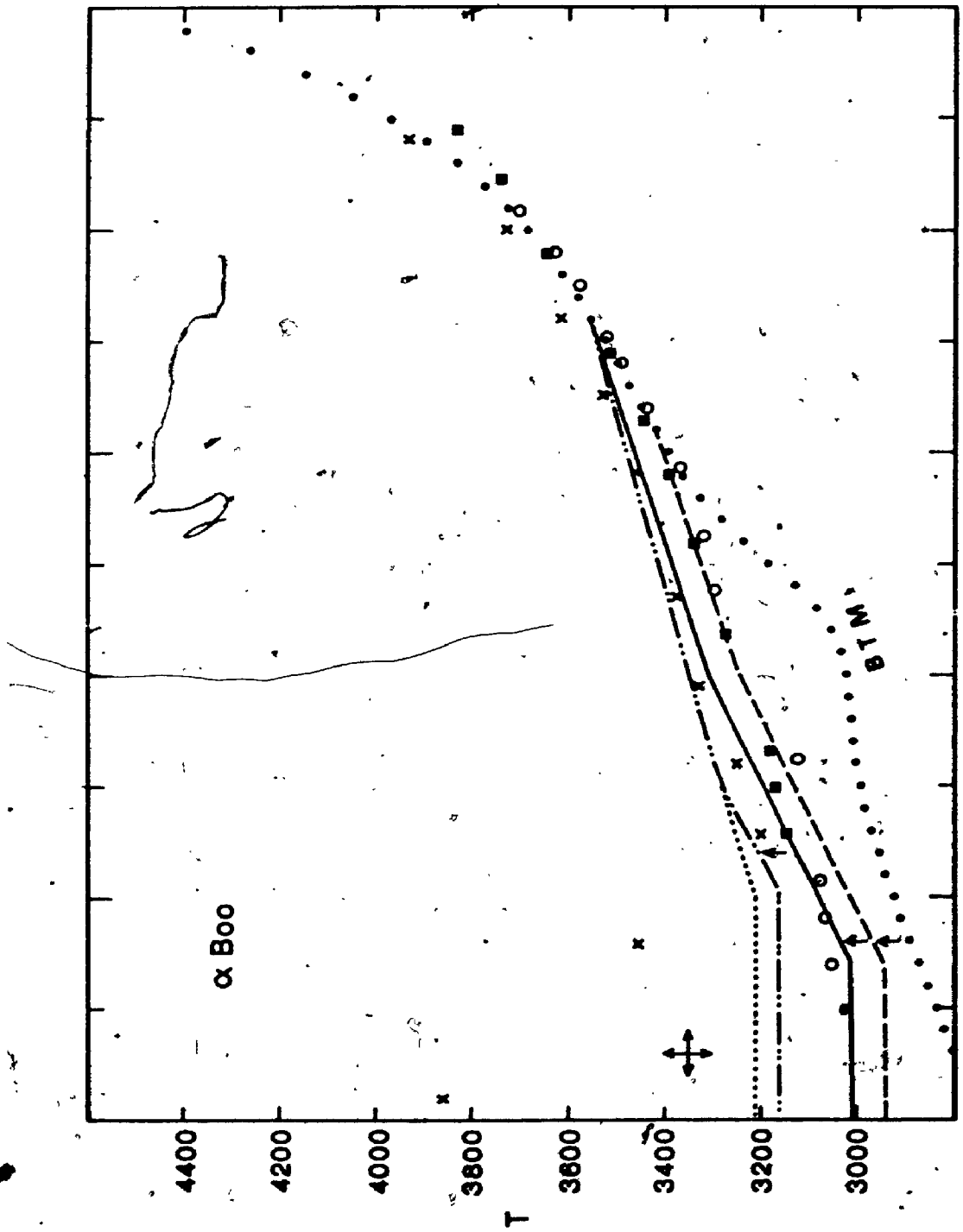

Fig 5.4. Temperature models for Arcturus.

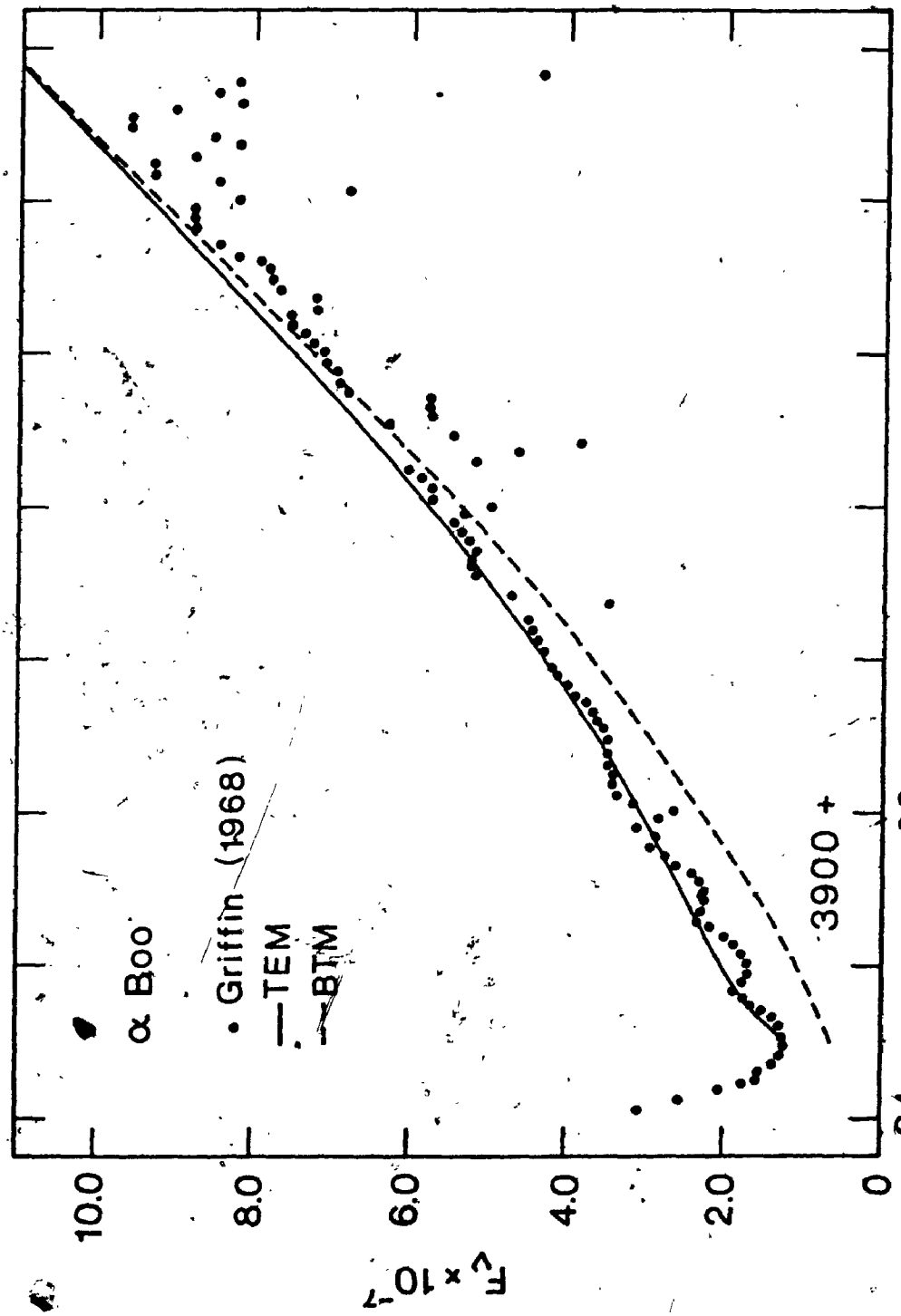

Fig.5.5. Griffin's high resolution K line profile of Arcturus is shown by dots. The dashed line represnts the theoretical profile obtained using BTM, while the solid line represents that obtained using TEM(-1.5,3526; -3.5,3275; -4.0,3160).

Fig.5.6 (Taken from Shine et al.,1975a)

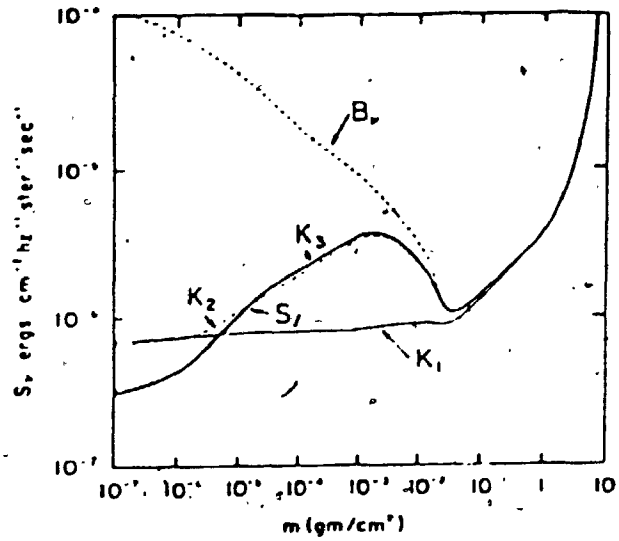

Source functions for the K line for a five-level atom in model 1. The CRD source function is labeled S_1; the Planck function is labeled B; the PRD source functions are labeled K_1, K_2, and K_3 for the appropriate wavelength positions in the line.

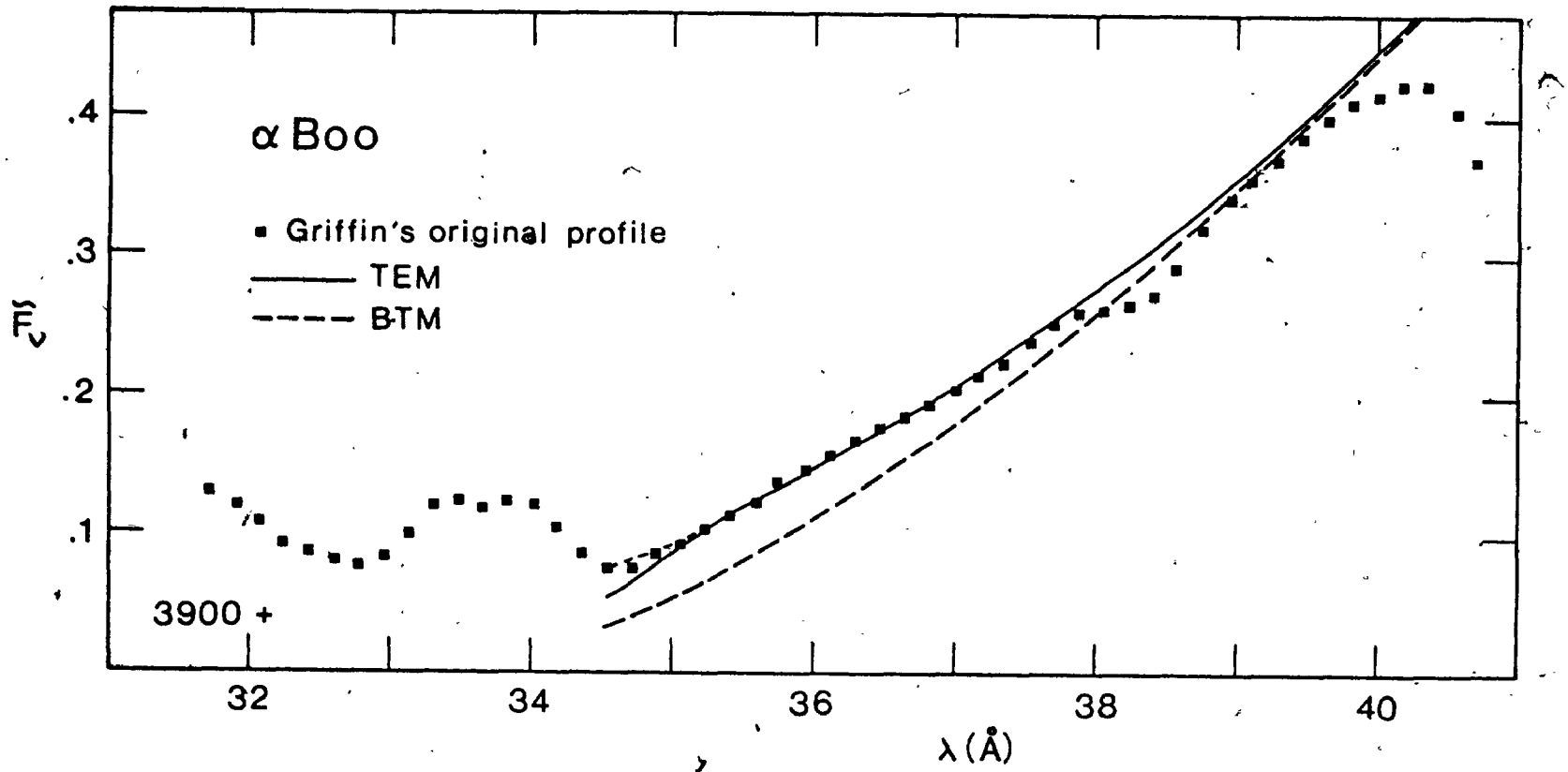

Fig.5.7. Squares represent Griffin's Arcturus atlas K line profile convolved with our instrumental profiles and normalised to the window at λ3950.8Å.The dashed line represents the profile synthesized with BTM(Bell et al.,4250,1.7,0.33), using an E_c=1.98 and an A_{Ca}= 0.642E-6. The solid line represents the profile synthesized with TEM(-1.5,3526; -3.5,3275; -4.0,3160), while the small-dashed line is the profile obtained with TEM(-1.5,3526; -3.5, 3275; -4.0,3220)

in the case of the low resolution profile of Arcturus in Fig.5.7. However, this effect rapidly diminishes away from K1, and at $\Delta\lambda$ = +0.17Å from K1 it is only ≃3%. This is reflected in the nature of the discrepancy found between the observed (squares) and computed (solid line) profiles near K1 in Fig.5.7. So, in order to fit the low resolution observations at K1, we have to enhance the temperatures of the T_{min} region in the above TEM by ∿50K. These temperature enhancements and the resulting fit at K1 are shown by small dashed lines in Figs.5.4 & 5.7 respectively. In conclusion, therefore, our low resolution leads to an overestimate of T_{min} by ∿50K in case of Arcturus.

5.4. EFFECT OF E_c ON THE ABSOLUTE AND RELATIVE FLUX PROFILES

The acceptable values of E_c for some of our program stars are as large as 2.4. Although E_c can be consistently determined (cf.§5.3) for a given BTM and A_{Ca}, it can be erroneous if these data are incorrect. So, it is important to investigate the effect of E_c on the absolute and relative flux profiles. In Fig.5.8 we have plotted the absolute flux ratio $F_\nu(E_c=1.0)/F_\nu(E_c=2.38)$ in the K wing in a model of Arcturus. It is seen that in the inner wing the flux ratio deviates only slightly from unity, implying that an E_c as large as 2.38 has only a small effect on the emergent fluxes. On the other hand, the flux ratio rapidly deviates from unity in the far wing (λ > 3939Å), and in the window $F_\nu(E_c=2.38)$ is only 60% of the $F_\nu(E_c=1.0)$. This behavior justifies the derivation of E_c from the far wing as in §5.3.

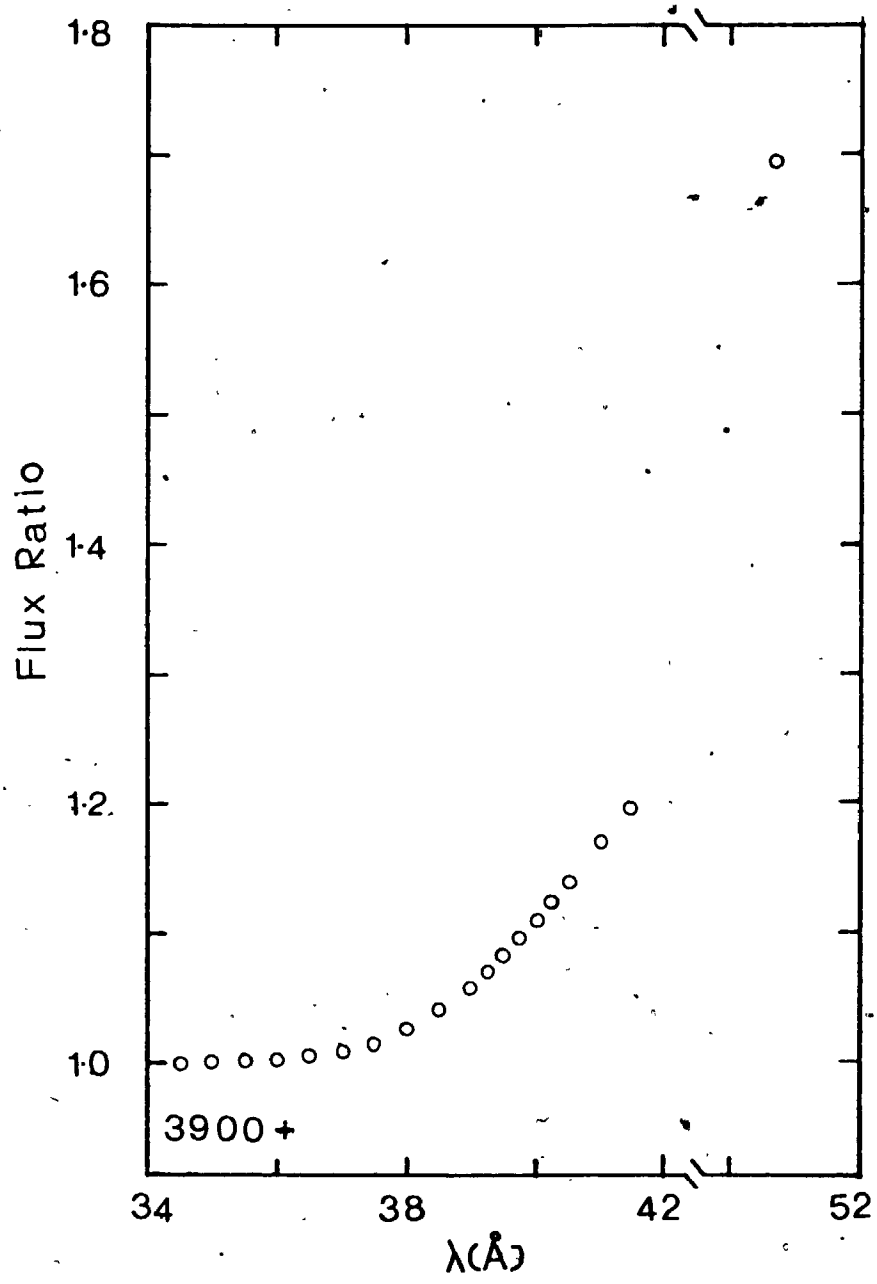

Fig.5.8. Plot of the flux ratio $F_\nu(E_c=1.0)/F_\nu(E_c=2.38)$ in the K wing in a model of Arcturus.

However, this also makes the relative flux profile(normalised to the window) more directly dependent upon the errors in E_c than the absolute flux profile. This underlines the importance of determining E_c as accurately as possible. Despite this sensitivity of the relative flux profile, $\tilde{F}_\nu$, to the errors in E_c, it turns out that the TEMs derived from this profile are no less accurate than those derived from the inner wing absolute fluxes (F_νs). This can be understood if we can attribute most of the uncertainty in E_c to errors in A_{Ca}, which is a good assumption in view of the strong dependence of E_c on A_{Ca} (cf. 3.4). To make further progress we must consider the $A_{Ca} \rightarrow E_c \rightarrow \tilde{F}_\nu$ dependence more explicitly, which is done in the next section.

5.5. EFFECT OF ERROR IN A_{Ca} ON THE TEMs

If one uses absolute fluxes to derive TEMs, these are hotter or cooler depending upon whether the adopted A_{Ca} is smaller or greater than the "correct" A_{Ca}. On the other hand, if one uses relative fluxes incorporating E_c, the situation is no longer as clear as this. In Chap.III we have seen that both κ_ν^K and E_c change in direct relation to a change in A_{Ca}, and these changes determine the relative flux profiles. In Fig.5.9, in a model of Arcturus, we have shown the relative flux profiles for various A_{Ca}s, and the E_cs consistent with these A_{Ca}s. One interesting result in this figure is that the relative flux profile is stronger the lower the A_{Ca}, in contrast to the absolute flux profiles shown in Fig.5.10 (upper). Thus, using the relative flux

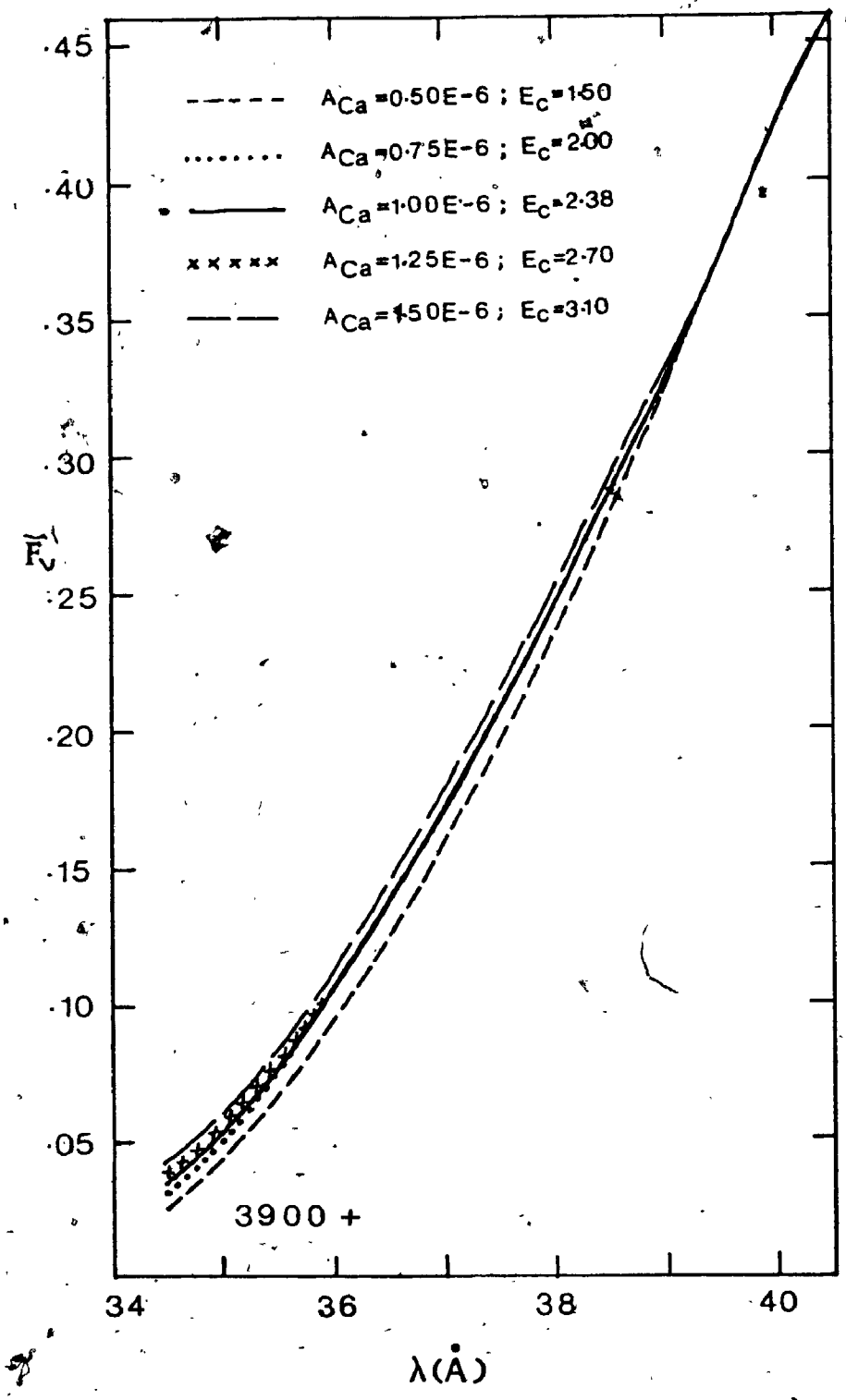

Fig.5.9. Behavior of the relative flux profiles of Ca II K as A_{Ca} is varied in a model of Arcturus. In each case an appropriate value of E_c is included to force agreement between different profiles in the "usable" far wing segment.

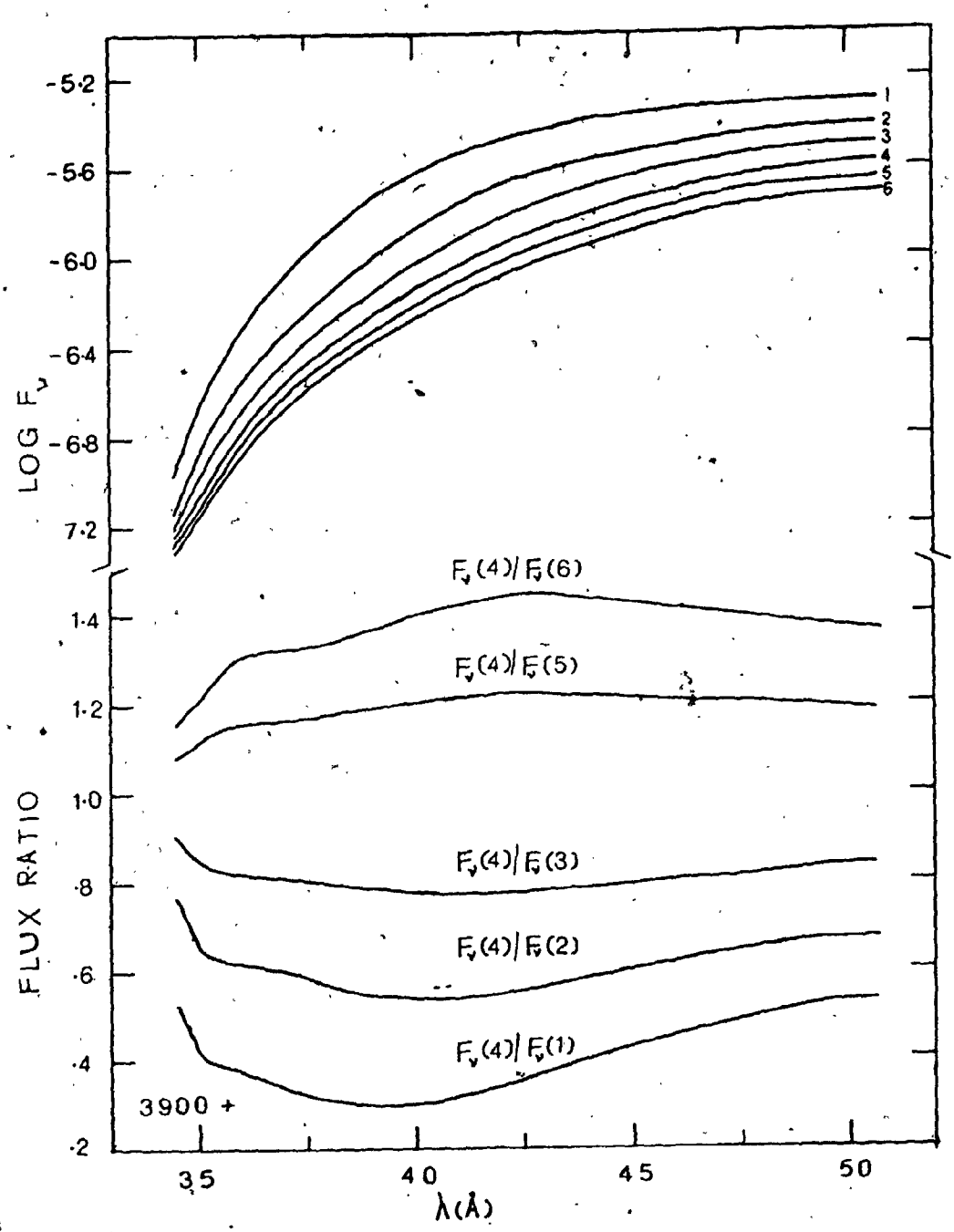

Fig.5.10. Absolute flux profiles of the K wing for various values of A_{Ca} in a model of Arcturus. The numbers denote the following A_{Ca}s: 1, A_{Ca}=0.25E-6; 2, A_{Ca}=0.50E-6; 3, A_{Ca}=0.75 E-6; 4, A_{Ca}=1.0E-6; 5, A_{Ca}=1.25E-6; 6, A_{Ca}=1.50E-6. The lower panel of this figure contains the flux ratios $F_\nu(A_{Ca}=1.0E-6)/F_\nu(A_{Ca}=x)$.

profiles as prescribed here, one obtains hotter or cooler TEMs depending upon whether the A_{Ca} is under or over-estimated. This is once again in contrast to the case using the absolute fluxes and can be understood as follows. In the upper panel of Fig.5.10 we have shown the absolute flux profiles without incorporating the opacity enhancement (i.e., E_c=1) for various values of A_{Ca}. In the lower panel we have shown the flux ratios $F_\nu(A_{Ca}=1.0E-6)/F_\nu(A_{Ca}=x)$. These reflect the changes in the shapes of the profiles as A_{Ca} is varied from A_{Ca}=1.0E-6. Suppose that the observed "usable" far wing segment is well fitted by the theoretical profile corresponding to the "correct" A_{Ca}=1.0E-6. Given this, let us explore what happens if we erroneously use an A_{Ca} different from this "correct" value. Firstly, suppose that we have underestimated A_{Ca}, i.e., used an A_{Ca}=0.5E-6 instead of 1.0E-6 for example. In this case, we have to include an E_c such that the whole profile is lowered by $\sim$0.55. While this operation fits the far wing segment very well, it also lowers the inner wing and part of the far wing (λ >3943Å) in relation to the "correct" profile with A_{Ca}=1.0E-6. This happens because in the inner wing and in the far wing with λ> 3943Å, the flux ratio $F_\nu(A_{Ca}=1.0E-6)/F_\nu(A_{Ca}=0.5E-6)>$ 0.55. On the other hand, if we have overestimated A_{Ca}, i.e., used A_{Ca}=1.5E-6 instead of 1.0E-6 for example, the reverse will happen. In this case we have to include an E_c such that the whole profile is raised by a factor $\sim$1.4. While this gives good fit to the far wing segment, this also raises

the inner wing and part of the far wing with $\lambda > 3948\text{Å}$, in relation to the correct profile with A_{Ca}=1.0E-6. This happens because the ratio $F_\nu(A_{Ca}=1.0E-6)/F_\nu(A_{Ca}=1.5E-6)<1.4$ in the inner wing and in the far wing with $\lambda>3948\text{Å}$ (cf.Fig. 5.10). To sum up, an error in A_{Ca} affects the absolute flux profile through its effect on κ_ν^K, while it affects the relative flux profile through its effect both on κ_ν^K and E_c. This underlines the necessity of using an accurate A_{Ca} in the spectrum synthesis. However, we would like to know the tolerances on the accuracy of A_{Ca}, and in particular if for a given error in A_{Ca} the relative flux approach leads to an error of the same magnitude as the absolute flux method. Sample calculations have shown that both methods lead to comparable errors for $\Delta\lambda<1.5\text{Å}$, while for $\Delta\lambda>1.5\text{Å}$ the relative flux method is less sensitive to an error in A_{Ca}. This follows from the similarity of the flux ratios for $\Delta\lambda>1.5\text{Å}$ (cf.Fig.5.10), and also from the fact that whatever A_{Ca} is adopted, we incorporate an E_c to force agreement with the observations near $\lambda 3939\text{Å}$. In all, it is heartening to see that the relative flux approach is no more sensitive to an error in A_{Ca} than the absolute flux method.

5.6. TEM FOR ARCTURUS USING AN A_{Ca}=1.0E-6

In Chap.IV we have derived an A_{Ca}=1.0E-6 for Arcturus from the Ca II λ8498 far wing profile of Anderson (1974). On the other hand, Ayres & Linsky (1975) have adopted an A_{Ca}=0.642E-6, and from an extensive curve of growth analysis Mackle et al. (1976) have obtained a value of 0.75±0.2E-6.

Ours and Ayres & Linsky's values constitute the upper and lower bounds implied by the analysis of Mackle et al., and in this sense they are not inconsistent. In any case, we feel that the A_{Ca}s determined to be consistent with our adopted BTMs in Chap.IV are to be preferred to the values available in the literature which are often based upon quite different BTMs. The λ8498 line profiles of Anderson, upon which our A_{Ca}s are based appear to be free of systematic errors as witnessed by the good agreement between his and Griffin's (1968) data for Arcturus (cf.Fig.4.3d). Hence, in this section we adopt an A_{Ca}=1.0E-6 for Arcturus and see how the resulting TEM differs from the one obtained in §5.2. Using this A_{Ca} we obtain an E_c=2.35 instead of the value (1.96) derived in §5.2 with Ayres & Linsky's A_{Ca}. The TEM that best fits Griffin's original (uncorrected for scattered light) low resolution K line profile is shown by a solid line in Fig.5.4. The profiles synthesized with this TEM and the BTM are compared with the observations in Fig.5.11. In accordance with the discussion in §5.5, we derive a cooler TEM by using A_{Ca}=1.0E-6 instead of 0.642E-6. Also, the depth of formation of the line moves outward in the atmosphere as we increase A_{Ca} (cf.§6.5c), hence we obtain a T_{min}=3030K and $\log \bar{\tau}(T_{min})$=-4.27 instead of the values 3210K and -3.8 derived in §5.2. Physically, an increase in A_{Ca} results in increased line opacity, hence in decreased contribution from the deeper layers to the emergent flux at a given Δλ. This is why the contribution functions peak at

shallower optical depths as we increase A_{Ca}. More about this will be said in the next chapter. In conclusion, we obtain a cooler TEM and a lower T_{min} and $\bar{\tau}(T_{min})$ by using A_{Ca}=1.0E-6 instead of A_{Ca}=0.642E-6 used by Ayres & Linsky.

In Chap.II we have seen that Griffin's observations are affected by ∿2% scattered light. So, it is more meaningful to derive a TEM after correcting his data for this effect. After this correction, his data agree very well with our own data for Arcturus as shown in Fig.5.12, where we have also shown the profiles synthesized with the BTM and the best fitting TEM. We derive an E_c=2.26 instead of a slightly higher value (2.35) obtained above from the uncorrected observations. The TEM itself is shown by a dashed line in Fig.5.4. It is clear from a comparison of this TEM with the TEM derived above from the uncorrected data that the ∿2% scattered light leads to a systematic overestimate of the upper photospheric temperature by ∿65K. Thus we derive a T_{min}=2965K located at $\log \bar{\tau}(T_{min})$=-4.27, instead of the T_{min}=3030K located at the same $\log \bar{\tau}(T_{min})$ obtained above from the uncorrected data.

The E_cs of 2.35 and 2.26 determined above are larger than the E_c=1.96 derived in §5.2. So, it is interesting to see how these larger E_cs affect the theoretical emergent fluxes in the window. We have

$F_\nu(\lambda 3950.8\text{Å})$=1.602E-6 ergs cm^{-2} sec^{-1} hz^{-1} for E_c=2.35,

and $F_\nu(\lambda 3950.8\text{Å})$=1.638E-6 ergs cm^{-2} sec^{-1} hz^{-1} for E_c=2.26,

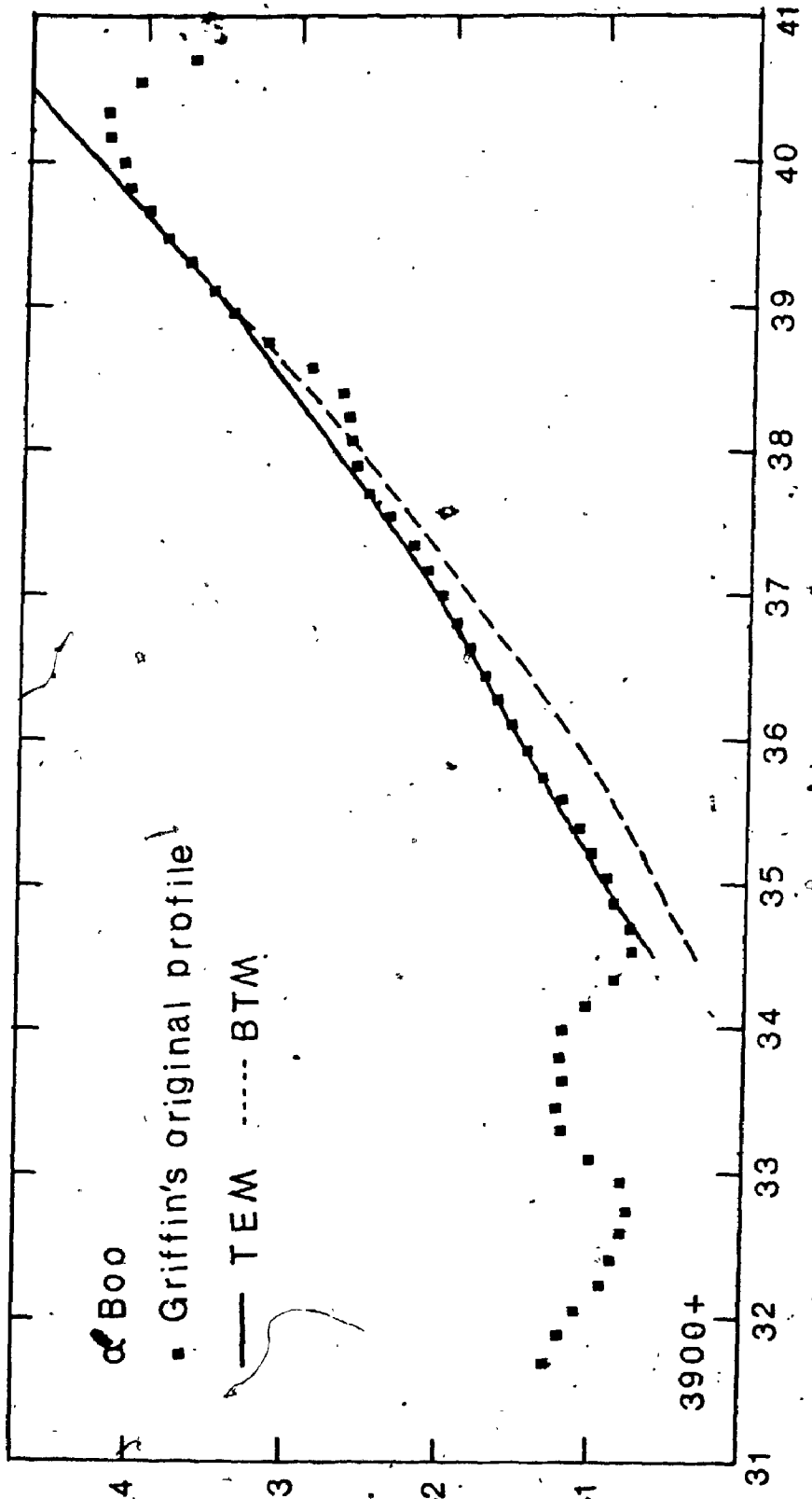

Fig.5.11. Comparison of Griffin's uncorrected (for scattered light) low resolution relative flux profiles with theory. ---- Profile synthesized using BTM(Bell et al.,4250,1.7, 0.33); ——— Profile synthesized using TEM(-1.40,3540; -3.0,3307; -4.3,3010). A_{Ca}=1.0E-6 and E_c=2.35 are used in the calculations.

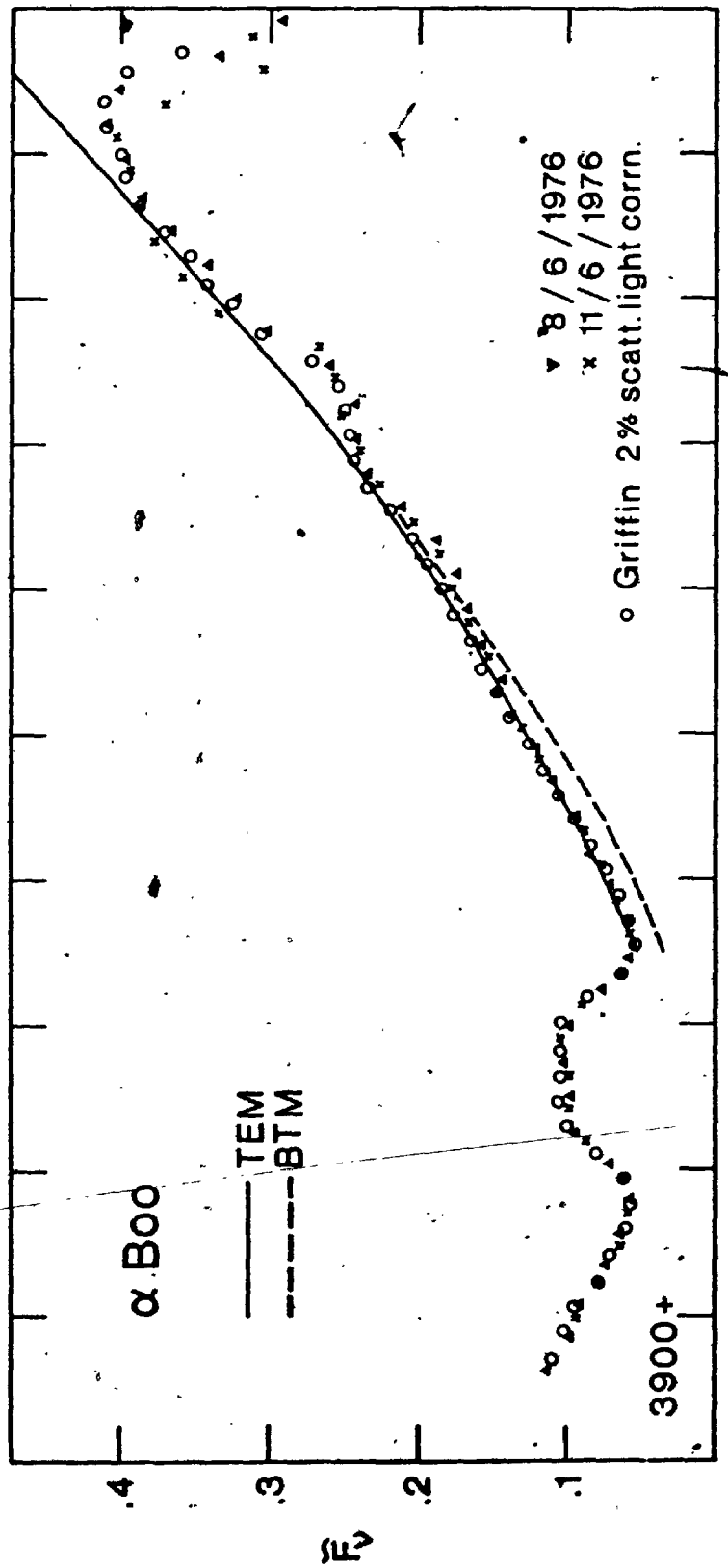

Fig.5.12. Comparison of Griffin's Arcturus atlas K line profile convolved with our instrumental profiles and corrected for 2% scattered light (circles) with theory. This profile is normalised to the window at λ3950.8Å. Triangles and crosses represent our own observations. - - - Profile synthesized using BTM(Bell et al.,4250,1.70,0.33); ——— Profile synthesized using TEM(-1.90,3370; -3.0,3240; -4.3,2940). A_{Ca}=1.0E-6, E_c=2.26 & E_6=1.45 are used in the calculations.

while Ayres & Linsky's calibration (which corresponds to an E_c=1.96) gives

$F_\nu(\lambda 3950.8\text{Å})$=2.12±0.64E-6 ergs cm^{-2} sec^{-1} hz^{-1}.

It is seen that the above theoretical fluxes, predicted by using an A_{Ca}=1.0E-6 and the associated E_{cs}, are consistent with Ayres & Linsky's value within the uncertainty of their absolute flux calibration.

5.7. TEMs FOR OTHER STARS

Having successfully tested our methodology on the Sun and Arcturus, we are now in a position to derive TEMs for the other K giants using the BTMs and A_{Ca}s determined in the last chapter. Below, we discuss the individual cases in some detail.

a) β Gem & ε Cyg

These two stars are described by the (same) BTM(Bell et al.,4750.2.8.1.0) and have the A_{Ca}s of 3.50E-6 and 2.70E-6, respectively. We have shown this BTM together with the derived TEMs in Fig.5.13. In this and in the following figures of similar kind, the insert shows the TEM at a higher magnification, so that the difference between the RE and K wing upper photospheric models is clearly seen. The stars β Gem & ε Cyg, which have the same BTMs also have very similar TEMs (within ∿50K). The profiles synthesized with the BTM and TEMs are compared with the observations of β Gem & ε Cyg in Figs.5.14 and 5.15, respectively. The values of E_c and the coordinates corresponding to the points P_i(i=1,3)

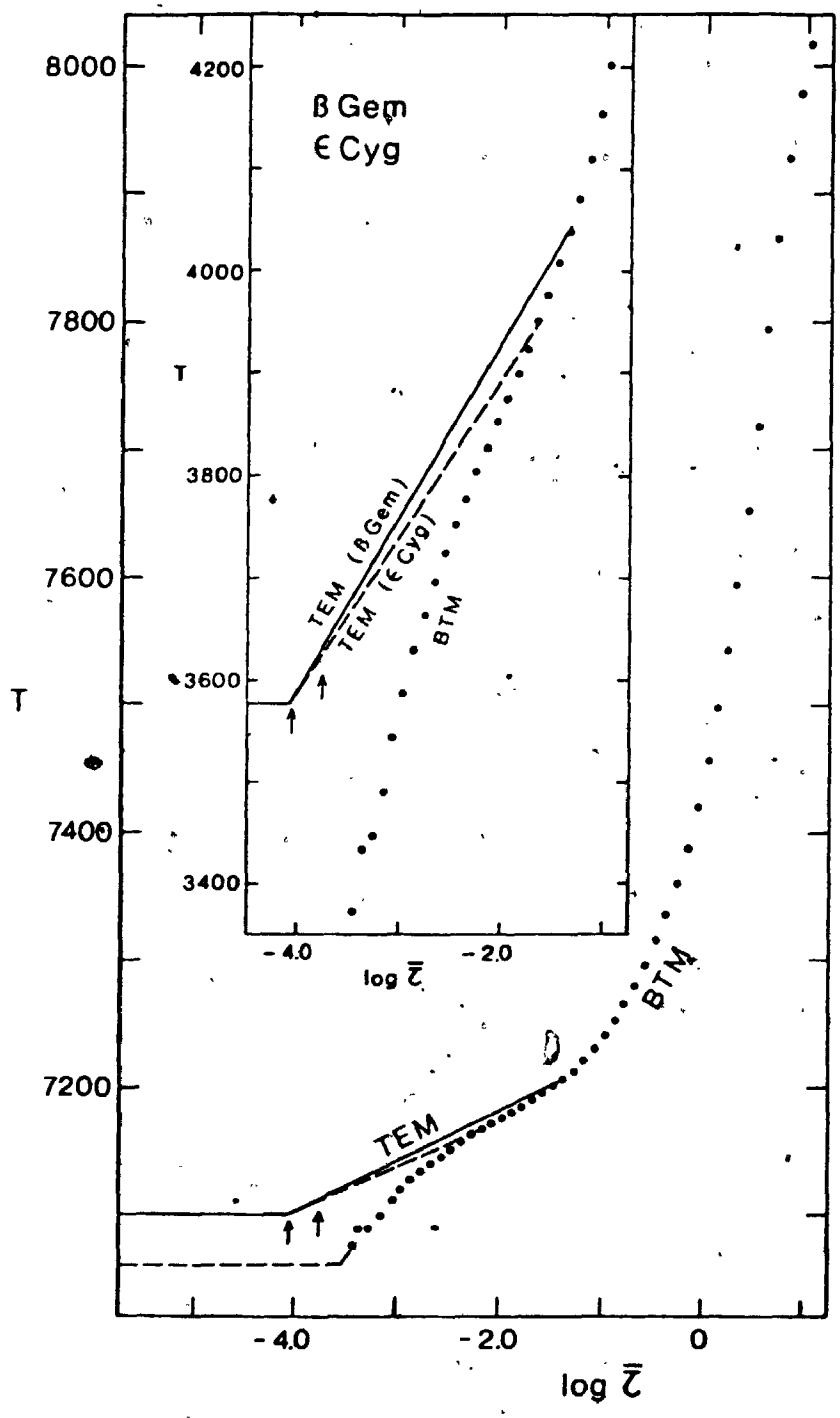

Fig.5.13. Temperature enhancement models for β Gem & ε Cyg.

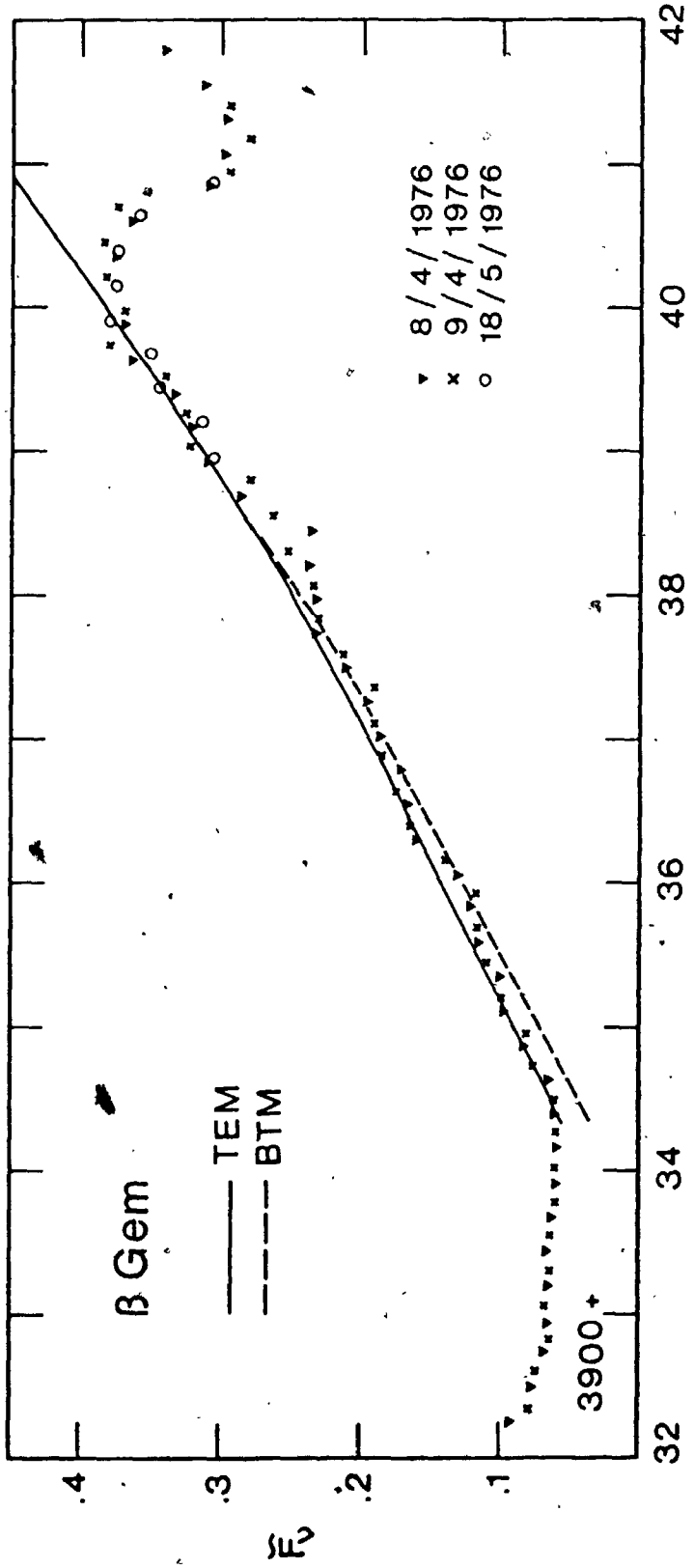

Fig.5.14. Comparison of the K line observations with theory. Dashed line represents the profile synthesized with BTM(Bell et al.,4750,2.8,1.0), while the solid line represents the profile obtained using TEM(-1.36,4036; -4.10,3575). A_{Ca}=3.50E-6 and E_C=1.10 are used throughout.

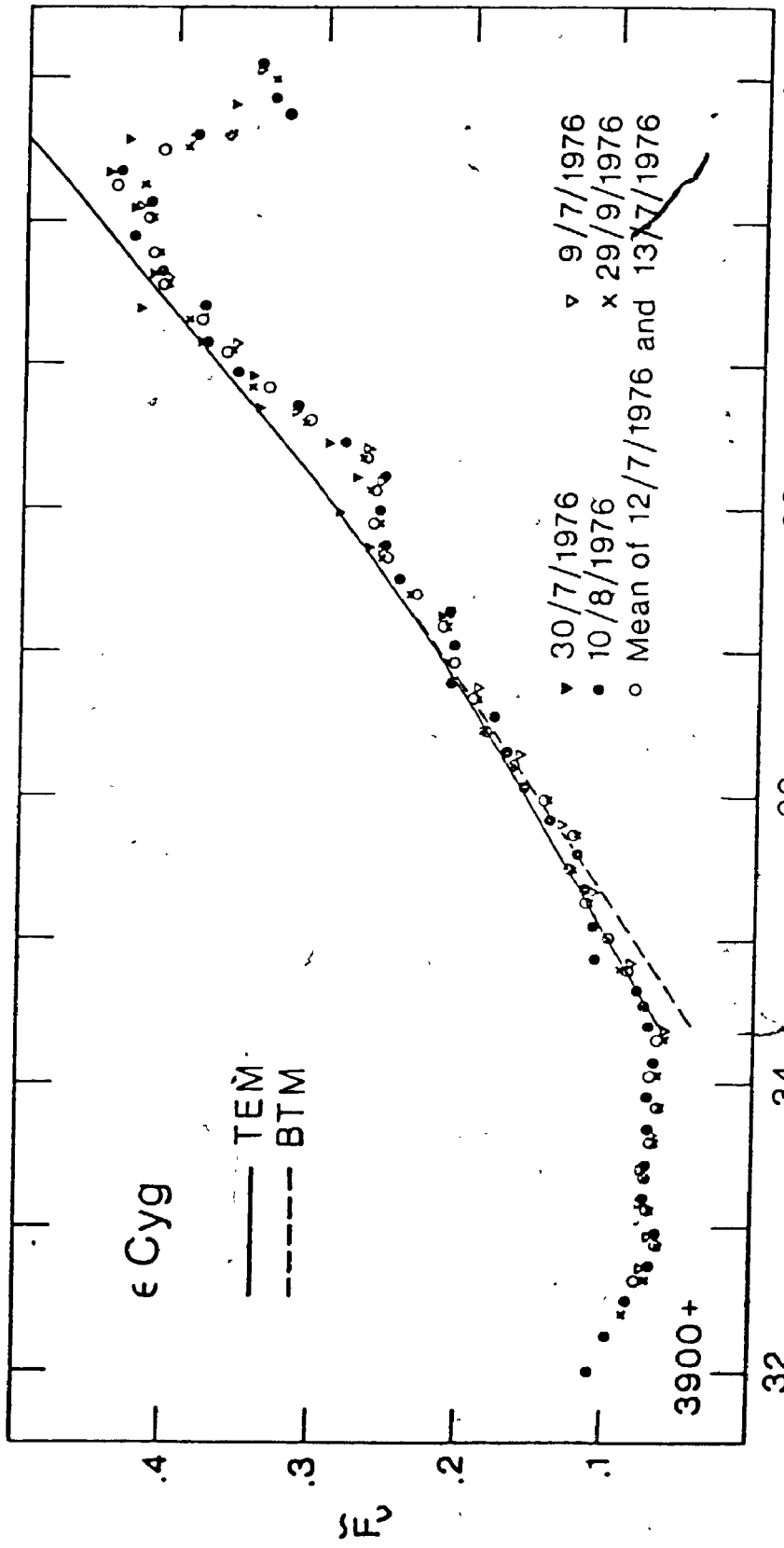

Fig.5.15. Comparison of observations with the thoory. Dashed line represents the profile obtained using BTN(Bell et al.,4750,2.8,1.0), while the solid line represents the profile synthesized with TEN(-1.66,3950; -4.10,3575). A_{Ca}=2.70E-6 & E_c=1.40 are used throughout.

between which linear temperature enhancement has been effected along with other data are listed in table 5.1.

b) α Ser & β Oph

These two SMR stars, which have the same T_e, log g values are described by BTM(Bell et al., 4650, 2.5, 1.0). Also, for β Oph we have derived an A_{Ca}=4.40E-6 from the Ca II λ8498 profile in the last chapter. Unfortunately, no observations of the λ8498 line are available for α Ser, so we can not obtain an A_{Ca} in the same manner for this star. However, the K line profile of α Ser is almost identical to that of β Oph, implying that A_{Ca} is identical too, as both stars have the same T_e, log g values. Therefore, we have adopted A_{Ca}(α Ser)≡A_{Ca}(β Oph). The TEMs derived with this A_{Ca} along with the BTM are shown in Fig.5.16. These two stars have identical TEMs. One striking difference between these TEMs and the TEMs of other stars is that these are considerably cooler. This is a very important result which will be further discussed in the next chapter. The profiles synthesized with these temperature models are compared with the observations of α Ser & β Oph in Figs.5.17 & 5.18, respectively. The E_cs along with other data are listed in table 5.1.

c) α Ari

This is the coolest of all the stars studied in this section. We have derived a BTM(Bell et al.,4450,2.5,1.0) and an A_{Ca}=2.20E-6 for this star in the last chapter. It is seen that this A_{Ca} is practically identical to the solar value.

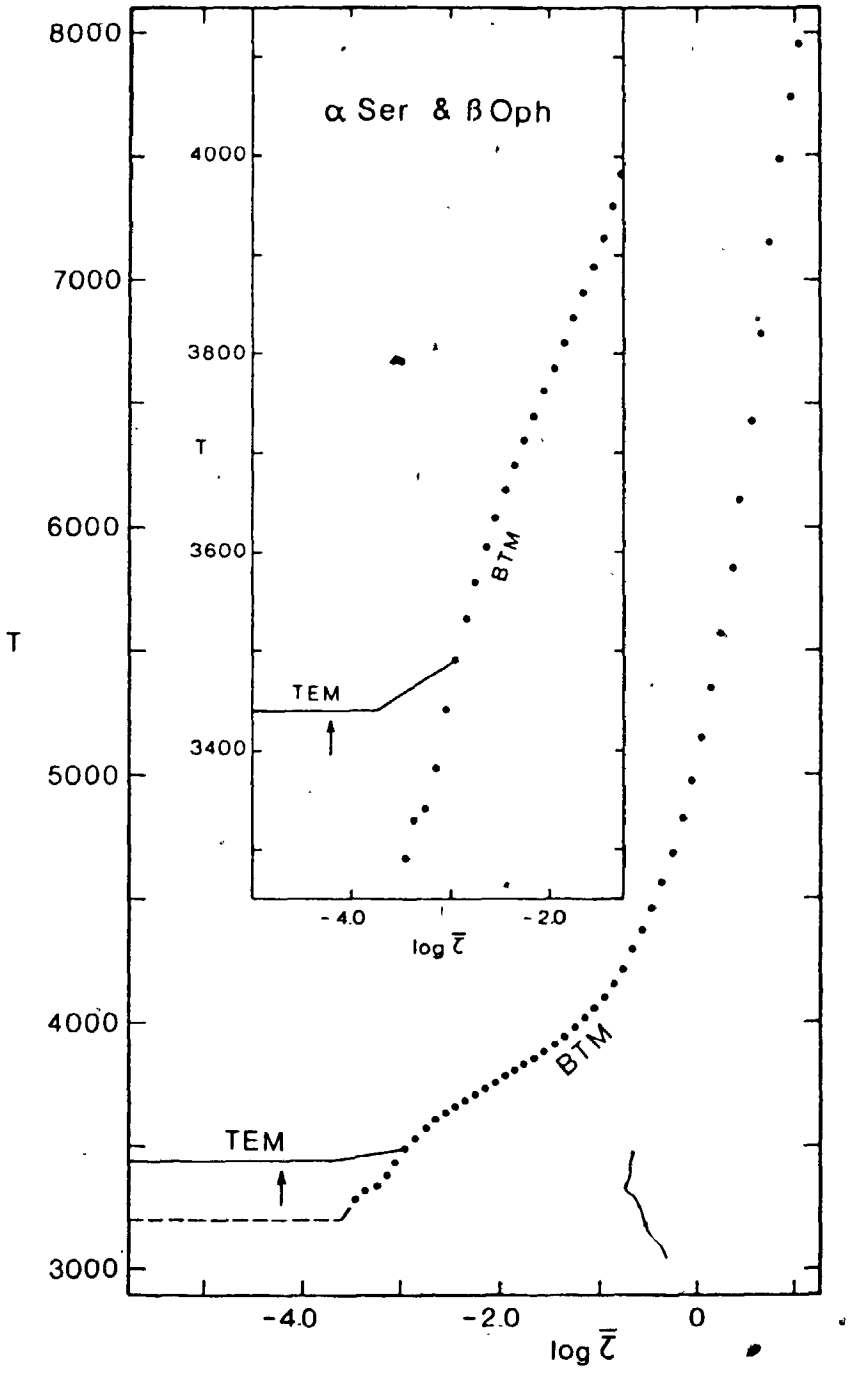

Fig.5.16. Temperature enhancement models for α Ser & β Oph.

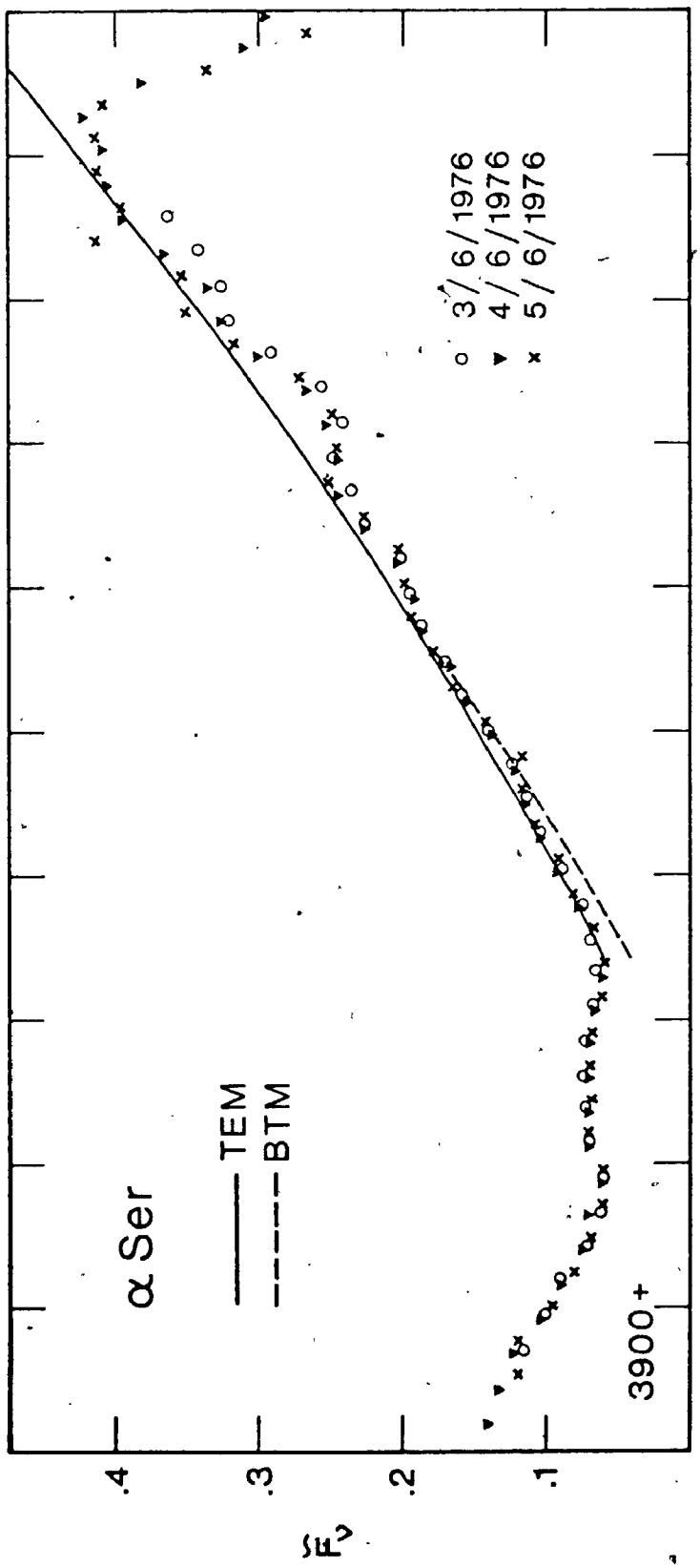

Fig.5.17. Comparison of observations with the theory. ---- Profile obtained using BTM(Bell et al.,4650,2.5,1.0); ——— Profile obtained using TEM(-2.96,3490; -3.75, 3440). A_{Ca}=4.4E-6 and E_c=1.96 are used in the calculations.

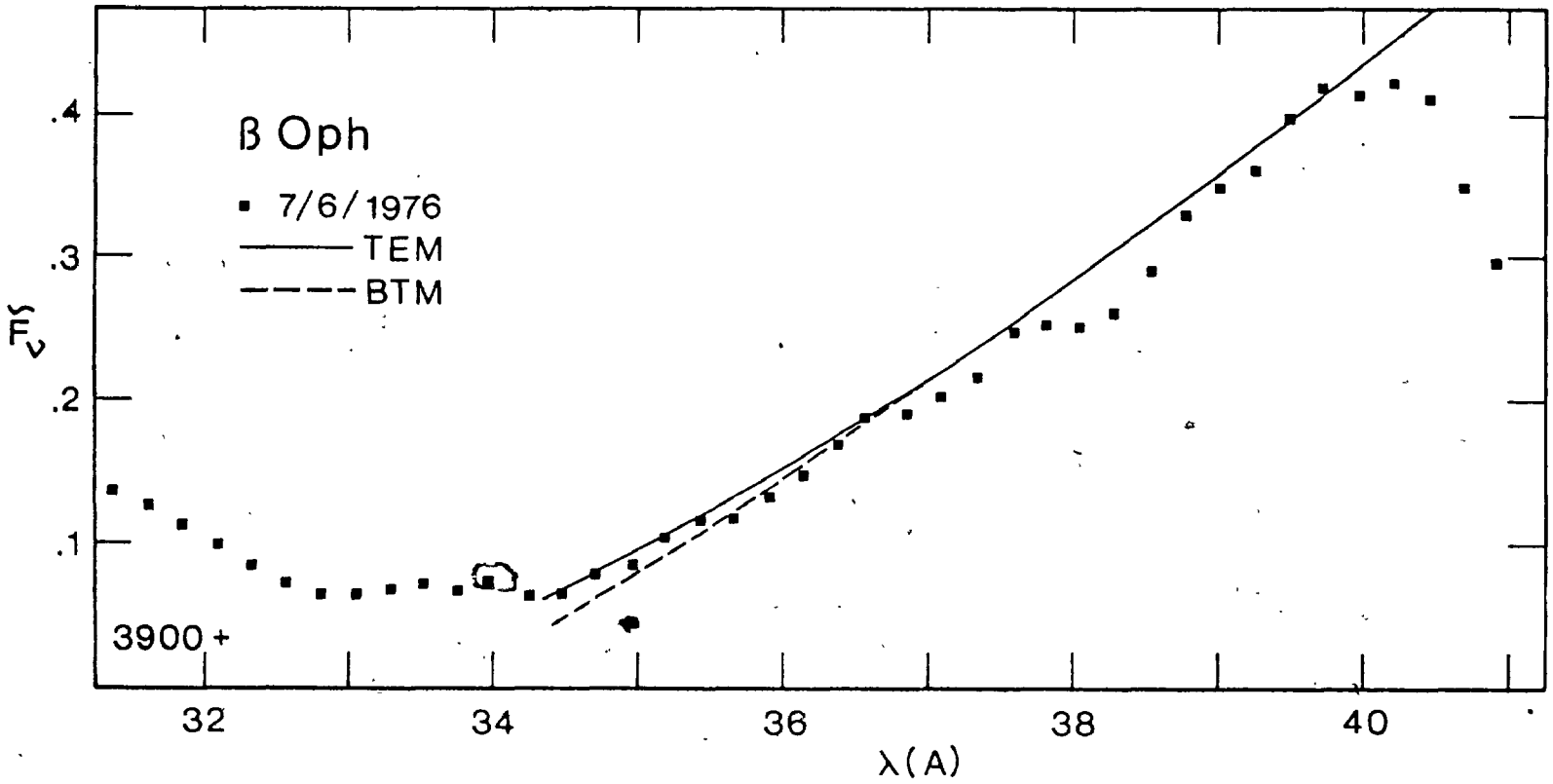

Fig.5.18. Comparison of observations with the theory. ---- Profile obtained using BTM(Bell et al.,4650,2.5,1.0); ——— Profile obtained using TEM(-2.96,3490; -3.75, 3440). A_{Ca}=4.4E-6 and E_c=2.06 are used in the calculations.

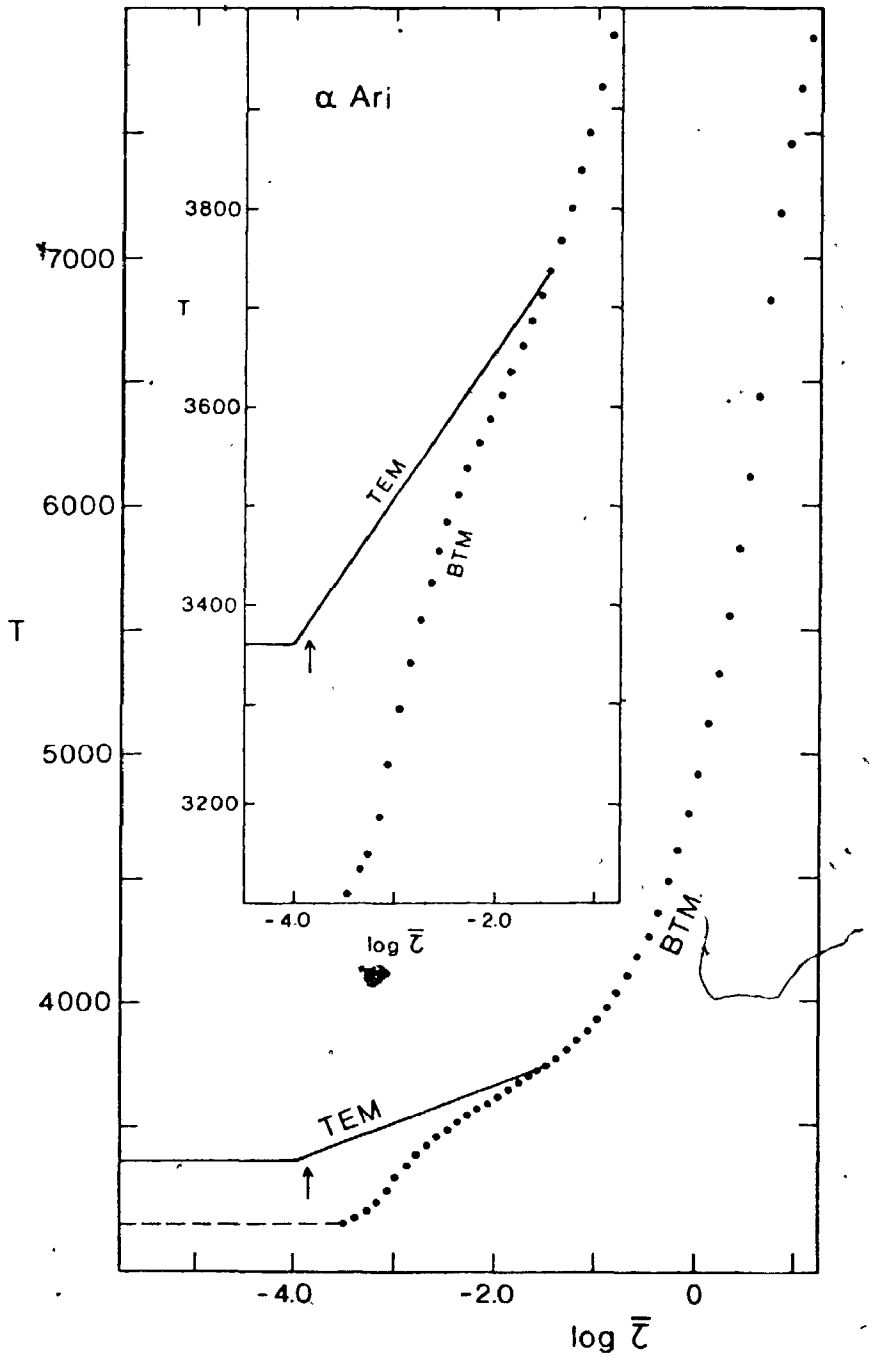

Fig.5.19. Temperature enhancement model for α Ari.

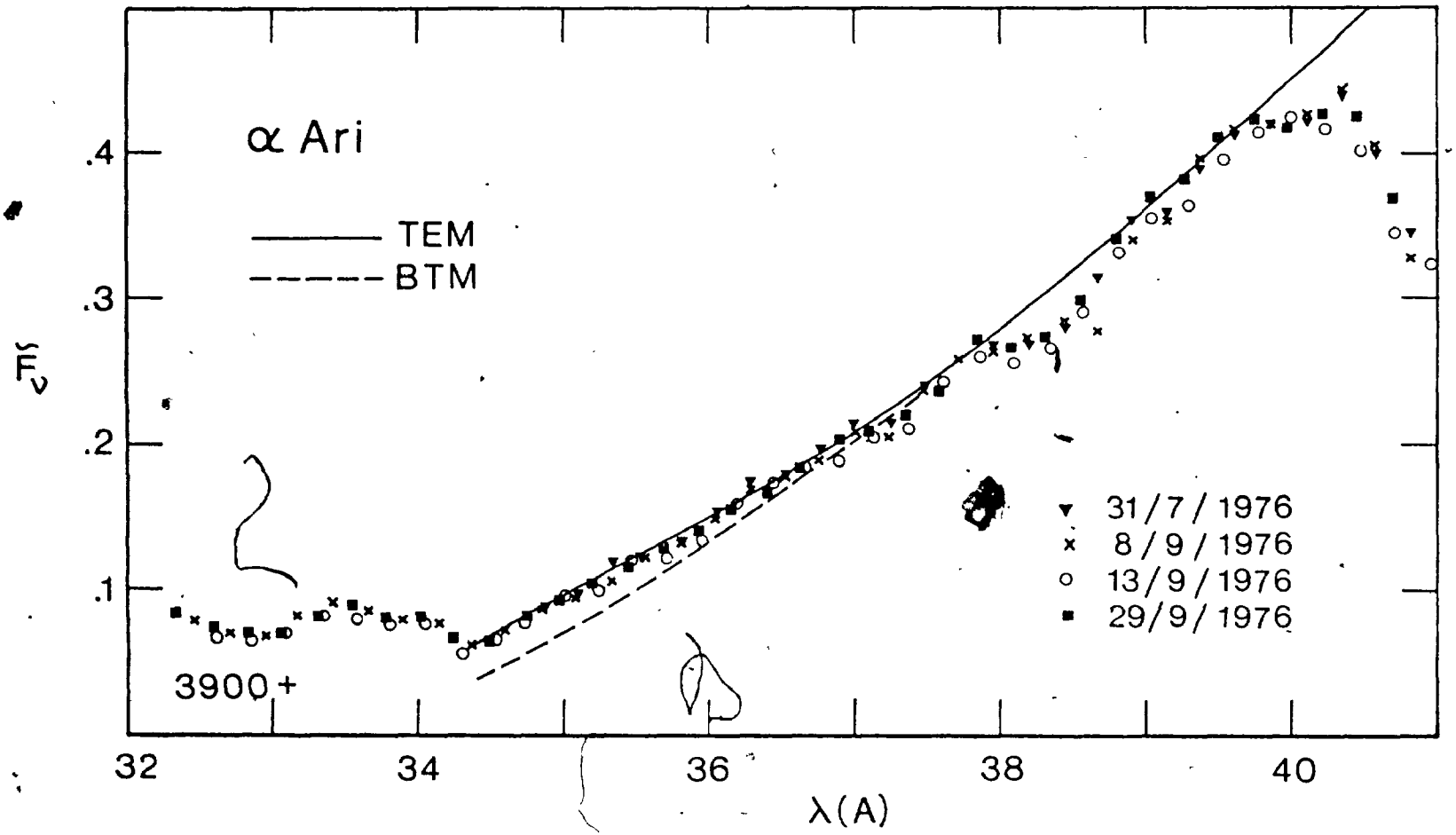

Fig.5.20. Comparison of observations with the theory. ---- Profile obtained using BTM(Bell et al.,4450,2.5,1.0); —— Profile obtained using TEM(-1.46,3738; -4.0, 3360). A_{Ca}=2.2E-6 and E_c=1.70 are used in the calculations.

We have shown the BTM and the TEM derived in Fig.5.19 and the K line profiles synthesized with these temperature models in Fig.5.20. The E_c and other data are listed in table 5.1.

d) κ Oph

This star was also studied by Peterson (1976) who derived a $T(\bar{\tau})$ model as follows. She obtained several initial $T(\bar{\tau})$ models by scaling the T_e=4000K, log g=3.0 model of Carbon & Gingerich (1969) and constrained them to satisfy the Fe I excitation equilibrium so that the abundances derived from a set of Fe I lines are independent of the equivalent width and excitation potential. Of the many initial models considered, she found that only one model with T_e=4600K and v_t= 1.5-2.0 km/sec, where v_t is the turbulent velocity, satisfied this constraint. She also noted that the scaling overestimated T_e, so that her T_e=4600K model in fact corresponded to the T_e=4500K model of Carbon & Gingerich. We find that her $T(\bar{\tau})$ model is very similar to the BTM(Bell et al., 4550,2.25,1.0).

Having fixed the $T(\bar{\tau})$ distribution of the deeper layers by satisfying the Fe I excitation equilibrium, she then turned to the Ti I excitation equilibrium to obtain the upper photospheric $T(\bar{\tau})$ model. In practice, she modified the above $T(\bar{\tau})$ distribution in the shallower layers by requiring that the abundances determined from a set of Ti I lines be independent of the equivalent width and excitation potential. Ti I lines are used because the number density of

Ti I, which is a minority species of Ti, is sensitive to the temperature distribution of the shallow layers. The gravity, g=200 cm sec^{-2} (log g=2.3), was determined by satisfying the Fe II/Fe I ionization equilibrium. Using this model, she also determined two values of A_{Ca}, viz. A_{Ca}=1.64E-6 & 2.64E-6, corresponding to the two values of the turbulent velocity given above.

Peterson has mentioned that her procedure is capable of yielding average temperatures in the vicinity of log $\bar{\tau}$=-0.3 and -1.3 only, and for log $\bar{\tau}$<-2.0 uncertainties as large as 120K are not ruled out. Likewise, the temperature gradient throughout the atmosphere is ill-defined. In any case, her observational approach appears to be less profound than the K line method to derive the upper photospheric T($\bar{\tau}$) models. So, it is interesting to see how the K line upper photospheric models compare with her model.

We have derived four TEMs for this star as follows. The first three TEMs were obtained by using an A_{Ca}=1.64E-6 and the three BTMs, BTM(Peterson,4600,2.3,1.0), BTM(Bell et al., 4550,2.3,1.0) and BTM(Bell et al.,4600,2.5,1.0). The first two BTMs, which are almost identical, give rise to identical TEMs shown by a dashed line in Fig.5.21. The third BTM is hotter and has a higher gravity and gives rise to a TEM that is ∿20K hotter than the above TEMs. This is shown by a thin line in Fig.5.21. We have included this BTM to allow for the possibility that Peterson's T($\bar{\tau}$), log g values were slightly underestimated. This possibility is indicated by the weakness

of the K line in κ Oph compared to other K giants considered here, which may be either due to a lower A_{Ca}, or a higher $T(\bar{\tau})$, or a higher g, or all these. This is why we have preferentially used the lower of the two A_{Ca}s given by Peterson in the above analyses. However, the modifications introduced in the TEMs by using this hogher T_e, log g model are only marginal. Using the same BTM but an A_{Ca}=2.64E-6, we have derived the fourth TEM which is shown by a wide line in Fig.5.21. In accordance with the discussion in §5.5, this higher A_{Ca} leads to a ~65K cooler TEM. Thus the TEMs corresponding to the lower and higher A_{Ca}s may be considered to represent two extreme cases, the truth lying somewhere in between. In any case all our TEMs, including the cooler one, are considerably hotter than Peterson's empirical $T(\bar{\tau})$ model. This is a very important result, the significance of which will be discussed in the next chapter.

Finally, let us comment upon the E_cs obtained with the various BTMs. Peterson's and the cooler of Bell et al.'s BTMs have very similar E_cs (within 2%) as the $T(\bar{\tau})$ distributions are very similar. However, the value of E_c=2.35 itself is quite large. The hotter of Bell et al.'s BTM requires a lower E_c (E_c=2.19) in accordance with the discussion in §3.4c. All the foregoing E_cs correspond to an A_{Ca}=1.64E-6. If we use an A_{Ca}=2.64E-6 instead, we obtain an E_c=3.1 using the hotter of Bell et al.'s BTMs. This E_c is about 1.5 times the typical values obtained for the other K giants and may be unrealistic. This indicates that of the two values of A_{Ca}, the lower one

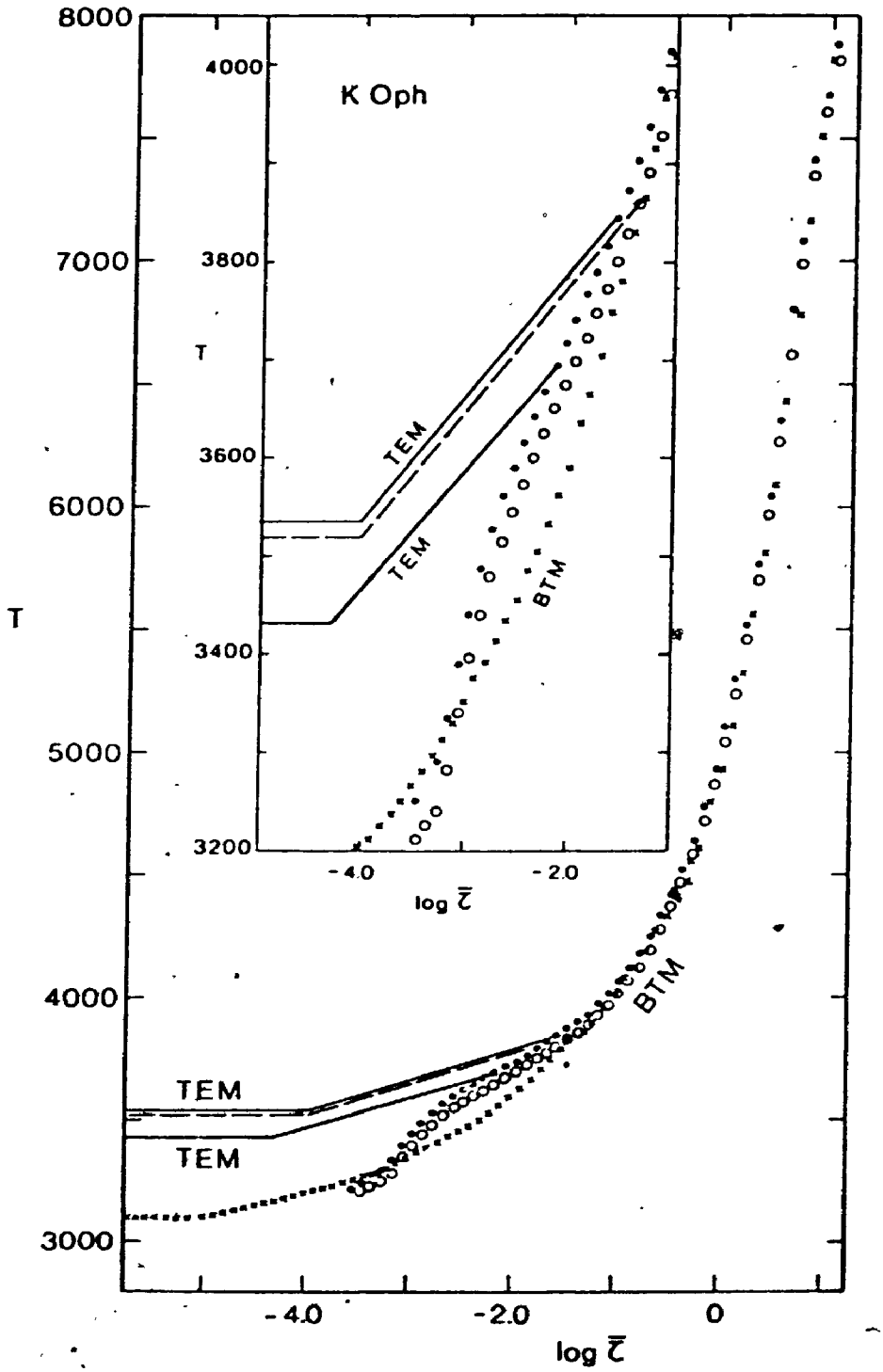

Fig.5.21. Temperature models for κ Oph. Crosses denote BTM(Peterson,4600,2.3,1.0) and circles represent BTM (Bell et al.,4550,2.3,1.0); dots denote BTM(Bell et al., 4600,2.5,1.0). Dashed line represents TEM(-1.36,3850; -4.0,3520) while the thin line represents TEM(-1.56,3842; -4.0,3530). Finally, the thick line represents TEM(-2.16, 3695;-4.3,3435). For computational details see the text.

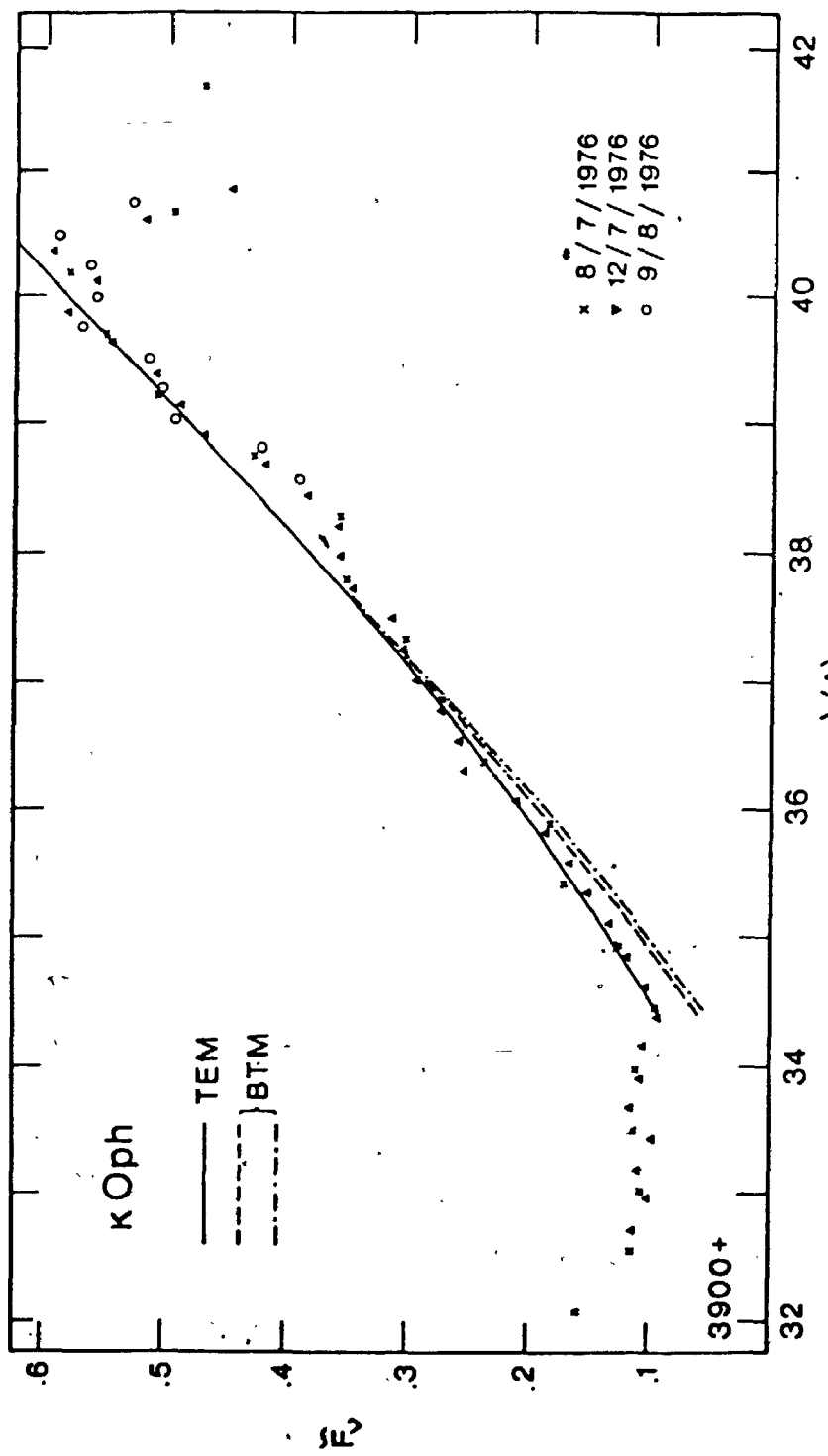

Fig.5.22. Comparison of the theory with observations. Dashed line represents the profile synthesized with the various BTMs (cf.Fig.5.21) using an A_{Ca}=1.64E-6, while the dot-dashed line represents that obtained using an A_{Ca}=2.64E-6.The solid line represents the profile synthesized with the various TEMs shown in Fig.5.21 and using either of the two values of A_{Ca} (i.e., either A_{Ca}=1.64E-6 or A_{Ca}=2.64E-6).

TABLE 5.1. PARAMETERS OF THE TEMPERATURE ENHANCEMENT MODELS

Star	Spectrum	T_e	log g	A_{Ca} x10-6	E_c	P1		P2		P3	
						log $\bar{\tau}$	T	log $\bar{\tau}$	T	log $\bar{\tau}$	T
Sun	G2 V	5770	4.44	2.14	1.04[a]	-1.10	5080	-4.0	4300	-	-
					1.13[b]	-0.83	5140	-4.0	4300	-	-
α Boo	K2 III	4250	1.70	0.642	1.96[c]	-1.40	3540	-3.5	3280	-4.0	3160
				1.00	2.35[d]	-1.4	3540	-3.0	3307	-4.3	3010
				1.00	2.26[e]	-1.9	3420	-3.0	3240	-4.3	2940
β Gem	K0 III	4750	2.80	3.50	1.10	-1.36	4036	-4.10	3575	-	-
ε Cyg	K0 III	4750	2.80	2.70	1.40	-1.66	3950	-4.10	3575	-	-
α Ser	K2 III	4650	2.50	4.40	1.96	-2.96	3490	-3.75	3440	-	-
β Oph	K2 III	4650	2.50	4.40	2.06	-2.96	3490	-3.75	3440	-	-
κ Oph	K2 III	4600[f]	2.30	1.64	2.35	-1.36	3850	-4.0	3520	-	-
		4550[g]	2.30	1.64	2.42	-1.36	3850	-4.0	3520	-	-
		4600[h]	2.50	1.64	2.19	-1.56	3842	-4.0	3530	-	-
		4600[k]	2.50	2.64	3.10	-2.16	3695	-4.3	3435	-	-
α Ari	K2 III	4450	2.50	2.20	1.70	-1.46	3738	-4.0	3360	-	-

a. TEM obtained adopting HSRA as BTM; b. TEM obtained adopting KREo as BTM; c. TEM obtained from calibrated Griffin's K line profile; d. TEM obtained using Griffin's K line relative flux profile; e. TEM obtained after correcting the above profile for 2% scattered light; f. TEM obtained using Peterson's $T(\bar{\tau})$ model as BTM; g. TEM obtained using Bell et al.'s T_e=4550K model as BTM; h. TEM obtained using BEll et al's T_e=4600K model as BTM; k. Same as (h) using A_{Ca}=2.64E-6.

is to be preferred. Evidence for this also comes from the weakness of the K line in κ Oph. So, it may be concluded that the TEMs obtained using the lower A_{Ca} are more realistic than the TEM derived using the higher A_{Ca}.

The synthesized profiles are compared with the observations in Fig.5.22 and the E_Cs and other data are listed in table 5.1.

In this chapter we have successfully tested our methodology on the Sun and Arcturus and derived TEMs for the program stars. This is the main body of information sought in this thesis. A further discussion of these results forms the topic of the next chapter.

CHAPTER VI

INTERPRETATION AND CONCLUSIONS

The principal aim of this thesis has been to quantitatively investigate if the SMR K giants have cooler upper photospheres than the normal K giants. We used the K line to obtain this information as it is the best tool available at present. In the last chapter we have already noticed that the SMR stars α Ser and β Oph do have cooler upper photospheres. In this chapter we elaborate upon this result and consider its limitations.

6.1. EVIDENCE FOR COOLER UPPER PHOTOSPHERES IN α Ser & β Oph

Fig.6.1 is a composite diagram of the upper photospheric $T(\bar{\tau})$ models of the stars studied in the last chapter*. In each case the solid line represents the temperature enhancement model (TEM) and the arrow locates the position of T_{min} (temperature minimum) in $\bar{\tau}$. It is clear from this figure that the SMR stars α Ser and β Oph have cooler upper photospheres — cooler than κ Oph and in parts even than α Ari! We must recall here that these latter two stars have respectively 100K and 200K cooler effective temperatures than the SMR stars. This is a very important result because it not only confirms the propositions of Strom et al. (1971) and Peterson (1976), but also proves the usefulness of the K line in delineating the effects of line blanketing on the

---

* The Sun and Arcturus for which no new information is being sought are not included.

surface temperatures of the late type stars. This result is better understood by referring to Fig.6.2, wherin we have plotted several probable TEMs which the SMR stars would have had if they behaved like the normal stars. These probable TEMs were obtained by scaling the $T(\bar{\tau})$ distributions of the normal stars to the effective temperature (T_e = 4650K) of the SMR stars. They encompass a large range of slopes, reflecting the differences in the T_e, log g and A_{Ca} values of these stars. Thus we believe that we have a fair sample of normal stars bracketing the physical parameters of the SMR stars, and if the SMR stars behaved like the normal stars they would have $T(\bar{\tau})$ distributions similar to the probable TEMs defined by these normal stars. But quite contrarily, the SMR stars have cooler TEMs — much cooler than the coolest probable TEM.

Now let us ask how cool is cooler? It is difficult to answer this question precisely as none of our normal stars is an exact twin of the SMR stars (Incidentally, the two SMR stars seem to be twins). However, we can set probable upper and lower limits to the extent of cooling. These are set by the two probable TEMs corresponding to the lower (1.64E-6) and higher (2.64E-6) values of A_{Ca} in κ Oph (cf.Fig.6.2). The truth may lie in between these two extremes, and the probable TEM corresponding to α Ari (which lies roughly midway) may be taken as the reference TEM with respect to which the cooling in the SMR stars has to be measured. Accordingly, cooling starts at log $\bar{\tau}$=-1.5

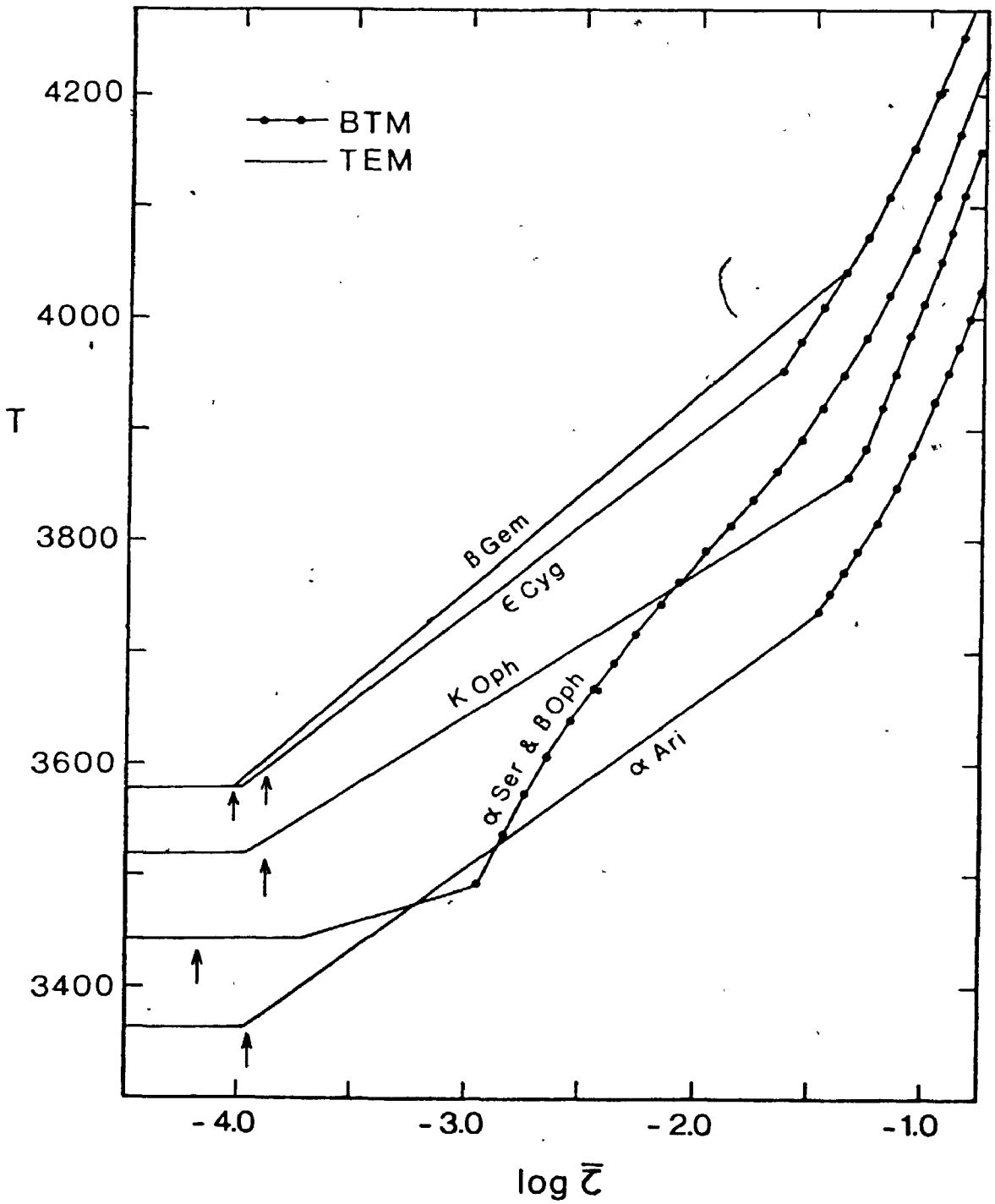

Fig.6.1. Compilation of the temperature enhancement models for the program stars. Arrows locate the temperature minima.

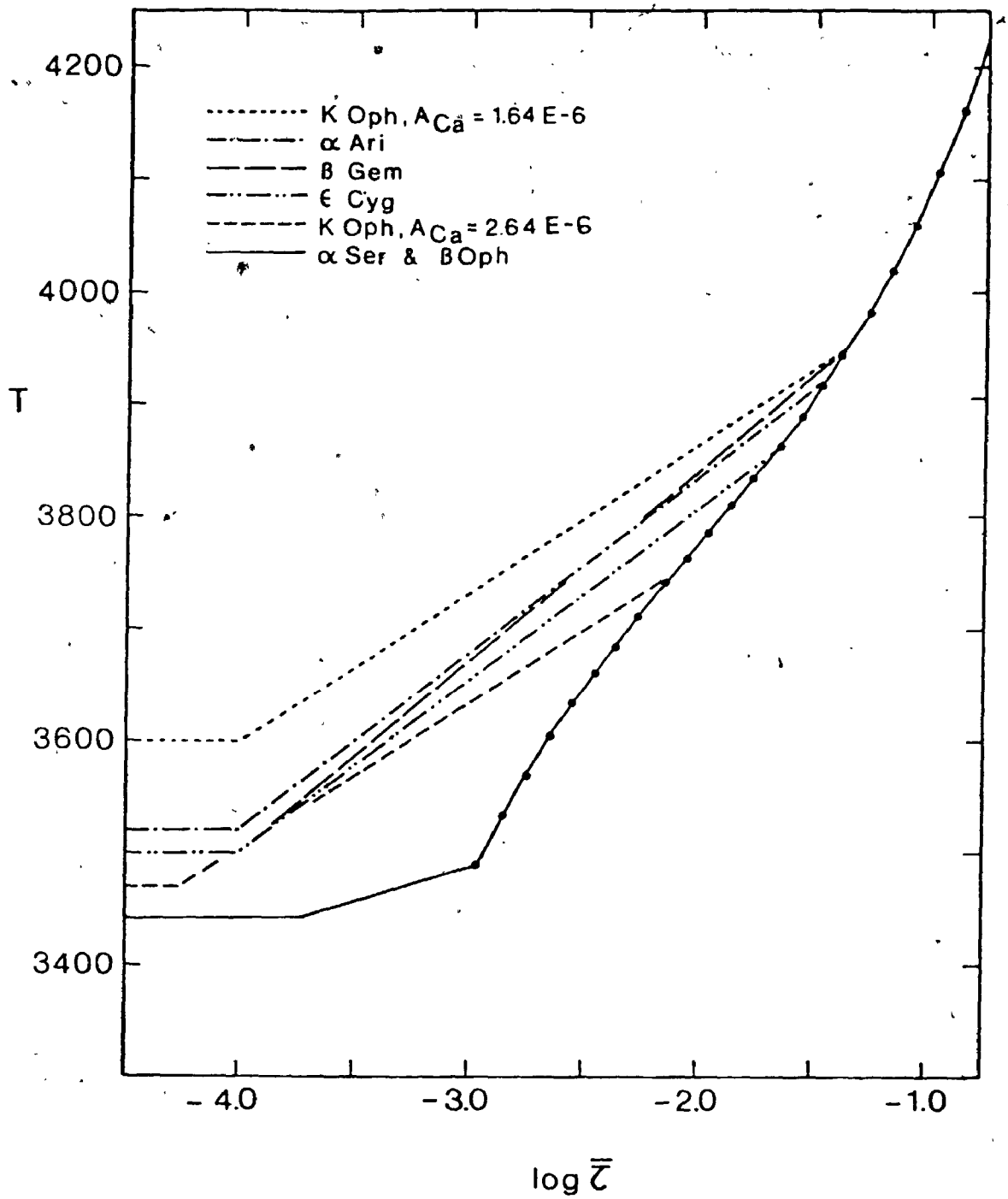

Fig.6.2. Probable temperature enhancement models defined by the normal stars (nonsolid lines) and temperature enhancement model for the SMR stars α Ser and β Oph (solid line).

and becomes more pronounced as log $\bar{\tau}$ decreases. The maximum cooling (ΔT = -180K) occurs near log $\bar{\tau}$ = -3.0, but the effect is smaller at other optical depths. The extent of this effect is in general agreement with that found in μ Leo by Peterson (1976) from a comparison of μ Leo with κ Oph.

6.2. HOW RELIABLE IS THIS RESULT?

The reliability of the TEMs depends upon the accuracy of the observations and the input parameters such as the BTM (Basic Temperature Model) and A_{Ca}. Here we consider how the uncertainties in these quantities affect the derived TEMs. Some general discussion of this nature has been given in the last chapter. Here we wish to be more specific in so far as our discussion concerns α Ser and β Oph. In Chap.II we have seen that the cumulative relative observational errors are about 4.5%. A crude estimate of how this error in the measured flux transforms into an error in T can be obtained by writing the Eddington-Barbier relation

$$F_\nu(\Delta\lambda) = \pi B_\nu(T_B(\Delta\lambda) \qquad (6.1)$$

where $T_B(\Delta\lambda)$ is the brightness temperature corresponding to the flux measured at $\Delta\lambda$ and is taken to be equivalent to the temperature of the star at the depth of formation of $\Delta\lambda$. Neglecting stimulated emission, we have

$$\frac{dF_\nu(\Delta\lambda)}{F_\nu(\Delta\lambda)} = \frac{dB_\nu}{B_\nu} \propto \frac{h\nu}{kT_{\Delta\lambda}} \frac{dT_{\Delta\lambda}}{T_{\Delta\lambda}} \simeq 9 \frac{dT_{\Delta\lambda}}{T_{\Delta\lambda}} \qquad (6.2)$$

where $T_{\Delta\lambda}$ is the temperature at the depth of formation

of $\Delta\lambda$ and $(h\nu/kT_{\Delta\lambda}) \simeq 9$ at the K line at a typical temperature of 4000K. Thus a 4.5% relative error in the observations causes only $\simeq$ 0.5% relative error in $T_{\Delta\lambda}$, or in absolute terms $\Delta T_{\Delta\lambda} \simeq 20K$ at $T_{\Delta\lambda}=4000K$.

It is important to consider exactly how the photometric and systematic errors affect the TEMs. The systematic errors which arise mainly in the slit width calibration (cf.Chap.II) cause a vertical shift in the K wing profile normalised to the window. The random photometric errors on the other hand introduce scatter into the observations. However, when we combine several nights' data together, the systematic shifts also partly contribute to the scatter. We have verified that purely systematic shifts as large as 5% have negligible effect on the TEMs, although they necessitate readjustment of E_c by $\sim$ 15%. This is an important result because it confirms that the expected $\sim$ 2% error in the slit width calibration does not directly affect the TEMs. But this affects them indirectly by adding scatter to the combined data set, thus accentuating the photometric errors. In any case, this effect has already been included in the 4.5% cumulative relative error, so that the estimate of $\Delta T_{\Delta\lambda}$ derived above remains unchanged.

Now let us consider the errors arising from the input parameters. We expect errors of < 100K in T_e, $\pm$0.3 in log g and $\pm$25% in A_{Ca} determined from Anderson's Ca II λ8498 profiles. This error in A_{Ca} corresponds to the estimated 3% error in Anderson's photometry. We varied our input

parameters (effectively A_{Ca} and BTM which is characterised by T_e and log g) over this range and found no changes in the theoretical profiles greater than the 4.5% error already present in the observations. In each of these calculations we have adjusted E_c so as to force agreement between different profiles in the far wings. The results are shown in Fig.6.3, the legend of which contains enough computational details. So, we conclude that the tolerances of our input parameters are such that the uncertainties introduced in the synthesized profiles are indistinguishable from the scatter already contained in the observations.

Other sources of error are the uncertainty in the van der Waals enhancement factor E_6 and the assumptions introduced in the partial redistribution formalism (cf.Chap.III). These errors should not effect the relative comparison of such a homogeneous group of stars as ours. We do not consider their absolute effect on the synthesized profiles as we are interested only in a relative comparison of the SMR and normal stars in this thesis.

The various sources of error considered above add up to 2%. But it is likely an overestimate as some of the sources (of error) tend to cancel each other and as we always determine an A_{Ca} consistent with the adopted BTM, thus partly reducing the effect of a wrong choice of BTM on TEMs. So, it is probable that a relative error of $\sim$1% is more realistic.This estimate leads to an absolute error of $\sim$36K in a typical upper photospheric temperature of 3600K.

Fig.6.3

a) Effect of changing A_{Ca} on the synthesized K line profiles. Squares and triangles represent the profiles synthesized using A_{Ca}=4.0E-6 and 5.0E-6 respectively. The $T(\tau)$ distribution used is that of BTM(Bell et al., 4650,2.5,1.0)

b) Effect of changing T_e on the synthesized K line profiles. Circles and dots represent the profiles synthesized using the $T(\tau)$ distributions corresponding to BTM(Bell et al.,4600,2.5,1.0) and BTM(Bell et al., 4700,2.5,1.0) respectively. An A_{Ca}=4.40E-6 has been used in all the calculations.

c) Effect of changing g on the synthesized K line profiles. Circles and triangles represent the profiles synthesized using g=200 cm/sec^2 (log g=2.3) and g=600 cm/sec^2 (log g=2.8) respectively. Every time g has been changed, a new A_{Ca} has been determined to be consistent with this changed g. Thus, A_{Ca}=4.0E-6 and 5.0E-6 were determined to be consistent with the above two values of gravity, and were used in the respective K line syntheses.

In every case, i,e., in all the Figs.a,b & c, appropriate values of E_c were included to force agreement between the different profiles in the "usable" far wing segment.

Fig.6.3.

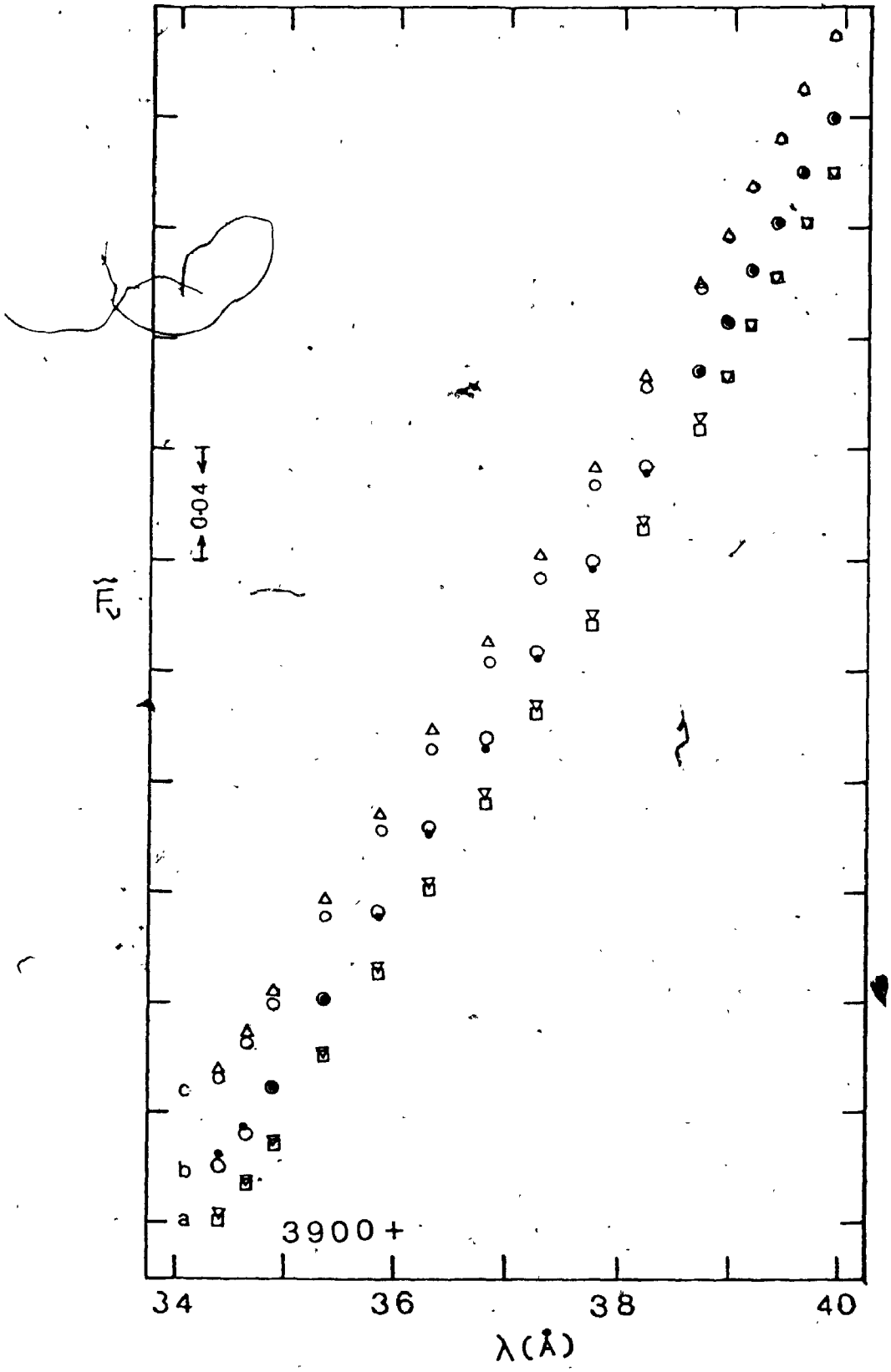

As can be seen from Fig.6.2, the extent of cooling in SMR stars exceeds this error estimate by 2-3 times.

6.3. ASTROPHYSICAL IMPLICATIONS OF COOLING

The cooling in the surface layers of SMR stars immediately points to the excess line blocking (cf. Fig.1.1) observed in these stars. It is well known, as was first shown by Chandrasekhar (1935), that lines cause back warming of the deeper layers while cooling the surface layers by redistributing the continuum flux in frequency. Since the work of Chandrasekhar, more effort has gone into constructing "realistic" line blanketed RE models of stars. Two such studies that are most relevant to the K giants are by Gustafsson et al. (1975) and Johnson & Krupp (1976). These authors have shown that the lines of CO and CN are very effective in surface cooling through their blocking action on the near infrared continuum flux, which forms the bulk of flux emitted by a K giant star. Even though a similar effect can result through increased metal content, this is less important in SMR stars as their overall metal content differs only mildly from the normal stars. Griffin (1969) and Oinas (1974) have shown that α Ser has $\sim$1.5 times more metal content than the Sun. Gustfsson et al. have quantitatively investigated the effect of changing metal content on the $T(\bar{\tau})$ distribution. They have found that in a T_e=4500K, log g=2.25 model, which is representative of the stars studied here, a three fold increase in the metal content results in an additional temperature drop of only $\lesssim$40K in

the surface layers ($\log \bar{\tau} < -1.5$). So, we can infer that the enhanced metal content in α Ser contributes only slightly ($\sim$ 20K) to the observed cooling. Hence, the major part of the cooling should arise from the increased strength of the CN and CO features. Observational evidence supports this view. For example, Spinrad & Taylor (1969) and Greene (1969) have noted strong CN features in this star, while Ridgeway (1974) has shown that the strong CN and SMR stars tend to have enhanced CO strengths too. Through a model atmosphere analysis, Greene has shown that the CNO abundances in α Ser are enhanced respectively by 1.6, 2.7, and 1.4 times compared to the Sun, thus explaining the excessive CN and CO line strengths. Gustafsson et al. have shown that CN and CO affect the $T(\bar{\tau})$ distribution quite differently. This is because of the differences in the distribution of the line opacity of these molecules with wavelength. The numerous CN lines of comparable and nonnegligible strength are quite evenly distributed, while the strong CO lines are confined to very narrow wavelength regions. Thus, the CO lines are more effective in surface cooling because of the strength of the opacity, but less effective in backwarming as they block only a small fraction of the continuum flux. The reverse holds true for CN. Therefore, Gustafsson et al. have concluded that in stars with normal CNO abundances surface cooling is mainly caused by CO. Similar results were obtained by Johnson & Krupp. However, if CN is abnormally strong, not only does it cause additional backwarming but

also significant surface cooling. In their trial calculations, Gustafsson et al. have found that a ten fold increase in the oscillator strength of the CN red system introduces an additional surface cooling of ∿100K at log $\bar{\tau}$= -3.0. It is difficult to quantitatively estimate the extent of this effect in α Ser as we do not know the exact magnitude of the CN enhancement. However, we can make a rough estimate as follows. The SMR prototype μ Leo and α Ser have similar Spinrad & Taylor's T and CN indices. If this CN index is a measure of the CN abundance, we can infer that both stars have similar CN abundances. In her comparison of μ Leo with κ Oph, Peterson has noted that the infrared CN lines are ∿50% stronger in the former star. Because of the similarity of α Ser to μ Leo, we can expect a similar conclusion to hold for this star too. According to Peterson, the CN enhancement in μ Leo is not a result of increased Carbon abundance but of a two fold increase in Nitrogen abundance. We have already seen that the CNO abundances in α Ser are enhanced respectively by factors of 1.7, 2.7, 1.4 with respect to the Sun. So, in α Ser excess CN strength may arise from the overabundance of both C and N. In addition, the overabundance of C and O can also enhance CO, which affects the surface temperature more strongly than CN. So, it appears that cooling in α Ser is caused by the overabundance of CN and CO, although we are unable to sort out the extent of contribution from each of these sorces.

Will the same explanation hold for β Oph? We expect so. Physically, β Oph and α Ser seem to be almost identical. They have identical K line profiles, effective temperatures, gravities and temperature enhancement models. They also have very similar line blocking coefficients (cf.Fig.1.1) and Spinrad & Taylor's T and CN indices. So, it is logical to expect the same processes to be responsible for surface cooling in both stars.

6.4. THE CASE OF κ Oph

Our K line upper photospheric models are always hotter than the RE models. What is more interesting and relevant to Peterson's explanation of the SMR phenomenon is the case of κ Oph. In the last chapter we have seen that our TEMs for this star are considerably hotter than the empirical model of Peterson. To be more quantitative, we have listed the temperature differences between the two models in table 6.1. It is clear that our model temperatures are higher by as much as 315K. It seems that Peterson's procedure underestimated the upper photospheric temperatures, as at some depths her model is even cooler than the corresponding RE model (cf. Fig.5.21) . We prefer the K line models as the K line is a better indicator of the upper photospheric temperatures than the data used by Peterson. By extending these considerations to μ Leo and ι Dra, which were studied by her but not included in our program, we expect her upper photospheric models to be cooler for these two stars too.

Despite this disagreement in an absolute sense, we do confirm the differential (SMR-Normal) cooling in the SMR stars found by her. But it is not clear if our temperature models are consistent with her equivalent width data. Should future work prove this consistency, her explanation of the SMR phenomenon as arising from a differential cooling effect would be upheld.

TABLE 6.1

DIFFERENCES BETWEEN OUR AND PETERSON'S $T(\bar{\tau})$ MODELS FOR κOph

Log $\bar{\tau}$	ΔT	Log $\bar{\tau}$	ΔT	Log $\bar{\tau}$	ΔT	Log $\bar{\tau}$	ΔT
-1.3	0	-2.0	180	-2.8	270	-3.6	295
-1.4	20	-2.2	218	-3.0	290	-3.8	305
-1.6	75	-2.4	235	-3.2	295	-4.0	315
-1.8	135	-2.6	255	-3.4	300		

Notes: ΔT is the temperature difference between Peterson's $T(\bar{\tau})$ model and the TEM obtained with BTM(Peterson,4600,2.3, 1.0) and A_{Ca}=1.64E-6. If we use A_{Ca}=2.64E-6 instead of 1.64E-6, ΔT will be reduced by ∿65K.

6.5. OTHER PROPERTIES OF THE TEMPERATURE MODELS

a) DEPARTURES FROM RE

Our K line upper photospheric models are always hotter than the RE models of Bell et al. (1976). Similar results were obtained by Ayres and his associates for the Sun, Arcturus, Procyon and α Cen A,B. These results point to non-radiative heating in the upper photospheres of these stars. In the case of the Sun, Ulmschneider (1974) has shown that the dissipation of the short period (∿10-20 sec) acoustic

waves generated by turbulence in the Hydrogen convection zone is responsible for heating of the lower chromosphere. However, he has also pointed out that the total acoustic energy contained in these waves is two orders of magnitude greater than the heating requirements of the lower chromosphere and suggested that this discrepancy may be removed if the upper photosphere is effective in dissipating some of these waves before they enter the chromosphere. In such a case, we expect to see higher upper photospheric temperatures than those predicted by RE models; the above observational evidence supports this view. It is possible to estimate the extent of mechanical energy dissipation by equating it to the total H^- radiative loss rate, as H^- is the principal cooling agent in the upper photosphere. Such calculations have been done by Ayres (1975) for the Sun and Procyon. In the Sun he has found that the H^- radiative loss rate is in rough accord with the theoretical acoustic energy production estimates. He has also found that the amount of energy dissipated is directly related to T_e, but is only very weakly dependent upon g. For example, it is more in Procyon than in the Sun. This is so because a star with a higher T_e produces more acoustic flux per unit area and also loses more radiative flux than a low T_e star. Hence, the mechanical dissipation is also greater. Thus, even though our program stars have similar upper photospheric temperature enhancements to the Sun and Procyon (cf. Chap.V), they dissipate less mechanical energy as they have lower T_es.

Following the above discussion it is logical to ask if the differential cooling observed in the SMR stars is due to differences in line blanketing or in nonradiative heating? The answer for this question appears to be straightforward. Since the mechanical energy dissipation is strongly dependent upon T_e and since the SMR stars have normal T_es, it is logical to expect no anamalous behavior in nonradiative heating in these stars. On the other hand, the presence of excessive line blanketing in these stars is well established. Hence, we feel that the differential cooling is principally caused by excessive line blanketing in these stars.

b) THE RATIO OF T_{min}/T_e

T_{min} is an important datum for stars with a chromospheric temperature rise. Besides, T_{min} is an indicator of the line blanketing effects on the photospheric temperature profile. Recently, Ayres et al. (1976) have shown that F and G stars have a $T_{min}/T_e \sim 0.78$, in good agreement with the theoretical ratios predicted by Carbon & Gingerich's (1969) line blanketed RE models; On the other hand, the cooler K type stars have a ratio close to 0.73, probably due to the increasing role of line blanketing in these stars. It is interesting to see if the K giant stars included in our study partake in this behavior. However, we have some uncertainty in locating $\Delta\lambda_{K1}$ and determining T_{min} from the K1 relative flux, as our low resolution (0.5Å) smears out the K1 region in the observed profiles. In the last

TABLE 6.2. PARAMETERS OF THE TEMPERATURE MINIMUM REGION

Star	T_e	A_{Ca}	$\Delta\lambda_{K1}$	log $\tau(T_{min})$	log $m(T_{min})$	T_{min}	T_{min}/T_e	$\Delta(T_{min}/T_e)$
β Gem	4750	3.5E-6	0.65§	-4.06	-0.78	3580	0.75	-0.015
ε Cyg	4750	2.7E-6	0.65	-3.76	-0.61	3595	0.76	-0.015
α Ser	4650	4.4E-6	0.72	-4.37	-0.64	3440	0.74	-0.015
β Oph	4650	4.4E-6	0.72	-4.37	-0.64	3440	0.74	-0.015
κ Oph	4600	1.64E-6	0.72	-3.76	-0.37	3520	0.77	-0.015
α Ari	4450	2.2E-6	0.72	-3.85	-0.52	3360	0.76	-0.015
α Boo	4250	1.0E-6	0.80	-4.27	-0.20	3030	0.71	-
α Boo*	4250	1.0E-6	0.80	-4.27	-0.20	2960	0.70	-
α Boo+	4250	6.42E-7	0.80	-3.70	+0.24	3150	0.74	-

* Using Griffin's (1968) observations corrected for 2% scattered light.

\+ Ayres & Linsky's (1975) values. § In Ångstroms.

chapter we have seen that in case of Arcturus this smearing has negligible effect on the position of K1, but increases the K1 relative flux by $\sim$ 25%, which in turn leads to an overestimation of T_{min} by $\sim$ 2%. We must recall here that this increase in the relative flux is caused by the spill-over of flux from the neighboring regions into K1 minimum. As this spillover flux is directly dependent upon the emission contrast, and as Arcturus has the largest emission contrast of all the stars studied here, the above $\sim$ 2% error in T_{min} has to be taken as the maximum possible error in our determination of T_{min} from the 0.5Å resolution line profiles. For β Gem and ϵ Cyg, which have much smaller emission contrasts, the spillover flux should be very small, hence the T_{min} may be accurate to better than 1%. But this small emission contrast in these stars also makes the location of $\Delta\lambda_{K1}$ rather uncertain. This difficulty can be surmounted by referring to Liller's (1968) high resolution K line profile of β Gem, where the $\Delta\lambda_{K1}$ can be clearly located. The same value applies to ϵ Cyg as its profile is very similar to that of β Gem. In table 6.2 we have listed T_e, log $\bar{\tau}(T_{min})$, T_{min}/T_e and other data for each star. The error in the T_{min}/T_e ratio noted in the last column of this table corresponds to a maximum 25% overestimate in the K1 relative flux.

c) DEPENDENCE OF T_{min} ON A_{Ca}

T_{min} and hence the T_{min}/T_e ratio are dependent upon the A_{Ca} used in the K line synthesis. The larger the A_{Ca}, the

higher in the photosphere lies the depth of formation of K1, hence the lower the T_{min} derived and vice versa. This can be seen as follows. In the radiative damping dominated inner wing we have

$$\tau^{K}_{\Delta\lambda} \propto A_{Ca}\, m \,/\, \Delta\lambda^{2} \qquad (6.3)$$

where m is the mass column density (gm cm^{-2}). According to the Eddington-Barbier relation K1 is formed where $\tau^{K}_{\Delta\lambda} \sim 1$, so that

$$m(\Delta\lambda_{K1}) \propto \Delta\lambda^{2}_{K1} \,/\, A_{Ca} \qquad (6.4)$$

which shows that $m(T_{min}) = m(\Delta\lambda_{K1})$ is inversely proportional to A_{Ca}. Hence, if we have incorrectly overestimated A_{Ca}, we would underestimate T_{min} because the depth of formation of K1 moves outward in the photosphere where the temperature is low. The reverse will happen if we have underestimated A_{Ca}. Following Ayres et al. (1975) we can relate $m(T_{min})$ to $\tau_c(T_{min})$, where $\tau_c(T_{min})$ is the continuum optical depth at the frequency corresponding to the K1 wavelength, as follows. Since most of the continuous opacity is contributed by H^-, we can write, $\tau_c(T_{min}) \simeq \tau^{H^-}(\lambda_{K1})$. Now the H^- opacity is directly proportional to P_e, which in turn can be related to P_g by

$$P_e \propto A_{el}\, P_g \qquad (6.5)$$

where A_{el} is the total abundance of the electron donor elements. Hence

$$\tau_c(T_{min}) \propto A_{el}\, P_g\, m(T_{min}) \propto g\, m^2(T_{min}) \qquad (6.6)$$

where we have used the hydrostatic equation, $P_g = mg$. Now replacing $m(T_{min})$ by Eq.6.4, we have

$$\tau_c(T_{min}) \propto A_{el}\, g\, \Delta\lambda_{kl}^{4} / A_{Ca}^{2} \qquad (6.7)$$

which shows that $\tau_c(T_{min})$ has an inverse square dependence on A_{Ca}. This has been verified in a model of Arcturus as shown in Fig.6.4*, where we have plotted log $\bar{\tau}(T_{min})$ against log A_{Ca}. This explains why we have obtained a lower $\bar{\tau}(T_{min})$ and T_{min} for Arcturus using an A_{Ca}=1.0E-6 instead of the value (A_{Ca}=0.642E-6) used by Ayres & Linsky (cf.table 6.2).

We expect that our derivation of A_{Ca} from the Ca II λ8498 profiles gives a reliable estimate of A_{Ca}, consequently, the $\bar{\tau}(T_{min})$ and T_{min} values given in table 6.2 are well determined. Hence, after allowing for the possible systematic errors noted in the last column of this table, we see that the T_{min}/T_e ratios for our stars are in general agreement with the value ≃0.73 obtained by Ayres et al. (1976) for other K type stars. As can be seen from Fig.6.2, the excess line blanketing in α Ser and β Oph has only a small effect on T_{min} and this is reflected in near normal T_{min}/T_e ratios for these stars. On the other hand, our T_{min}/T_e ratio for Arcturus is smaller than the value obtained by Ayres & Linsky (1975). This difference is attributable to the larger A_{Ca} used in our analysis, which has been chosen to be consistent with our adopted BTM. Ayres & Linsky's A_{Ca} was not determined in this way, but was adopted to be

---

* Notice that in this and in the following figures we have plotted $\bar{\tau}(T_{min})$ instead of $\tau_c(T_{min})$ after transforming τ_c into $\bar{\tau}$.

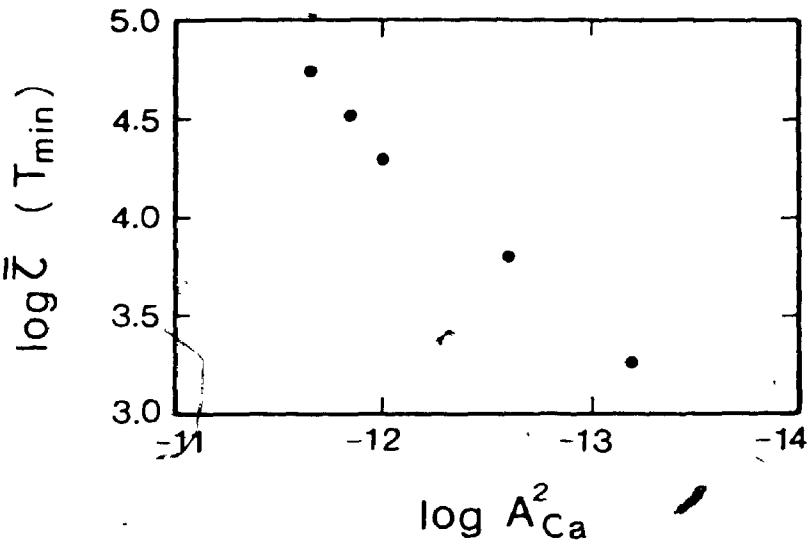

Fig.6.4. $\bar{\tau}(T_{min})$ vs. A_{Ca} dependence in a model of Arcturus

$(1/3)A_{Ca}^{\odot}$, assuming an overall three fold metal deficiency in Arcturus compared to the Sun. As noted in the last chapter, these two values are consistent within the uncertainties of the best possible curve of growth abundance estimates (Mackle et al., 1976) available for this star. Granted these uncertainties, it can be argued that ours and Ayres & Linsky's T_{min}/T_e ratios are not inconsistent with one another.

d) $m(T_{min})$ VERSUS g RELATION AND AYRES ET AL'S (1975) INTERPRETATION OF THE K1 WILSON-BAPPU EFFECT

Ayres et al. (1975) have shown that $\Delta\lambda_{K1}$ is correlated with the absolute visual magnitude M_V of the star through the relation

$$M_V = (-12 \pm 2) \log \Delta\lambda_{K1} + \text{Const.} \qquad (6.8)$$

where $\Delta\lambda_{K1}$ is expressed in km sec^{-1}. By relating M_V to M_{Bol} and M_{Bol} to fundamental physical parameters g and T_e through the mass-luminosity relation, Ayres et al. have shown that Eq.6.8 is equivalent to

$$\Delta\lambda_{K1} \propto g^{-0.27\pm0.04}\, T_e^{1.4\pm0.2} \qquad (6.9)$$

Assuming that a) the dependence on T_e can be neglected in the above relation as T_e changes by a small factor compared to g going from main sequence stars to giants; and b) $\tau_c(T_{min})$ is roughly independent of g in Eq.6.6, Ayres et al. have deduced* from Eq.6.7, the following relation

---

* Ayres et al. assumed that A_{Ca} scales with A_{el} whereas we have not made this assumption.

$$\Delta\lambda_{K1} \propto A_{el}^{-0.25} A_{Ca}^{0.5} g^{-0.25} \qquad (6.10)$$

which has the same functional dependence upon g as the empirical relation 6.9. A consequence of assumption (b) is that

$$m(T_{min}) \propto A_{el}^{-0.5} g^{-0.5} . \qquad (6.11)$$

Accordingly, the K1 width-luminosity relation is a consequence of the increasing $m(T_{min})$ with decreasing g. If this explanation is correct, we must see a tight correlation between log $m(T_{min})$ and log g, although some scatter may be introduced into this relation due to differences in A_{Ca} and A_{el} among the stars. Fig.6.5a shows a plot of this relation for our program stars plus the stars studied by Ayres et al. (1976). The solid line in this figure represents the theoretical relation, $m(T_{min}) = \text{Const.}\ g^{-0.5}$. It is seen that the overall fit between the theory and the data points is quite good, even though there is some scatter. As already noted, part of this scatter must arise from the dispersion in A_{Ca}. We believe that this correlation supports the Ayres et al.'s explanation of the K1 Wilson-Bappu effect.

As shown in Fig.6.5b, we can also plot log $\bar{\tau}(T_{min})$ vs. log g to test the validity of assumption (b). This plot is more strongly affected by dispersion in A_{Ca} than the above plot, because of the stronger dependence of $\bar{\tau}(T_{min})$ on A_{Ca} (cf.Eqs.6.4 & 6.6). This is seen in Fig.6.5b. In this figure our program stars show a large dispersion in the continuum optical depth although they span a narrow range (2.3-2.8)

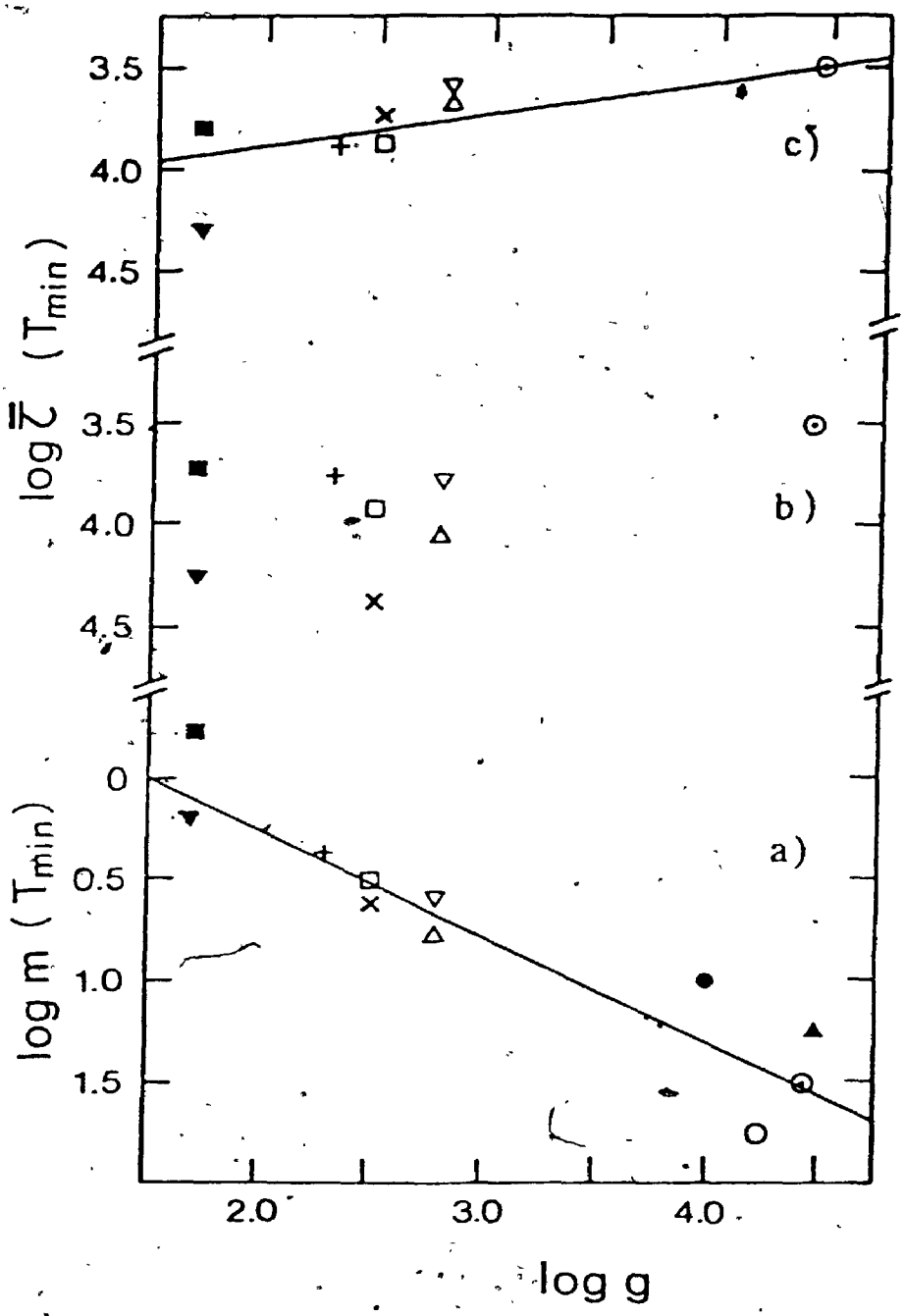

Fig.6.5.a) $m(T_{min})$ vs. g relation. Solid line represents the theoretical relation $m(T_{min})=const.g^{-1/2}$; b) $\bar{\tau}(T_{min})$ vs. g relation; c) Same as (b) with $\bar{\tau}(T_{min})$ corrected for the dependence on A_{Ca}. Symbols denote the following objects; ⊙ Sun; ● Procyon; ○ α CenA; ▲ α CenB; ▼ α Boo, A_{Ca}=1.0 E-6; ■ α Boo, A_{Ca}=0.642E-6; △ β Gem; ▽ ε Cyg; X α Ser and β Oph; □ α Ari; + κ Oph.

in log g. We can reduce this abundance dependent scatter by referring all the $\bar{\tau}(T_{min})$ to a standard A_{Ca}, say A_{Ca}=2.2 E-6. This is possible because of the tight correlation between A_{Ca} and $\bar{\tau}(T_{min})$ as shown in Fig.6.4. Having thus minimised the abundance effect on $\bar{\tau}(T_{min})$, we will be able to see if there is any correlation between $\bar{\tau}(T_{min})$ and g. Fig.6.5c shows a plot of log $\bar{\tau}(T_{min})$ referred to the standard A_{Ca} vs. log g. As expected, the dispersion in log $\bar{\tau}(T_{min})$ is much smaller in this figure than in Fig.6.5b. This figure is suggestive of a weak correlation between $\bar{\tau}(T_{min})$ and g ($\bar{\tau}(T_{min}) \propto g^{1/7}$?), but we feel our data are insufficient to establish the reality of this correlation unambiguously. So, we can conclude that Ayres et al.'s assumption that $\bar{\tau}(T_{min})$ is roughly independent of g is approximately satisfied. As this assumption is the basis for their explanation of K1 Wilson-Bappu effect, we believe that this finding lends support to their explanation.

6.6. SUMMARY OF RESULTS

In this thesis we have applied a method which does not require direct absolute flux calibration of the observed K line profiles, hence has greater flexibility in application to stars with unknown radii and distances, to derive upper photospheric $T(\bar{\tau})$ distributions of the SMR stars α Ser and β Oph and the normal stars β Gem, ε Cyg, κ Oph and α Ari. We have found that:

a) The SMR stars have cooler (upto 180K) upper photospheres

than the normal stars. This differential (SMR-Normal) cooling effect is in agreement with a similar result found by Peterson(1976) in her comparison of the SMR prototype μ Leo with the normal stars κ Oph ι Dra. Despite this agreement in a differential sense, our K line upper photospheric models are considerably (upto 300K) hotter than the empirical $T(\bar{\tau})$ models derived by Peterson from her consideration of Ti and Fe ionization-excitation equilibria. This conclusion is based on κ Oph, which is common to our analysis and hers. By extending this conclusion to μ Leo and ι Dra, which have not been included in our study, we expect a similar situation to hold even though differential cooling in μ Leo may still be present. However, it is not clear if the K line models are consistent with the conditions of excitation and ionization demanded by Peterson's data. If the future work establishes their consistency, her explanation of the SMR phenomenon as arising from a differential cooling effect will be upheld.

b) The differential cooling in SMR stars appears to be caused by enhanced CN and CO line absorption.

c) The temperature enhancements of 200-300K (in excess of Bell et al.'s RE models) needed by the K line upper photospheric models are in general agreement with similar results found by Ayres and his associates for other K type stars. These enhancements are indicative of departures from RE in the upper photospheres of these stars.

d) The T_{min}/T_e is not significantly different in the SMR stars from the normal stars. It appears that the cooling mechanisms operating in these stars have only a small effect on the temperature at the depth of formation of K1. The T_{min}/T_e ratios for our stars are in general agreement with the values derived for other K type stars by Ayres et al. (1976).

e) We have shown that T_{min} and $\bar{\tau}(T_{min})$ are dependent upon the Ca abundance used in the K line synthesis. We find that $\bar{\tau}(T_{min})$ is roughly independent of g. Since this independence is the basis for Ayres et al.'s (1975) explanation of the K1 Wilson-Bappu effect, we feel that this finding lends support to their explanation.

6.7. FOR THE FUTURE

Several future extensions and verifications of the studies conducted in this thesis are possible. Below, we have outlined a few of them.

a) We have seen that the K wing $T(\bar{\tau})$ models are clearly different from the RE models in having excessive upper photospheric temperatures. So, it is very important to check if they are consistent with the formation of other strong lines such as Na I D, whose cores are formed near the temperature minimum (Kelch & Milkey, 1976). If consistency can be established, it will be advantageous to use Na I D lines instead of Ca II K lines in future investigations, because the continuum is well defined near the

D lines and the late type stars are much brighter at D than at K. This latter fact enables us to extend our studies to fainter stars.

b) Na I D line strength is one of the criteria used by Spinrad & Taylor (1969) for their SMR classification. So, it will be intersting to see if the derived upper photospheric temperature drop in these stars is consistent with their Na I D line strengths. This study can ofcourse be extended to other strong features like Ca I λ4226 and Mg I b lines.

c) It is important to derive K line upper photospheric models for μ Leo and ι Dra and compare them with the $T(\bar{\tau})$ models of Peterson. By extending our conclusions for α Ser and β Oph to μ Leo, we expect it to have a differential temperature drop in the upper photosphere. However, it is important to observationally confirm this point as μ Leo is the SMR prototype. We must also investigate the consistency of the K line $T(\bar{\tau})$ models for κ Oph, μ Leo and ι Dra with the observational data of Peterson, as such a study will have important implications for her explanation of the SMR phenomenon.

d) Since the lower boundary temperatures in the SMR stars are possibily caused by excessive CN and CO line strengths, it is necessary to investigate the detailed relationship between the CN and CO abundances and the upper photospheric temperature structure. For this purpose it is necessary to do a

detailed abundance analysis of these molecules in the above stars.

REFERENCES

Ayres,T.R. 1975, Ap.J.201,799.

_____ and Linsky,J.L. 1975, Ap.J.200,383.

_____ 1976, Ap.J.205,874.

_____and Shine,R.A.1974,Ap.J.192,93.

_____1975,Ap.J.195,L121.

Ayres,T.R.,Linsky,J.L.,Rodgers,A.W., and Kurucz,R.L.1976, Ap.J.210,199.

Anderson,C.M. 1974,Ap.J.190,585.

Bell,R.A.,Eriksson,K.,Gustafsson,B.,and Nordlund,A.1976, Astron. Astrophys. Suppl.23,37.

Blackwell,D.E.,Ellis,R.S.,Ibbertson,P.A.,Petford,A.D.,and Willis,R.B. 1975,M.N.R.A.S.171,425.

Blanc-Vaziaga,M.,Cayrel,G., and Cayrel,R.1973,Ap.J.180,871.

Bohm,K.H. 1961,Ap.J.134,264.

Carbon,D.F., and Gingerich,O.1969, Proceedings of the 3rd Harvard-Smithsonian conference on stellar atmospheres, Ed.O.Gingerich, MIT press,P.377.

Chandrasekhar,S. 1935, M.N.R.A.S.96,21.

Connes,P. 1970, Ap.J. Suppl.19,1.

De Jager,C., and Neven,L.1967, B.A.N. Suppl.1,325.

Edmonds,F.N. 1973, P.A.S.P.85,24.

Gingerich,O.,Noyes,R.W.,Kalkofen,W., and Cuny,Y. 1971, Solar Phys.18,347.

Gray,D.F. 1971, B.A.A.S.3,387.

Gray,D.F. 1976, Observation and Analysis of Stellar Photospheres, Wiley & Sons, New York.

Greene,T.F. 1969, Ap.J.157,737.

Griffin,R.F. 1968, A Photometric Atlas of the Spectrum of Arcturus, Cambridge Philosophical Society, Cambridge, England.

Griffin,R. 1969, M.N.R.A.S.143,223.

_____ 1976, M.N.R.A.S.175,225.

_____ and Griffin,R. 1967, M.N.R.A.S.137,253.

Gustafsson,B., Kjaergaard,P., and Anderson,S. 1974, Astron. Astrophys.34,99.

Gustafsson,B., Bell,R.A., Eriksson,K., and Nordlund,A. 1975, Astron. Astrophys.42,407.

Hays,D.S., and Latham,D.W. 1975, Ap.J.197,593.

Holweger,H. 1972, Solar Phys.25,14.

Houtgast,J. 1970, Solar Phys.15,273.

Kelch,W.L., and Milkey,R.W. 1976, Ap.J.208,428.

Kurucz,R.L. 1974, Solar Phys.34,17.

Jefferies,J.T., and White,O.R. 1960, Ap.J.132,767.

Johnson,H.R., and Krupp,B.M. 1976, Ap.J.206,201.

Labs,D., and Neckel,H. 1962, Z. Astrophys.55,269.

_____ 1968, Z. Astrophys.69,1.

Liller,W. 1968, Ap.J.151,589.

Linsky,J.L. 1968, Smithsonian Special Report No.274.

Linsky,J.L.,and Ayres,T.R. 1973, Ap.J.180,473.

Lites,B.W. 1973, Solar Phys.32,283.

Mackle,R., Holweger,H., Griffin,R., and Griffin,R. 1975, Astron. Astrophys.38,239.

Mihalas,D. 1970, Stellar Atmospheres, W.H. Freeman & Co, San Fransisco.

Milkey,R.W., and Mihalas,D. 1974, Ap.J.192,769.

Milkey,R.W., Ayres,T.R., and Shine,R.A. 1975, Ap.J.197,143.

Oinas,V. 1974, Ap.J. Suppl.27,391, and 405.

_____ 1975, Private Communication.

Peach,G. 1970, Mem.R.A.S.73,1.

Peterson,R.C. 1976, Ap.J. Suppl.30,61.

Ridgeway,S.T. 1974, Ap.J.190,591.

Rodriguez,M.G. 1969, Astrophysika,5,269.

Shine,R.A. 1973, Ph.D. Thesis, University of Colorado.

Shine,R.A., and Linsky,J.L. 1974, Solar Phys.39,49.

Shine,R.A., Milkey,R.W., and Mihalas,D. 1975a, Ap.J.199,724.

_____ 1975b, Ap.J.201,222.

Spinrad,H., and Taylor,B. 1969, Ap.J.157,1279.

Strom,S.M., Strom,K.M., and Carbon,D.F. 1971, Astron. Astrophys.12,177.

Travis,L.D., and Matsushima,S. 1968, Ap.J.154,689.

Ulmschneider,P. 1974, Solar Phys.39,327.

Unsold,A. 1955, Physik der Sternamospharen, Springer-Verlag, Berlin.

Van Paradijs,J. 1976, Astron. Astrophys. Suppl.24,53.

Vernazza,J.E., Avrett,E.H.,

and Loeser,R. 1976, Ap.J. Suppl.30,1.

White,O.R., and Suemoto,Z.1968, Solar Phys.3,523.

Williams,P.M. 1971, M.N.R.A.S.153,171.

_____ 1972, M.N.R.A.S.158,361.

Withbroe,G.L. 1971. NBS Special Publication #353,

p.127.